

Research Programme of the Research Fund for Coal and Steel  
Steel RTD

TGS8

## **Two INnovations for Earthquake Resistant Design The INERD Project.**

A. PLUMIER, C. DONEUX Catherine  
Université de Liège  
Institut de Mécanique et Génie Civil – Bât.B52/3  
Chemin des Chevreuils, 1, B – 4000 LIEGE 1, BELGIUM

C.CASTIGLIONI, J. BRESCIANINI, A. CRESPI , S. DELL'ANNA , L.LAZZAROTTO  
Politecnico di Milano  
Dipartimento di Ingegneria Strutturale, POLITECNICO DI MILANO  
Piazza Leonardo da Vinci, 32, I-20133 Milano, ITALY

L.CALADO, J.FERREIRA Joao, S. FELIGIONI  
IST  
Instituto Superior Técnico , Department of Civil Engineering and Architecture  
Av. Rovisco Pais, P-1049-001 Lisboa, PORTUGAL

O.BURSI , F.FERRARIO, M.SOMMAVILLA  
University of Trento  
Universita Degli Studi di Trento,Dipartimento di Ingegneria Mecc. e Strutturale  
Via Mesiano 77,I-38050 Trento ,ITALY

I.VAYAS , P.THANOPOULOS  
NTUA  
National Technical University of Athens,Department of Civil Engineering  
Patission Str. 20,GR-10682 Athens,GREECE

T.DEMARCO  
ProfilArbed Recherches  
Profil ARBED Recherches,B.P. 14, L – 4009 Esch sur Alzette  
GRAND DUCHE DE LUXEMBOURG

CEC Agreement No7210-PR-316  
1 July 2001 to 30 June 2004

**Final Report**

## **ABSTRACT.**

The project develops two innovations.

The first innovation promotes a construction measure by which the "soft storey" mechanism is obviated in the lower storeys of reinforced concrete (R.C.) frames by encasing steel profiles in R.C. columns in order to provide them with a basic reliable shear, bending and compression resistance. Tests are performed and comparison of the behaviour of reference reinforced concrete and composite specimens made. Several parameters are studied: axial load, length of anchorage, stiffeners in the panel zone, weak and strong axis bending, configurations with and without infills. The study defines design rules for steel profiles to be encased in ductile R.C. columns, formulas for the behaviour of local strut and tie mechanism in presence of infills and formulas for the calculation of the shear resistance of a composite beam-to-column panel zone in configurations without infills.

The second innovation consists in using dissipative connections for diagonals of frames with concentric bracings. Two types of connections are studied: the "pin" connections, made of bent rounded or rectangular bars, and "U-device" connection, made of plates bent in U. Their behaviour is studied experimentally on connections and on complete bracings. Design rules are defined, especially for the pin connection, and fatigue curves obtained. The applicability and interest are set forward by numerical studies and comparative design of structures with classical and with dissipative connections. The innovation demonstrates a higher capacity to dissipate energy. It can be translated into higher behaviour factor  $q$ .

## **STRUCTURE OF THE REPORT.**

There are three distinct parts in the report of the INERD project.

The first part is a document focused on the presentation of the design relationships or methods developed in the course of the INERD project. Calling the document a “design guide” might be too ambitious, because there are still assessments to be made in the future for some of the proposed design relationships. It is a “**Design Report**”. It is presented at the front of this document, in Sections 1 and 2.

The second part is a report explaining the meaning of the research activity in the INERD project, the background and the conclusions. It is a “**Research Report**”, which is presented in Sections 3, 4 and 5 of this document.

The third part of the INERD Report compiles all the experiments, either physical or numerical, with measurements, graphs, curves, etc. It is a “**Laboratory Report**”. The “Laboratory Report” is not included in the present document, due to its size. It can be obtained separately upon request by email at: [a.plumier@ulg.ac.be](mailto:a.plumier@ulg.ac.be)



## **TABLE OF CONTENT.**

STRUCTURE OF THE REPORT .....	3
SYMBOLS.....	7
1. DESIGN REPORT ON COMPOSITE COLUMNS.....	9
1.1 Design conditions for the encased steel profile.....	9
1.2 Local failure mechanism in case of pilotis structure (presence of infills at all floors except the first one) Verification formulas. ....	11
1.3. Seismic design of composite beam-to-column joint .....	15
2. DESIGN REPORT ON DISSIPATIVE CONNECTIONS.....	17
2.1. Description of the INERD connections.....	17
2.2. Benefits of braced frames with INERD connections .....	18
2.3. Mechanical characteristics of pin INERD connections.....	19
2.4. Code rules for braced frames with pin INERD-connections.....	21
2.5. Practical design procedure and design example.....	22
2.6. Design example .....	23
2.7. Design proposal for fatigue.....	25
3. RESEARCH REPORT ON DISSIPATIVE COMPOSITE COLUMNS FOR MITIGATION OF SOFT STOREY FAILURES IN REINFORCED CONCRETE COLUMNS. ....	31
3.1 Definition of the problem and proposal for a solution.....	31
3.2. Research approach. Design requirements for the encased steel profile. ....	32
3.3. Test set up and testing procedure. ....	35
3.4. Plastic hinges in columns as dissipative mechanism. ....	37
3.4.1. Specific features of the test set up.....	37
3.4.2. Global behaviour of the tests specimens. ....	38
3.4.3. Conclusions from the tests. ....	45
3.4.4. Effect of discrepancies between the concrete design resistance and actual resistance. .....	46
3.4.5. Design resistance of potential local failure mechanisms. ....	48
3.5. Composite panel zone as dissipative mechanism.....	56
3.5.1. Forces acting at the beam-to-column joint.....	56
3.5.2. Analytical procedure for an effective composite joint design.....	59
Panel Zone Resistance.....	60
Horizontal Bearing Resistance .....	61
Concrete Compression Field Resistance .....	62
Bond Shear Resistance .....	62
3.5.3. Conclusions from the tests. ....	63
3.5.4. Experimental and numerical validation of the analytical formulas.....	67
3.6. Conclusions on composite columns. ....	73
4. RESEARCH REPORT ON DISSIPATIVE CONNECTIONS FOR FRAMES WITH CONCENTRIC BRACINGS. ....	75
4.1. Motivation for using dissipative connections in frames with concentric bracings. ....	75
4.2. Description of the INERD connections and research approach.....	76
4.3. Tests on single connections.....	78
4.3.1. Test setup and test programme.....	78
Pin connections .....	79
U connections.....	79
4.3.2. Results in terms of energy dissipation capacity .....	81
U connections.....	83

Global comparisons.....	85
4.3.3. Results in terms of Fatigue.....	85
4.4. Tests on frames with concentric bracings and dissipative connections. ....	90
4.4.1. Test set up and test programme.....	90
4.2.2. Results .....	93
Global comparisons.....	97
4.5. Theoretical assessment of dissipative connections and of frames with concentric bracings using dissipative connections. ....	100
4.5.1. Analysis of pin INERD connections .....	100
4.5.2. Frame and connection kinematics .....	110
4.5.3. Response of braced frames with INERD connections under static loading.....	113
4.5.4. Response of braced frames with INERD connections under seismic loading .....	115
4.6. Conclusions on dissipative connections in concentric bracings.....	122
 5. GENERAL CONCLUSION AND FUTURE WORK.....	 125
 5. LIST OF REFERENCES .....	 129

## Symbols.

The symbols used in Section 3 are the following.

$a_c$	height of the Stress Block, equal to: $(0,58h_b/2)$ .
$A_{cs}$	area of the inner concrete strut of the panel zone mechanism.
$A_{s,tie}$	total area of a layer of the transversal reinforcement.
$A_{s,teel}$	cross sectional area of the steel profile.
$A_{total}$	cross sectional area of the composite section.
$A_v$	cross sectional shear area of the steel column.
$b_{cf}$	width of the steel column flange.
$b_{cs}$	effective width of the outer concrete strut, equal to: $(b_c - b_{cf} - 2c_c)$ .
$d$	effective height of the reinforced concrete column, equal to: $(h_{col} - c_c)$ .
$d_s$	panel zone height measured centre to centre line of the axis of the continuity plates.
$E_c$	concrete Young modulus.
$E_s$	steel Young modulus.
$f_{bd}$	bond design strength.
$f_{cd}$	concrete cylindrical design strength in compression.
$f_{ck,c}$	concrete cylindrical characteristic strength in compression accounting for the confinement effect.
$f_{yd,w}$	yield design strength of the transversal reinforcement.
$f_{ym,d,cw}$	mean yield design strength of the steel column web.
$f_{yk,w}$	characteristic yield design strength of the transversal reinforcement.
$G$	dead load.
$h_b$	height of the reinforced concrete beam.
$h_c$	depth of the column steel profile.
$L_{beam}$	distance between inflection points in the beam.
$L_{col}$	distance between inflexional points in the column equal to the its free length.
$M_g$	bending moment acting in the beam due to the gravity loads.
$M_{j,Rd}$	design resisting moment of the joint.
$M'_{j,Rd}$	design resisting moment of the joint, taking into account the Capacity Design.
$M'_{j,Rd,BF,col}$	design resisting moment of the bond mechanism in the composite column.
$M'_{j,Rd,CCF}$	design resisting moment of the concrete compression field mechanism.
$M'_{j,Rd,CCS}$	design resisting moment of the inner concrete compression strut.
$M'_{j,Rd,HBF}$	design resisting moment of the horizontal bearing mechanism.
$M'_{j,Rd,INNER}$	design resisting moment of the inner part of the joint.
$M'_{j,Rd,OUTER}$	design resisting moment of the outer part of the joint.
$M'_{j,Rd,SWP}$	design resisting moment of the shear web panel.
$M_{j,Sd}$	design stressing moment of the joint.
$M_p$	plastic bending moment.
$M_{Rd,beam}$	design resisting moment of the beam region next to the joint.
$M_s$	bending moment acting in the beam due to the seismic loads.
$N_{rd}$	design compressive resistance of the column.
$N_{sd}$	design compressive force acting on the column.
$Q$	live load.
$r$	radius of the steel profile between the web and the flange.
$S_{tie}$	longitudinal spacing of the transversal reinforcement in the joint region.
$t_{bf}$	thickness of the steel beam flange.
$t_{cf}$	thickness of the steel column flange.
$t_{cw}$	thickness of the steel column web.
$T_{cb}$	compressive force acting on a set of longitudinal re-bars of the column.
$T_{mb}$	friction design force developed by a set of longitudinal re-bars of the column.
$T_{tb}$	tensile force acting on a set of longitudinal re-bars of the column.
$V_c$	shear resistance of the concrete part in the joint region, equal to: $(V_{c,inner} + V_{c,outer})$ .
$V_{col,wp,u}$	ultimate mean shear acting on the web panel in the joint.
$V_{j,bf,col}$	shear resistance of the bond mechanism.
$V_{j,ccs}$	shear resistance of the concrete strut in the inner joint region.

$V_{j,ccf}$	shear resistance of the concrete compression field in the outer joint region.
$V_{j,hbf}$	shear resistance of the horizontal bearing mechanism.
$V_{j,Rd}$	shear design resistance of the composite joint.
$V_{j,Sd}$	design shear force acting on the joint.
$V_{j,swp}$	nominal shear resistance of the steel column web.
$V_s$	shear resistance of the transversal reinforcement.
$x_{rb,c}$	distance between the barycentres of the two sets of longitudinal re-bars resisting in bonding.
$\alpha_c$	magnification factor defined in Eurocode 2.
$\phi_b$	total perimeter of a set of longitudinal re-bars encased in the outer zone of the joint, equal to: $T_{cb}$ o $T_{tb}$ .
$\gamma_c$	partial safety factor for the concrete at the ULS.
$\gamma_g$	partial safety factor for the dead load.
$\gamma_q$	partial safety factor for the live load.
$\gamma_s$	partial safety factor for the reinforcement steel at ULS.
$\nu$	reduction factor from Eurocode 2.
$\theta$	angle formed by the concrete compression strut.



# **1. DESIGN REPORT ON COMPOSITE COLUMNS**

## **1.1 Design conditions for the encased steel profile**

The proposed innovation for the problem of soft storey consists in encasing steel profiles (HE or UC) in the lowest levels of reinforced concrete (R.C.) columns in order to provide them a basic reliable shear and compression resistance. The idea is to use encased steel section as a ductile fuse able to dissipate cyclically the energy of the earthquake in the columns of the lower storey of the buildings which otherwise remain reinforced concrete buildings. The objective is to ensure a minimum structural reliability especially in the possible tricky circumstances of either a bad concrete mix utilisation or an awkward concrete hardening process.

In the concept of the proposal, the steel profiles are "safety belts": if circumstances are such that a soft storey mechanism would form under earthquake action, the plastic hinges in the R.C. column at ground level would not provide much ductility; then the steel profile would come into action.

The objectives are:

To achieve this goal, it is necessary to satisfy some simple criteria to design the steel profiles:

- to maintain axial strength, (plastic) moment resistance, and stiffness similar to those of the RC column at the ultimate stage when concrete is locally crushed.
- to provide ductility.

The corresponding detailed design criteria are:

- I. The steel section alone should at least be able to take the design axial force of the seismic loading case:

$$N_{Rd} \geq N_{sd}(\gamma_g \cdot G + \gamma_q \cdot Q) \quad [1.1]$$

with  $\gamma_g = 1$  and  $\gamma_q = 0,3$

- II. The steel section alone (not acting composedly) should be able to substitute the deficient concrete section due to the bending moment and shear actions at collapse:

$$M_{Rd,steel} > M_{Rd,concrete} \quad [1.2]$$

$$V_{Rd,steel} > V_{Rd,concrete} \quad [1.3]$$

for axial force  $N_{sd}$  considered equal to zero

- III. The steel sections should not much modify the local stiffness  $EI$  of the single RC column (maximum modification level in the order of 10%) in order not to change the distribution of stiffness in the entire and original RC structure. In fact, a change in stiffness distribution may also signify a variation of the building periods of vibration closely tied to the inertial forces, e.g. seismic forces.

- IV. The following ratio should be close to unity in order to achieve a suitable performance of the steel profile along major and minor axis bending:

$$\frac{r_{major}}{r_{minor}} = \frac{\left( \frac{M_{Rd,comp}}{M_{Rd,concrete}} \right)_{major}}{\left( \frac{M_{Rd,comp}}{M_{Rd,concrete}} \right)_{minor}} \quad [1.4]$$

The idea developed is to insert steel profiles in columns at ground level. It raises the problem of how to realize the details of the anchorage and how far to extend the anchorage of these steel profiles into the concrete structure of the 1st storey and of the ground level.

At the present state of knowledge, the good behavior of the encased steel profile is ensured provided that the following requirements are met:

- “long” anchorage of the steel profile in the concrete column of the second floor

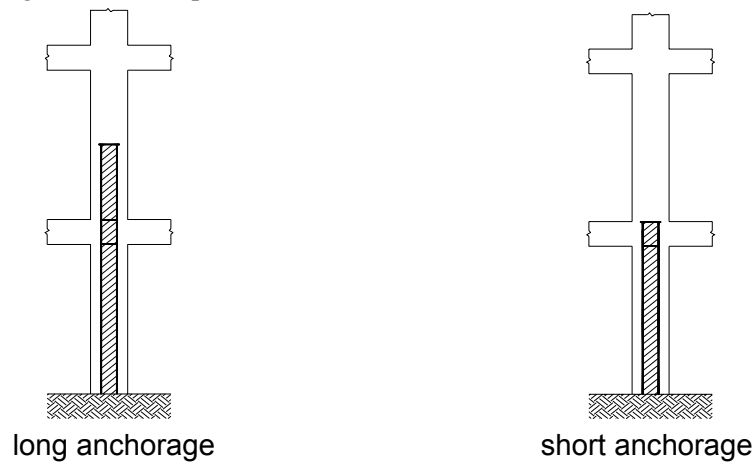


Figure 1.1. Anchorage of the steel profile into the second floor

- presence of an endplate at the end of the steel profile, to transmit axial forces and bending moment

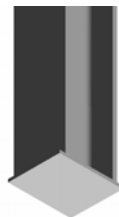


Figure 1.2. Endplate at the end of the steel profile

- stiffeners in the panel zone of the steel profile
- confinement is present in the anchorage zone by the same density of stirrups in the anchorage length as in the critical zones of the reinforced concrete node.

It is clear that all these criteria are on the safe side. It has been seen in the INERD research that short anchorage was also effective and that stiffeners were not absolutely necessary. Unfortunately, these very positive results are linked to a very strong concrete combined with very effective confinement. Some additional research is still needed to allow less severe design rules.

**1.2 Local failure mechanism in case of pilotis structure (presence of infills at all floors except the first one) Verification formulas.**

This part is not complete, in the sense that the following formulas represent the “resisting” parts of the possible failure mechanism in case of pilotis structures. The “action effect” part to be considered in the verifications has not been defined. Calculations had been done with possible maximal actions, with the idea that if the verifications were ok with secure actions, the design was ok. But the verifications were not ok, even though the tests showed that no failure occurred. So, it seems that this procedure is too secure and additional work is still needed.

The link between the whole pilotis structure and the beam-to-column node where the local failure mechanism is supposed to occur is presented at Figure 1.3.

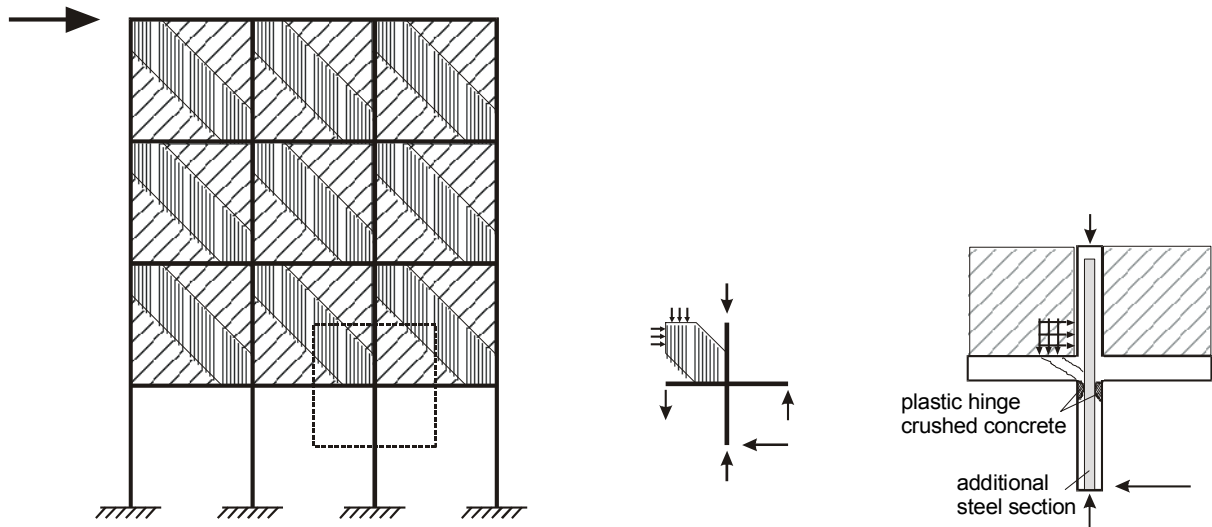


Figure 1.3 . Link between global pilotis structure and local failure mechanism

In the following, the drawings are given for a configuration with the first floor at the top and the second floor at the bottom of the beam-to-column node.

The formation of the compressive strut in the beam is conditioned by local equilibrium in the node, implying steel ties in tension and concrete struts in compression, as shown in Figure 1.4.

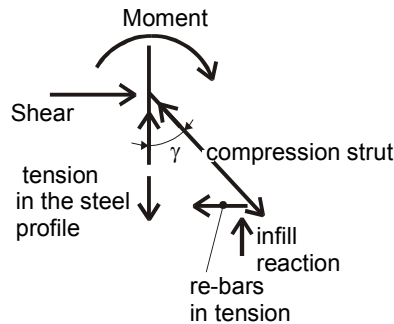


Figure 1.4 . Global equilibrium of the steel profile

If the column is in compression (as it was assumed in the tests), the steel profile applies a compression directly equilibrated by the concrete of the column (see Figure 1.5).

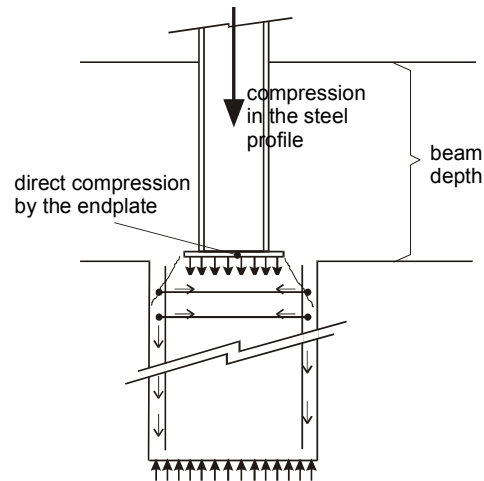


Figure 1. 5. Equilibrium of steel profile in compression

The compression strut force (1) in Figure 1.6 is equilibrated at both ends by compression perpendicular to contact surface (steel profile at one end, infill at the other end (2)) and by tension in re-bars of column and beam (3). The tension in the beam re-bar is also equilibrated by a compressed strut bearing on the vertical side of the infill.

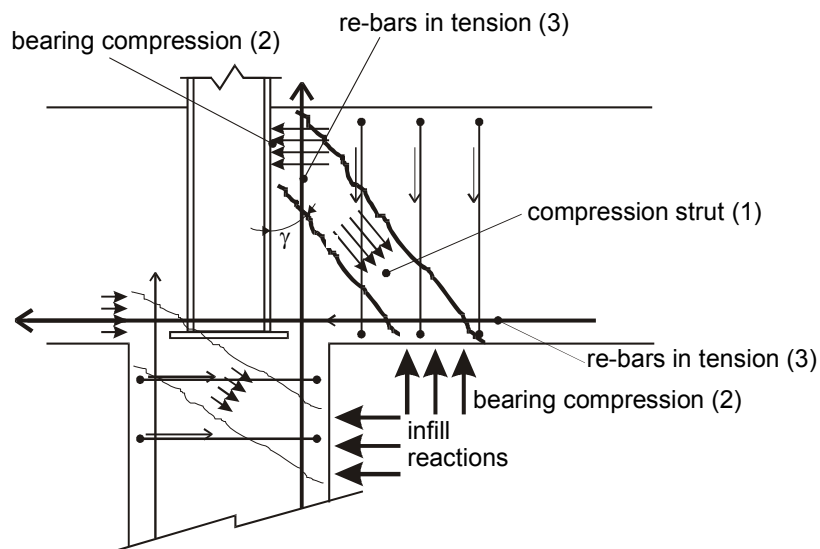


Figure 1. 6. Equilibrium of one compressed concrete strut

The steel profile in tension is equilibrated by the additional compression coming from the applied vertical load, and also superposed and equilibrated by the compressed strut in the beam. No mechanism is independent. But the estimations of resistance will be done separately because the different mechanisms here are beneficial for each other. So, it is secure to work partly independently.

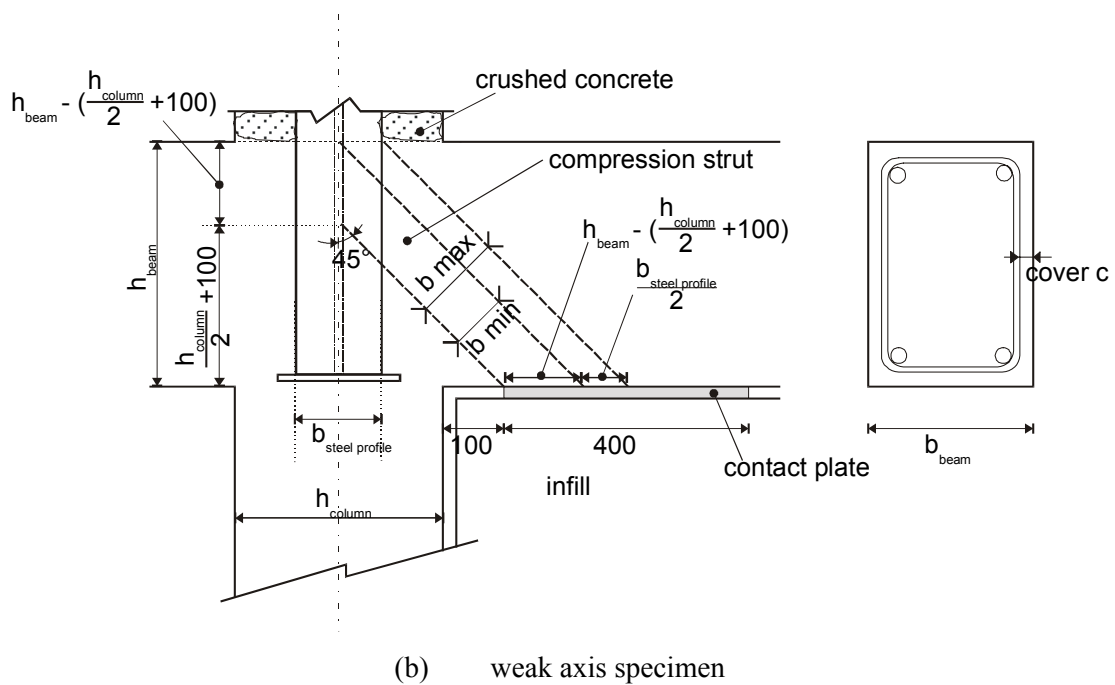
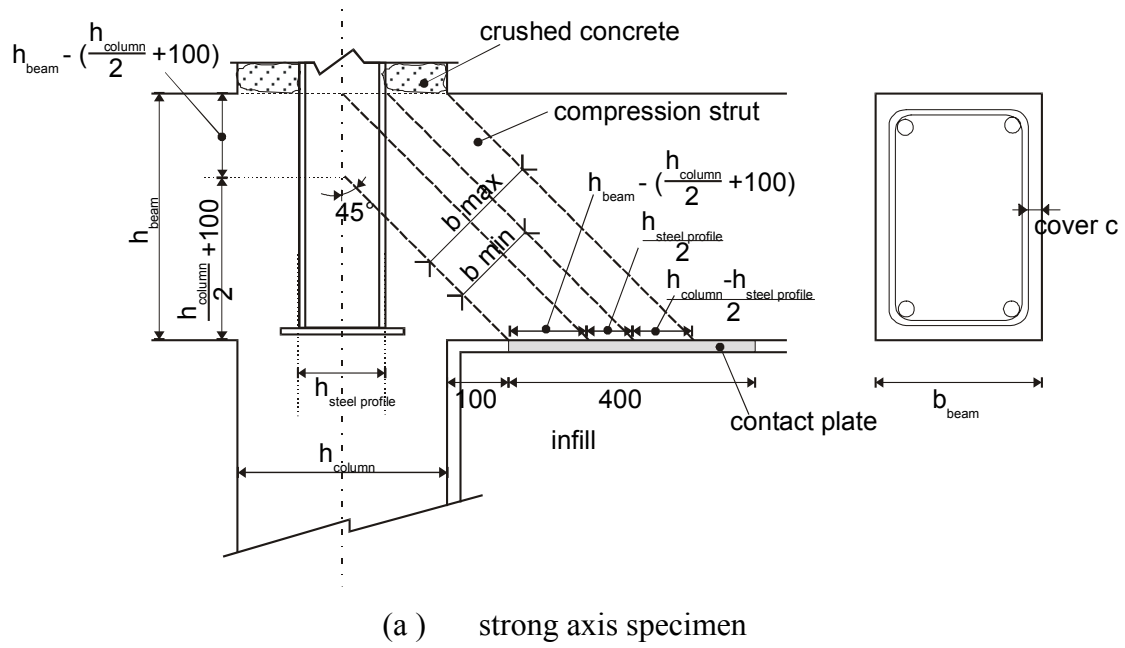


Figure 1.7. Notations to define the dimensions of the compressed strut

The dimensions of the compressed strut (1) are represented on Figure 1.7 with the assumption of a 45° slope for the compressed strut. Their resistance are calculated in function of minimum and maximum widths given in the following equations.

Width of the compressed strut for the strong axis specimens

$$b_{\text{strut min}} = \frac{\sqrt{2}}{2} \left( h_{\text{beam}} - \left( \frac{h_{\text{column}}}{2} + 100 \right) + \frac{h_{\text{steel profile}}}{2} \right) \quad [\text{mm}] \quad [1.5]$$

$$b_{\text{strut max}} = \frac{\sqrt{2}}{2} (h_{\text{beam}} - 100) \quad [\text{mm}] \quad [1.6]$$

Width of the compressed strut for the weak axis specimens

$$b_{\text{strut min}} = \frac{\sqrt{2}}{2} (h_{\text{beam}} - (\frac{h_{\text{column}}}{2} + 100)) \quad [1.7]$$

$$b_{\text{strut max}} = \frac{\sqrt{2}}{2} (h_{\text{beam}} - (\frac{h_{\text{column}}}{2} + 100) + \frac{b_{\text{steel profile}}}{2}) \quad [1.8]$$

Thickness of the compressed strut

$$t_{\text{strut}} = b_{\text{beam}} - 2 c_{\text{cover}} - \phi_{\text{stirrup}} \quad [1.9]$$

Resistance of the struts

$$N_{\text{Rd strut}} = \nu f_c b_{\text{strut}} t_{\text{strut}} \quad [1.10]$$

With  $\nu = 0,6$

The bearing compression of the concrete of the strut on the steel profile (2) is also estimated for both strong and weak axis specimens.

For the strong axis specimens, the bearing compression of the concrete is located on the flanges of the steel profile. The resistance to the bearing compression is calculated as follows:

$$h_{\text{bearing}} = b_{\text{strut min}} \sqrt{2} = h_{\text{beam}} - (\frac{h_{\text{column}}}{2} + 100) + \frac{h_{\text{steel profile}}}{2} \quad [1.11]$$

$$w_{\text{bearing}} = b_{\text{steel profile}} \quad [1.12]$$

$$\text{Resistance} = N_{\text{Rd bearing}} = f_c h_{\text{bearing}} b_{\text{steel profile}} \quad [1.13]$$

For the weak axis specimens, the bearing compression is located on the web of steel profile instead of on the flanges. The resistance to the bearing compression is calculated as follows:

$$h_{\text{bearing}} = b_{\text{strut min}} = h_{\text{beam}} - (\frac{h_{\text{column}}}{2} + 100) \quad [1.14]$$

$$w_{\text{bearing}} = h_{\text{steel profile}} - 2 t_{\text{flanges steel profile}} \quad [1.15]$$

$$\text{Resistance} = N_{\text{Rd bearing}} = f_c h_{\text{bearing}} (h_{\text{steel profile}} - 2 t_{\text{flanges steel profile}}) \quad [1.16]$$

The tension in the re-bars of the beam (3) is limited by the equation:

$$N_{\text{Rd re-bars}} = A_{\text{re-bars}} f_y \quad [1.17]$$

### 1.3. Seismic design of composite beam-to-column joint

This part concerns the design of beam-to-column node of moment resisting frames, without infills or without taking into account the possible effect of infills.

The main type of failures occurring at the joint location are a) panel shear failure and b) bearing failure for inner joint region, whereas the outer part of the joint deals with c) concrete shear and d) bond failure. The behaviour of the beam-to-column joint area is tied to the resistance mechanisms reacting to the forces stressing the area under consideration:

- Panel Zone Resistance: this is obtained from the sum of the column steel web panel resistance ( $V_{j,wps}$ ) and of the concrete compression strut resistance ( $V_{j,ccs}$ ) generated between the continuity plates (stiffeners) and the steel profile flanges. The web is considered to carry pure shear stress over an effective panel length  $d_s$ , which is dependent on the location of the stiffeners in the column or on the distribution of horizontal bearing stresses. The concrete compression strut is similar to the mechanism used to model shear in a reinforced concrete connection, in which the concrete compression strut could be mobilized in resisting the connection shear either due to the presence of the horizontal stiffener plates welded to the column or due to the friction and the flexural forces acting in the steel column flange.

$$V_{j,wps} = 0,7 \cdot (f_{ym,d,cw} \cdot \min(A_v; t_{cw} \cdot d_s) + \Delta V_{j,wps}) \quad [1.18]$$

$$V_{j,ccs} = \frac{1}{1,3} \cdot v \cdot 0,85 \cdot f_{cd} \cdot A_{cs} \cdot \sin\theta \quad [1.19]$$

- Horizontal Bearing Resistance ( $V_{j,hbf}$ ): this resistance is determined through a standard Stress Block model similar to that used for flexural strength calculation in reinforced concrete members and depends on the confinement of the joint area;

$$V_{j,hbf} = \frac{1}{1,3} \cdot \left( 0,85 \cdot \frac{f_{ck,c}}{\gamma_c} \right) \cdot a_c \cdot b_{cf} \quad [1.20]$$

- Concrete Compression Field Resistance ( $V_{j,ccf}$ ): the concrete compression field mechanism consists of several compression struts that act with the horizontal reinforcement to form a truss mechanism. Shear is transferred horizontally from the beam into the compression field by the concrete bearing against the embedded steel column;

$$V_{j,ccf} = \frac{1}{1,3} \cdot \min \left( \alpha_c \cdot v \cdot f_{cd} \cdot b_{cs} \cdot 0,9 \cdot d \cdot \frac{1}{(\cot\theta + \tan\theta)_c}; \frac{A_{s,tie}}{s_{tie}} \cdot f_{yd,w} \cdot 0,9 \cdot d \cdot \cot\theta_s \right) \quad [1.21]$$

- Bond Shear Resistance ( $V_{j,bf}$ ): this resistance depends on the longitudinal rebars acting in friction with concrete. The bond failure occurs if the compression and tension forces compatible with the moment equilibrium (along with the forces mobilised in the concrete compression field) are greater than the bond strength provided by one set of longitudinal reinforcing bars embedded in the outer most joint region.

$$V_{j,bf} = \frac{1}{1,3} \cdot f_{bd} \cdot \phi_b \cdot x_{rb,c} \quad [1.22]$$

In Eurocode 8, the beam-to-column joints in moment frames are required to have a high enough moment resistance  $M_{j,Rd}$  in order to enhance the ductile capacity of the columns and to avoid the local formation of plastic hinges in the column panel zone. Provided that, at the design stage, the plastic hinge formation in the beams is envisaged, it is necessary in any case to take into account the increase in the beam moment values in order to derive the design joint forces.

$$M_{j,Rd} \geq 1,3 (M_{beam,Rd,right} + M_{beam,Rd,left}) \quad [1.23]$$

Moreover, focusing the attention on the behaviour of an internal beam-to-column joint belonging to a frame free to deform in plane and subjected both to gravitational and seismic loads it is possible to

define the shear force acting in the joint, that depend obviously on the bending moments acting at the left and at the right of the joint.

Considering that the gravitational loads reduce the effects of the seismic action in terms of bending moment acting at the joint and that the column shear reduces the total joint shear action at the beam-to-column joint position and thus increases the shear joint strength. In accordance with these assumptions, and by considering the mechanism mentioned above, in seismic conditions, for an internal beam-to-column composite joint it is to check that:

$$V_{j,Rd} \geq V_{j,Sd} = 0,8 \cdot \frac{\sum M_{Rd,beam}}{d_s} - V_{col,wp,u} \quad [1.24]$$



## 2. DESIGN REPORT ON DISSIPATIVE CONNECTIONS

### 2.1. Description of the INERD connections

Innovative dissipative (INERD) connections are used in seismic resistant braced steel frames for the connection of the braces to the adjacent members (columns or beams). Two types of INERD connections were developed:

#### a) Pin connections

The pin connections consist of two external eye-bars welded or bolted to the adjacent member (column or beam), two internal eye-bars welded to the brace and a pin running through the eye-bars (Figure 2.1). In this type of connection the pin exhibits inelastic bending deformations and dissipates energy due to the fact that the eye-bars are placed at some distance between each other.

#### b) U-connections

The U-connections consist of one or two bent, U-shaped thick plates that connect the brace to the adjacent member (Figure 2.2). Here again, energy dissipation takes place in the bent plate(s).

The advantage of these connections is that, by appropriate sizing, inelastic deformations are limited within exactly predetermined zones, the pins or the U-plates, whereas the adjacent parts remain elastic. Consequently, braces are protected from buckling and damage is restricted in the pins or the U-plates. These are small parts that may be easily replaced if they are largely deformed, after an unusually strong earthquake.

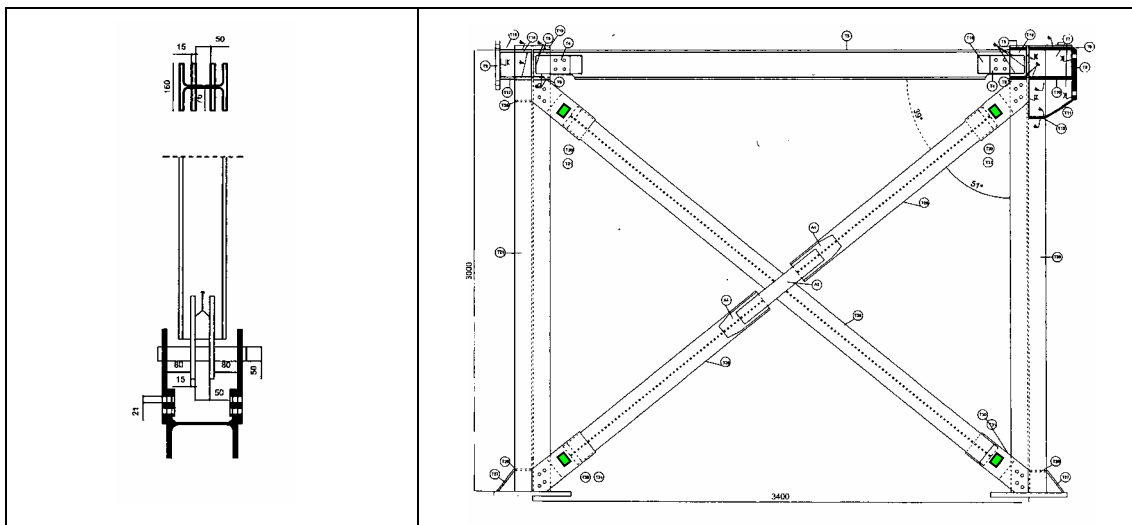


Figure 2.1: INERD pin connections

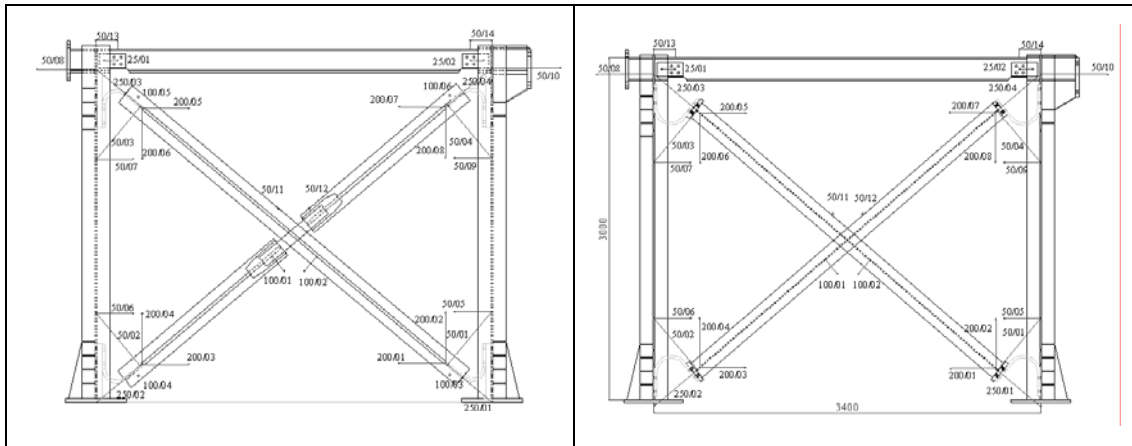


Figure 2.2 : INERD U-connections

## 2.2. Benefits of braced frames with INERD connections

Seismic resistant steel structures are designed for stiffness, strength and ductility. Stiffness requirements are imposed in order to limit non-structural damage in case of minor to moderate earthquakes and limit instability effects, strength in order to ensure the capacity of the structure to resist safely the action effects and ductility in order to dissipate part of the seismic input energy through inelastic deformations and therefore reduce the action effects. Conventional frames, both unbraced and braced, have certain disadvantages in respect to the above design criteria (Table 2.1, columns 2 to 4). In addition, braced frames that are widely applied in Europe, face following problems after unusually strong earthquakes that result in some degree of damage: a) the need for strengthening or replacement of damaged and buckled braces which have a certain length and are difficult to handle, b) the need for strengthening and repair of the links or the beams that are part of the main system that supports gravity loading. Such works require therefore considerable skill and are associated with high material and labour costs.

Table 2.1: Structural typologies and main characteristics for Steel Frames

1	2	3	4	5
	Moment resisting Frames (MRF)	Concentric Braced Frames (CBF)	Eccentric Braced Frames (EBF)	CBF or EBF with dissipative INERD-connections
Stiffness	Low	High	Moderate	High
Ductility	High	Low	Moderate	High
Strength	As required	As required	As required	As required
Dissipative zones at	Beam-ends	Braces	Link beams	Connections

Braced frames with INERD-connections exhibit following benefits compared to conventional steel frames:

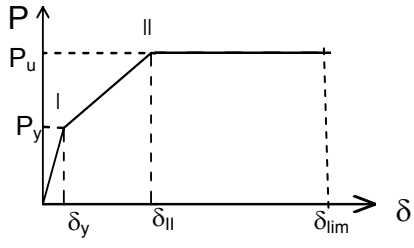
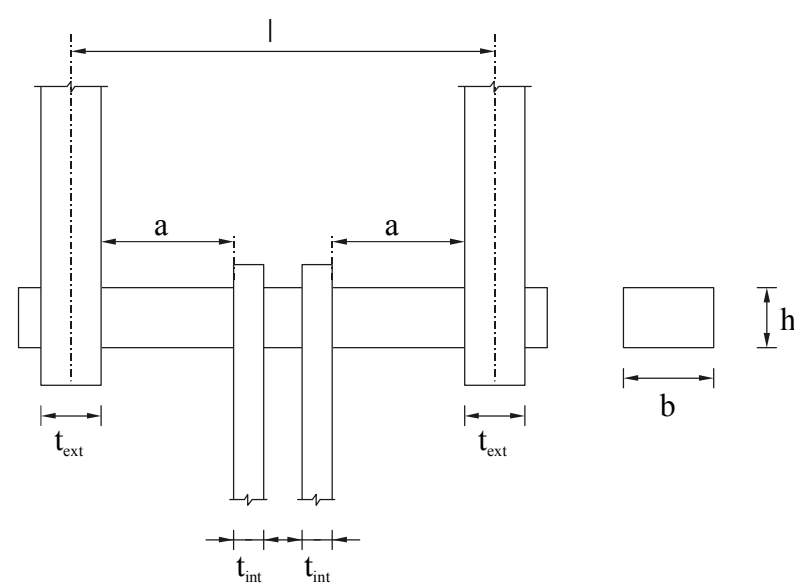
- a) Better compliance with the seismic design criteria (Table 2.1, column 5).
- b) Protection of compression braces against buckling.
- c) Activation of all braces, either in compression or in tension, even at large storey drifts.
- d) Limitation of inelastic action in small parts that may be easily replaced.
- e) Possibility for easy inexpensive repair after very strong earthquakes, if required.
- f) Reduction of overall structural costs for the same performance level.

### **2.3. Mechanical characteristics of pin INERD connections**

The mechanical characteristics of pin INERD connections may be described by their force-deflection-curves. These curves may be approximated by a tri-linear curve with two characteristic points (yield and ultimate). The relevant values, as well as the deformation capacity of the connection, are given in Table 2.2.

Due to further analysis of the research data, this table is slightly different from the table presented in the research report.

Table 2.2. Design formulae for the connection with 2 internal plates

	Eye-bars in	Force	Displacement
Point I “yielding y”	Compression	$P_{y,Rk} = \frac{2 \cdot M_p}{(a/1,1)}$	$\delta_y = 1,5 \cdot \frac{M_p}{E \cdot I} \cdot \ell^2 \cdot \frac{\alpha}{6} \cdot (3 - 4\alpha)$
Point II “ultimate u”	Compression	$P_{u,Rk} = \frac{4 \cdot M_p}{(a/1,1)}$	$\delta_{II} = 0,2 \cdot a$
Points I and II	Tension	90% of the above values for $P_y$ and $P_u$	
Over-strength for capacity design checks		30% beyond $P_u$	
Deformation capacity			$\delta_{lim} = 0,8 \cdot a$
<p> <math>M_p = W_{pl} \cdot f_y</math>      <math>\alpha = a/\ell</math>  <math>\ell</math> = pin length (axial distance between external eye-bars)  <math>a</math> = clear distance between internal and external eye-bars  <math>f_y</math> = yield stress of pin  <math>W_{pl}</math> = plastic modulus of pin cross section  <math>I</math> = moment of inertia of pin cross section  <math>E</math> = elastic modulus of pin 's material                 </p>  <p>For rectangular pins, <math>W_{pl} = bh^2/4</math> and <math>I = bh^3/12</math>  <math>h</math> = pin height, <math>b</math> = pin width</p>			

## 2.4. Code rules for braced frames with pin INERD-connections

Braced frames with pin INERD-connections may be designed according to the general rules of Eurocode 8, duly modified in order to consider that energy dissipation is taking place in the pin connections and not in the tension braces. Table 2.3 gives the original EC 8 rules for concentric braced frames and the proposed modified rules of such frames with pin INERD connections.

Table 2.3. Code formulation for concentric braced frames with pin INERD connections

Paragraph	Original Code text	Modified text
6.7.1 Design criteria	(1)P Concentric braced frames shall be designed so that yielding of the diagonals in tension will take place before failure of the connections and before yielding or buckling of the beams or columns.	(1) P Concentric braced frames with pin INERD connections shall be designed so that: (a) yielding of the pins will take place before compression failure of the diagonals and before yielding or buckling of the beams or columns. (b) failure of the connections precedes buckling failure of the diagonals (c) yielding of the pins is limited at the damage limitation state (d) the other connection elements shall be designed with adequate overstrength relevant to the pins.
	(2)P The diagonal elements of bracings shall be placed in such a way that the structure exhibits similar load deflection characteristics at each storey in opposite senses of the same braced direction under load reversals.	(2)P The diagonal elements of bracings and their connections shall be placed in such a way that the structure exhibits similar load deflection characteristics at each storey in opposite senses of the same braced direction under load reversals.
6.7.2 Analysis	(2)P The diagonals shall be taken into account as follows in an elastic analysis of the structure for the seismic action:  – in frames with diagonal bracings, only the tension diagonals shall be taken into account;  (3) .....	(2)P The diagonals shall be taken into account as follows in an elastic analysis of the structure for the seismic action:  – in frames with diagonal bracings, both the tension and compression diagonals shall be taken into account;  (3) Does not apply
6.7.3 Diagonal members	(1) to (9)	(1) to (9) Do not apply, except (8)
6.7.4 Beams and columns	(1) ...	(1) as in the original text, with: $\Omega$ is the minimum value of $\Omega_i = P_{u,Rd,i}/N_{Ed,i}$ over all the connections of the diagonals of the braced frame system; where $P_{u,Rd,i}$ is the ultimate strength of the pin INERD connection.

## 2.5. Practical design procedure and design example

For practical applications, the following design steps are recommended:

1. Selection of the pin dimensions, according to the following requirements:

$$a. \delta_{lim} = 0,8 a \geq \frac{D \cdot H \cdot \cos \varphi}{2} \quad [2.1]$$

$$b. P_{y,Rd} = \frac{P_{y,Rk}}{\gamma_{Mser}} \geq N_{E,ser} \quad [2.2]$$

$$c. P_{u,Rd} = \frac{P_{u,Rk}}{\gamma_{M0}} \geq N_{Ed} \quad [2.3]$$

where:

$\delta_{lim}$  = deformation capacity of the pin connection (see Table 2.2.)

$a$  = clear distance between internal and external eye-bars

$D$  = lateral drift ratio

$H$  = storey height

$\varphi$  = angle of inclination of the diagonal

$P_{y,Rk}$ ,  $P_{u,Rk}$  yield and ultimate strength of the connection according to Table 2.2.

$\gamma_{M0}$  partial safety factor of resistance (=1,0)

$\gamma_{Mser}$  partial safety factor of resistance (=1,0)

$N_{Ed}$  design force of the diagonal

$N_{E,ser} = \frac{N_{Ed}}{\nu}$  design force of the diagonal at the damage limitation state

$\nu$  reduction factor which takes into account the lower return period of the seismic action associated with the damage limitation requirement.

2. Verification of the brace dimensions

$$P_{u,Rk} \leq N_{b,Rd} \quad [2.4]$$

where:

$N_{b,Rd}$  buckling resistance of the diagonal

3. Dimensioning of eye-bars, welds etc

All connection elements (eye-bars, bolts, welds etc.) shall be verified for the capacity design force, equal to:

$$P_{Ed} = 1,3 P_{u,Rk} \quad [2.5]$$

The thicknesses of the eye bars shall additionally verify the following requirements:

$$t_{ext} \geq 0,75 h \quad [2.6]$$

$$t_{int} \geq 0,5 t_{ext} \quad [2.7]$$

$$a \geq h$$

[2.8]

With  $h$  = pin height,  
 $t_{\text{ext}}$  = thickness of external eye bars,  
 $t_{\text{int}}$  = thickness of internal eye bars  
 $a$  = clear distance between external and internal eye-bars

Steel quality of the eye-bars has to be equal to or higher than that of the pin.

## 2.6. Design example

The lateral stability of a three storey steel building is provided by X-braces (Figure 2.3). For the first storey, the columns sections are HEB 320, S 355 and the brace sections HEB 180, S 355. The pin INERD connections between braces and columns for the first storey shall be designed. The analysis design force for the seismic combination is equal to  $N_{\text{Ed}} = 850$  kN.

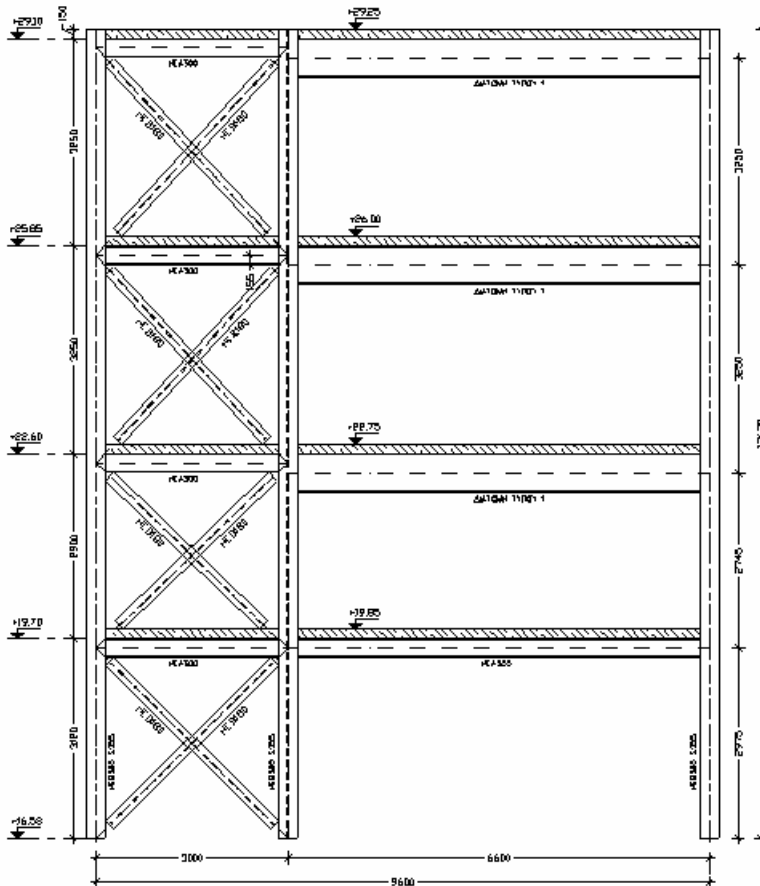


Figure 2.3 : Design example

### Step 1. Verification of the pin

The pin dimensions are 65 x 75 mm, S 235. The clear distance between external and internal eye-bars is equal to  $a = 87$  mm.

The value of the reduction factor is  $v = 2,5$ . Accordingly it is:

$$N_{E,ser} = \frac{870}{2,5} = 348 \text{ kN}$$

From Table 2.2, it is:

$$W_{pl} = \frac{7,5 \cdot 6,5^2}{4} = 79,2 \text{ cm}^3$$

$$M_p = 79,2 \cdot 23,5 = 1861 \text{ kNcm}$$

$$\rightarrow P_{y,Rk} = \frac{2 \cdot 1861}{(8,7/1,1)} = 470 \text{ kN}$$

$$\rightarrow P_{u,Rk} = \frac{4 \cdot 1861}{(8,7/1,1)} = 941 \text{ kN}$$

$$\text{eq. [2.2]: } P_{y,Rd} = \frac{470}{1,0} = 470 \text{ kN} > N_{E,ser} = 348 \text{ kN}$$

$$\text{eq. [2.3]: } P_{u,Rd} = \frac{941}{1,0} = 941 \text{ kN} > N_{Ed} = 850 \text{ kN}$$

### Step 2. Verification of the brace dimensions

For the brace, it is  $N_{b,Rd} = \chi_z \cdot A \cdot f_y / \gamma_{M1} = 0,43 \cdot 65,3 \cdot 35,5 / 1,1 = 997 \text{ kN}$

$$N_{t,Rd} = A \cdot f_y / \gamma_{M1} = 65,3 \cdot 35,5 / 1,1 = 2.107 \text{ kN}$$

$$\text{eq. [2.4] } P_{u,Rd} = 941 \text{ kN} < N_{b,Rd} = 997 \text{ kN}$$

### Step 3. Dimensioning of eye-bars, welds etc

All connection elements (eye-bars, bolts, welds etc.) shall be verified for the capacity design force:

$$\text{eq. [2.5] } P_{Ed} = 1,3 \cdot 941 = 1223 \text{ kN}$$

The design criteria for eye-bars are as following:

- Net section failure  $P_{Ed} \leq N_{t,net,Rd}$
- Gross section yielding  $P_{Ed} \leq N_{t,,Rd}$
- Bearing failure  $P_{Ed} \leq F_{b,Rd}$

The design criteria for bolts (connection of eye-bars to column flanges) are as following:

- Bearing failure  $P_{Ed} \leq F_{b,Rd}$
- Shear failure  $P_{Ed} \leq F_{v,Rd}$

The design criteria for welds (connection of eye-bars to braces) are as following:

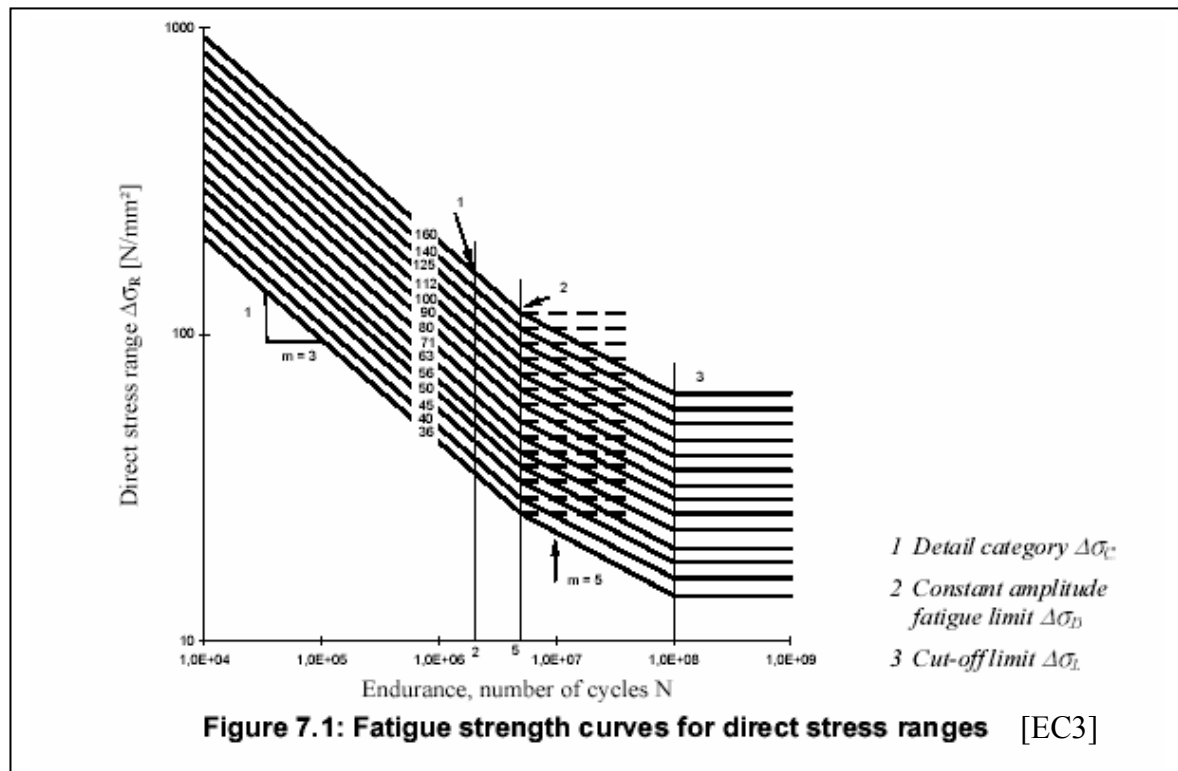
- Shear failure



## 2.7. Design proposal for fatigue.

These design suggestions are based on the experimental tests performed in two types of dissipative devices at Instituto Superior Técnico.

In order to allow the development of possible code provisions these designers guide are made in terms of fatigue curves like the ones shown in EC3.



### Fatigue Pin Comparisons

Fatigue behaviour of circular Pin is better than rectangular Pin independently of distance of plates.  
 Fatigue behaviour of circular Pin increases with decreasing of distance of plates.

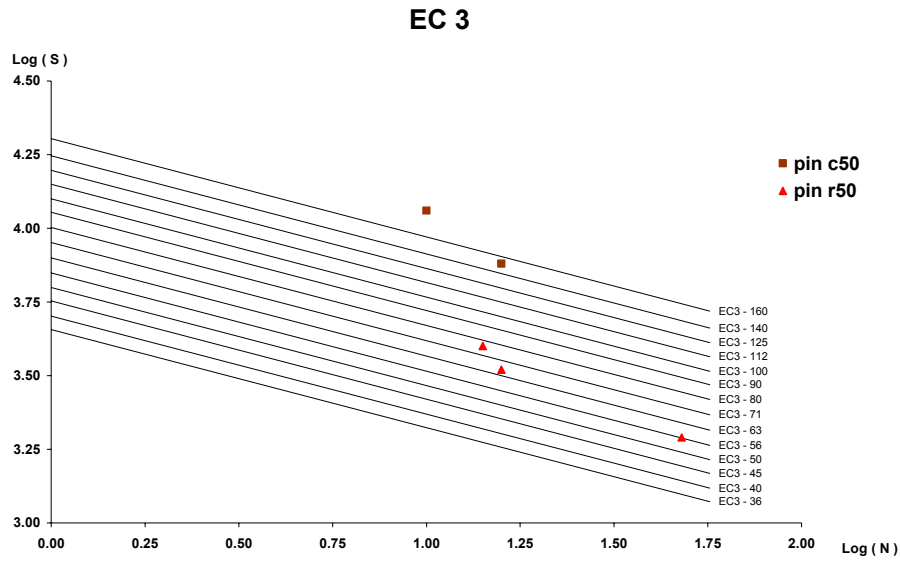


Figure 2.4 . Fatigue behaviour of Pin c50 (circular pin whit distance of plates of 50mm) and Pin r50 (rectangular pin whit distance of plates of 50mm)

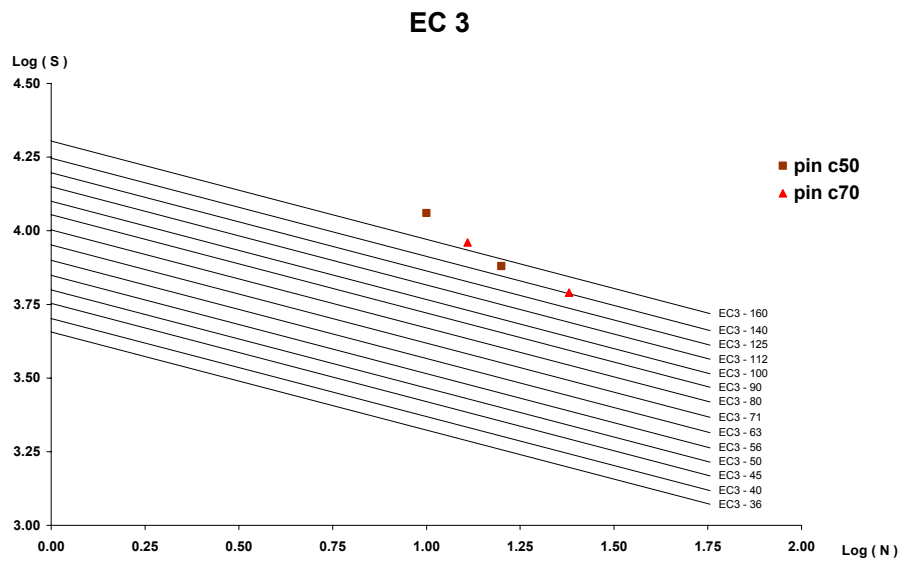


Figure 2.5. Fatigue behaviour of Pin c50 (circular pin with distance of plates of 50mm) and Pin c70 (circular pin with distance of plates of 70mm)

## Fatigue U-Devices Comparisons

Fatigue behaviour of U-Devices loaded parallel (mola8) is better when compared with those loaded perpendicular (mola 10).

Relative to U-Devices loaded parallel:

1. Fatigue behaviour of U-Devices is better when the angle ( $\alpha$ ) is different of  $45^\circ$
2. Fatigue behaviour of U-Devices increases partially with decreasing of thickness(e)
3. Fatigue behaviour of U-Devices increases partially with increasing of radius (R)

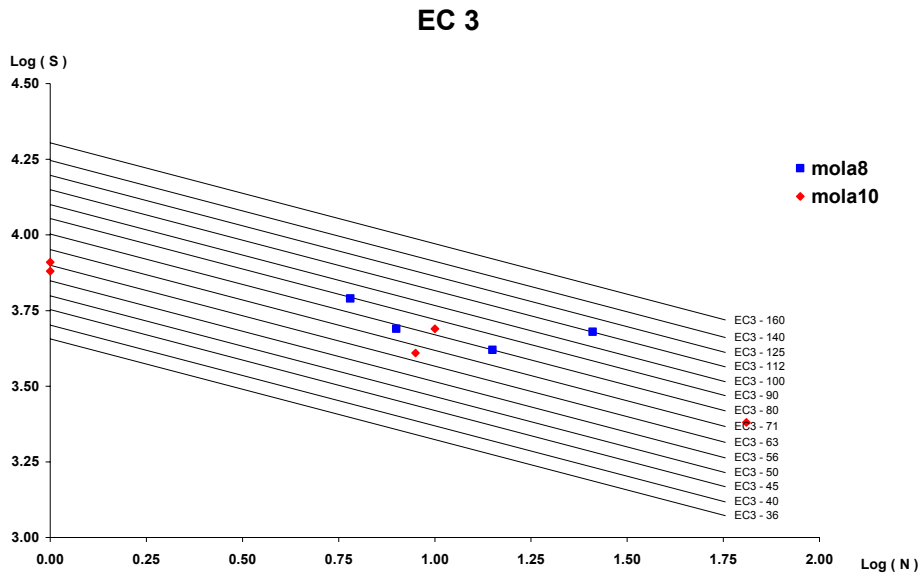


Figure 2.6. Fatigue behaviour of U-Devices loaded parallel (mola8) and perpendicular (mola 10).

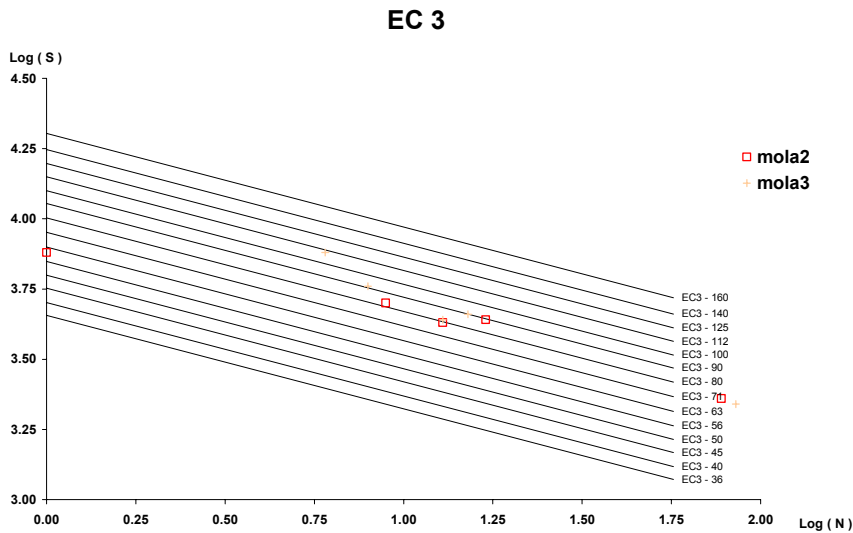


Figure 2.7. Fatigue behaviour of U-Devices mola2 ( $\alpha=45^\circ$ ) and mola3 ( $\alpha=50^\circ$ )

### EC 3

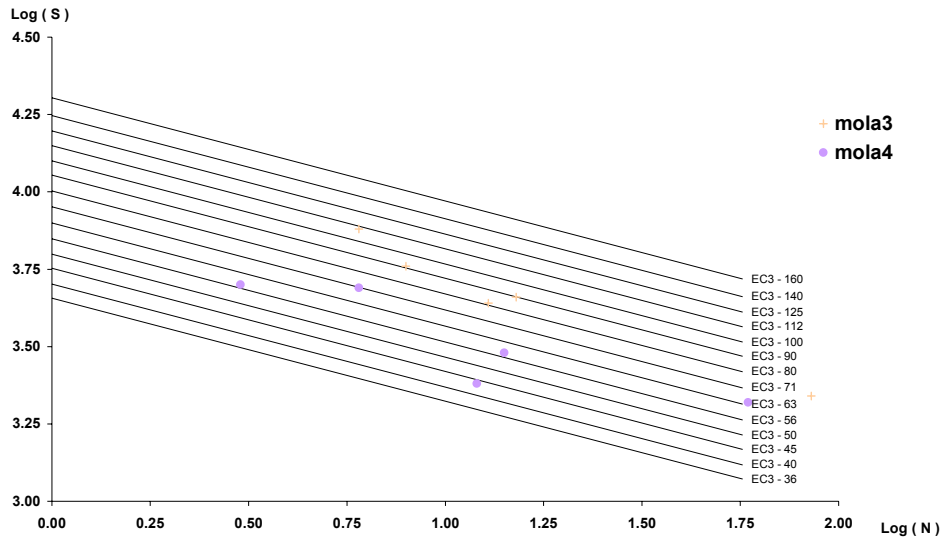


Figure 2.8 . Fatigue behaviour of U-Devices mola3 ( thickness e=25mm) and mola4 (e=30mm)

### EC 3

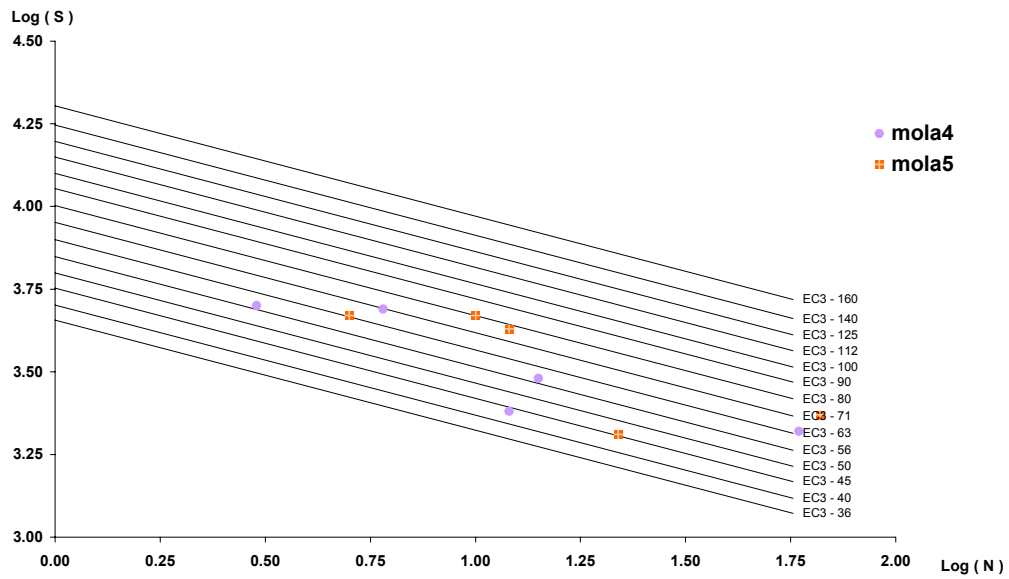


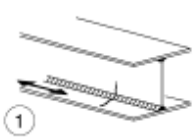
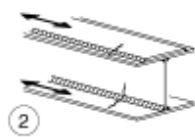
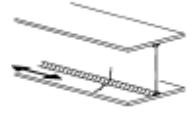

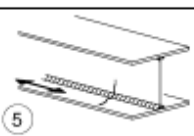
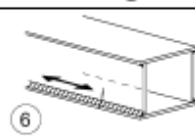
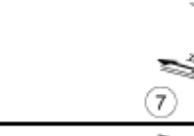



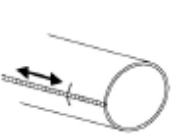
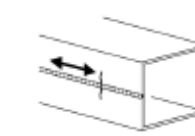
Figure 2.9. Fatigue behaviour of U-Devices mola4 (Radius R=100mm) and mola5 (R=125mm)

Description of EC3

Plain members and mechanically fastened joint

Detail category	Constructional detail	Description	Requirements
160	<p>NOTE: The fatigue strength curve associated with category 160 is the highest. No detail can reach a better fatigue strength at any number of cycles.</p>	<p><u>Rolled and extruded products:</u></p> <p>1) Plates and flats; 2) Rolled sections; 3) Seamless hollow sections, either rectangular or circular.</p>	<p><u>Details 1) to 3):</u></p> <p>Sharp edges, surface and rolling flaws to be improved by grinding until removed and smooth transition achieved.</p>
140		<p><u>Sheared or gas cut plates:</u></p> <p>4) Machine gas cut or sheared material with subsequent dressing.</p>	<p>4) All visible signs of edge discontinuities to be removed. The cut areas are to be machined or ground and all burrs to be removed.</p> <p>Any machinery scratches for example from grinding operations, can only be parallel to the stresses.</p>
125		<p>5) Material with machine gas cut edges having shallow and regular drag lines or manual gas cut material, subsequently dressed to remove all edge discontinuities.</p> <p>Machine gas cut with cut quality according to EN 1090.</p>	<p><u>Details 4) and 5):</u></p> <p>- Re-entrant corners to be improved by grinding (slope <math>\leq \frac{1}{4}</math>) or evaluated using the appropriate stress concentration factors.</p> <p>- No repair by weld refill.</p>
100 m = 5		<p>6) and 7) Rolled and extruded products as in details 1), 2), 3)</p>	<p><u>Details 6) and 7):</u></p> <p><math>\Delta\sigma</math> calculated from: <math>\tau = \frac{V S(t)}{I t}</math></p>
For detail – 5 made of weathering steel use the next lower category.			
112		<p>8) Double covered symmetrical joint with preloaded high strength bolts.</p>	<p>8) <math>\Delta\sigma</math> to be calculated on the gross cross-section.</p>
		<p>8) Double covered symmetrical joint with preloaded injection bolts.</p>	<p>8) ... gross cross-section.</p>
		<p>9) Double covered joint with fitted bolts.</p>	<p>9) ... net cross-section.</p>
		<p>9) Double covered joint with non preloaded injection bolts.</p>	<p>9) ... net cross-section.</p>
90		<p>10) One sided connection with preloaded high strength bolts.</p>	<p>10) ... gross cross-section.</p>
		<p>10) One sided connection with preloaded injection bolts.</p>	<p>10) ... gross cross-section.</p>
		<p>11) Structural element with holes subject to bending and axial forces</p>	<p>11) ... net cross-section.</p>
80		<p>12) One sided connection with fitted bolts.</p>	<p>12) ... net cross-section.</p>
		<p>12) One sided connection with non-preloaded injection bolts.</p>	<p>12) ... net cross-section.</p>
50		<p>13) One sided or double covered symmetrical connection with non-preloaded bolts in normal clearance holes.</p> <p>No load reversals.</p>	<p>13) ... net cross-section.</p>
50	<p>size effect for <math>d &gt; 30\text{mm}</math>: <math>k_s = (30/d)^{0.25}</math></p>	<p>14) Bolts and rods with rolled or cut threads in tension.</p> <p>For large diameters (anchor bolts) the size effect has to be taken into account with <math>k_s</math>.</p>	<p>14) <math>\Delta\sigma</math> to be calculated using the tensile stress area of the bolt. Bending and tension resulting from prying effects and bending stresses from other sources must be taken into account.</p> <p>For preloaded bolts, the reduction of the stress range may be taken into account.</p>

## Welded built-up sections

Detail category	Constructional detail	Description	Requirements
125	 	<u>Continuous longitudinal welds:</u> 1) Automatic butt welds carried out from both sides. 2) Automatic fillet welds. Cover plate ends to be checked using detail 6) or 7) in Table 8.5.	<u>Details 1 and 2:</u> No stop/start position is permitted except when the repair is performed by a specialist and inspection is carried out to verify the proper execution of the repair.
112	 	3) Automatic fillet or butt weld carried out from both sides but containing stop/start positions. 4) Automatic butt welds made from one side only, with a continuous backing bar, but without stop/start positions.	4) When this detail contains stop/start positions category 100 to be used.
100	 	5) Manual fillet or butt weld. 6) Manual or automatic butt welds carried out from one side only, particularly for box girders	5), 6) A very good fit between the flange and web plates is essential. The web edge to be prepared such that the root face is adequate for the achievement of regular root penetration without break-out.
100		7) Repaired automatic or manual fillet or butt welds for categories 1) to 6).	7) Improvement by grinding performed by specialist to remove all visible signs and adequate verification can restore the original category.
80		8) Intermittent longitudinal fillet welds.	8) <del>As based on direct stress in flange.</del>
71		9) Longitudinal butt weld, fillet weld or intermittent weld with a cope hole height not greater than 60 mm. For cope holes with a height > 60 mm see detail 1) in Table 8.4	9) <del>As based on direct stress in flange.</del>
125		10) Longitudinal butt weld, both sides ground flush parallel to load direction, 100% NDT	
112		10) No grinding and no start/stop	
90		10) with start/stop positions	
140	 	11) Automatic longitudinal seam weld without stop/start positions in hollow sections	11) Free from defects outside the tolerances of EN 1090. Wall thickness $t \leq 12,5$ mm.
125		11) Automatic longitudinal seam weld without stop/start positions in hollow sections	11) Wall thickness $t > 12,5$ mm.
90		11) with stop/start positions	

For details 1 to 11 made with fully mechanized welding the categories for automatic welding apply.

### **3. RESEARCH REPORT ON DISSIPATIVE COMPOSITE COLUMNS FOR MITIGATION OF SOFT STOREY FAILURES IN REINFORCED CONCRETE COLUMNS.**

#### **3.1 Definition of the problem and proposal for a solution.**

The most frequent failure mode of reinforced concrete (R.C.) buildings is the so called “soft storey” mechanism. It consists in a localisation of buildings’ seismic deformations and rupture in the bottom storey of the building (see Fig.3-1).

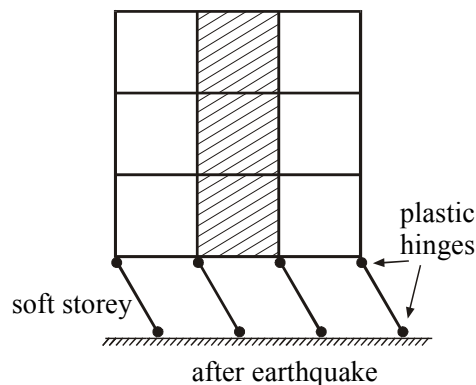


Figure 3-1: The soft storey mechanism for which composite columns would be of interest.

This phenomenon is basically caused by the fact that the overall shear force applied to the building by an earthquake is higher at the base and by the following factors:

- geometric irregularities and discontinuities in plan and section;
- wide openings in lower storeys which are not present at upper levels and weaken the structure - ground level is often used for offices, shops, lobby in hotels, etc;
- slender columns at ground level – so called “pilotis” type buildings;
- if the lower storey is not originally weakened, it is however there that infills are the most stressed, so that they fail first and create then the openings at ground level;
- the sequence of concreting generally results in an interface between two different concrete in the top section of the column, which is then a section weaker than computed;

The “soft storey” mechanism induces very localised deformations to which correspond local brittle mechanisms: bending combined with compression resulting in the crushing of concrete, or shear due to alternate inclined cracks resulting in the decohesion of the section.

The proposed innovation for the problem of soft storey consists in encasing steel profiles (HE or UC) in the lowest levels of reinforced concrete (R.C.) columns in order to provide them a basic reliable shear and compression resistance. The idea is to use encased steel section as a ductile fuse able to dissipate cyclically the energy of the earthquake in the columns of the lower storey of the buildings which otherwise remain reinforced concrete buildings. The objective is to ensure a minimum structural reliability especially in the possible tricky circumstances of either a bad concrete mix utilisation or an awkward concrete hardening process.

Because the position of the infills in a real structure is not always well known or the infills are not always as effective as it is assumed in the design, the study bear on

- composite column in a configuration with infills, which is studied in the University of Liege

- composite column in a configuration without infills in which the sheared panel of the composite column is a crucial weak point, which is studied in the University of Trento.

### **3.2. Research approach. Design requirements for the encased steel profile.**

The R.C. reference building chosen in order to study the problem corresponds to a 6 storeys office building resisting as a pure moment frame, without concrete core. The soft storey situation comes, like in real life situation, from the fact that infills placed in the structure from 1<sup>st</sup> storey to top prevent the effective work as moment resisting frame, so that all deformations are concentrated in columns at ground level (see Fig. 3-1).

The design was made according to Eurocode 2 (EC2) [prEN1992], Eurocode 4 (EC4) [prEN1994] and Eurocode 8 (EC8) [prEN1998-1 (2001)] and sections of concrete and steel reinforcements were established corresponding to 3 reference design situations of the R.C. sections:

- Static design: EC2 (gravity loading only), earthquake not considered;
- Low ductility design (“DCL”): EC2 + EC8 considering earthquake with PGA 0,2g (low seismicity), low ductility class building (q=1,5);
- Medium ductility design (“DCM”): EC2 + EC8 considering earthquake with PGA 0,2g (low seismicity), medium ductility class building (q=3,9);

In the concept of the proposal, the steel profiles are "safety belts": if circumstances are such that a soft storey mechanism would form under earthquake action, the plastic hinges in the R.C. column at ground level would not provide much ductility; then the steel profile would come into action.

To achieve this goal, it is necessary to satisfy some simple criteria to design the steel profiles:

- to determine a steel cross section with a low  $A_{steel}/A_{total}$  ratio: the steel profiles are inserted in some critical and limited regions, e.g. the joint regions with a quite high quantity of horizontal, vertical and transversal reinforcing bars. That is, the impact of the steel profile cross sectional area on the overall transverse section has to be minimised.
- to maintain axial strength, (plastic) moment resistance, and stiffness similar to those of the RC column at the ultimate stage when concrete is locally crushed.
- to provide ductility.

Hence, more detailed design criteria have been defined allowing the achievement of the mentioned requirements:

- V. The steel section alone should at least be able to take the design axial force of the seismic loading case:

$$N_{Rd} \geq N_{Sd}(\gamma_g \cdot G + \gamma_q \cdot Q) \quad [3-1]$$

$$\text{whit } \gamma_g = 1 \text{ and } \gamma_q = 0,3$$

Equation 3-1 should entail the erection of composite columns which resist the dead load of the structure under severe seismic load conditions providing enough residual stiffness to minimise the risk of collapse.

- VI. The steel section alone (not acting composedly) should be able to substitute the deficient concrete section due to the bending moment and shear actions at collapse:

$$M_{Rd,steel} > M_{Rd,concrete} \quad [3-2]$$

$$V_{Rd,steel} > V_{Rd,concrete} \quad [3-3]$$

The criteria defined in I and II provide a beneficial residual strength after the concrete crushing with a gain in the ductile behaviour too.



VII. The steel sections should not much modify the local stiffness  $EI$  of the single RC column (maximum modification level in the order of 10%) in order not to change the distribution of stiffness in the entire and original RC structure. In fact, a change in stiffness distribution may also signify a variation of the building periods of vibration closely tied to the inertial forces, e.g. seismic forces.

VIII. The following ratio should be close to unity in order to achieve a suitable performance of the steel profile along major and minor axis bending:

$$\frac{r_{\text{major}}}{r_{\text{minor}}} = \frac{\left( \frac{M_{\text{Rd,comp}}}{M_{\text{Rd,concrete}}} \right)_{\text{major}}}{\left( \frac{M_{\text{Rd,comp}}}{M_{\text{Rd,concrete}}} \right)_{\text{minor}}} \quad [3-4]$$

The computed sections were too large to be tested in laboratory and were scaled down. The test sections are shown on Fig. 3-2.

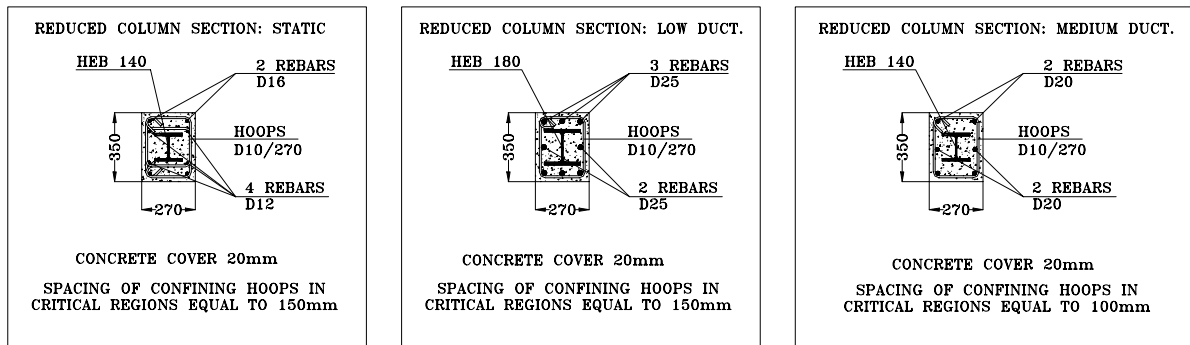


Figure 3-2 : Reduced sections for the composite columns to be tested

The idea developed in the project is to insert steel profiles in columns at ground level. It raises the problem of how to realize the details of the anchorage and how far to extend the anchorage of these steel profiles into the concrete structure of the 1st storey and of the ground level. Basically 3 designs (C1-C2-C3) were considered (see Fig.3-3):

- in Liege,
  - anchorage limited within the depth of the 1<sup>st</sup> storey beams – C2 (400mm).
  - anchorage expanded up to mid height of the 1<sup>st</sup> storey level columns – C1.
- in Trento,
  - typology in which the steel profile extends from the base up to mid height of the 1<sup>st</sup> storey level columns – C1.
  - typology in which a steel stump covers only the critical joint region – C3.

In order to ensure that the axial load transfer between the concrete and the steel is efficient in the critical region of the composite column, an endplate is welded at the end of the steel profile (see Fig. 3-4). No shear connectors were used in the load introduction area and in areas with change of the cross section, both to realize an easier solution and to minimize the cost for the fabrication of the specimens.

Moreover specimens with and without the presence of stiffeners delimiting a clear shear panel zone were tested (see Fig.3-4) to study their influence both on the global behaviour of the joint and on the actions transmitted from the concrete column to the inserted steel profile.

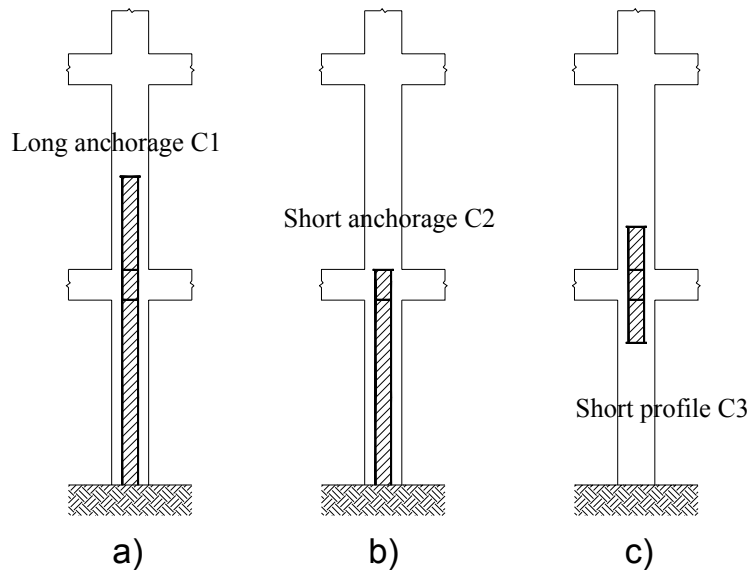


Figure 3-3. : Geometrical characteristics of the anchorage and length of steel profiles in the Liege and Trento tests specimens

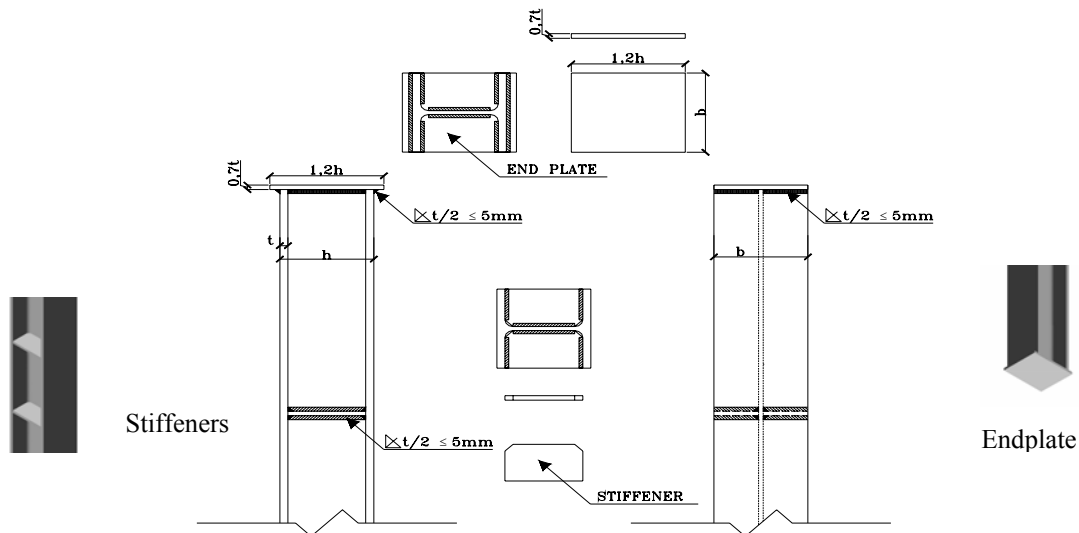


Figure 3-4 : Geometrical characteristics of the end plate and stiffeners

Both situations of weak axis and strong axis of the steel profile are considered

All composite tests can be compared to reference reinforced concrete R.C. situations; practically this means that a total of 10 tests on 38 tests are indeed reference R.C. tests; this is a price to pay to assess properly the positive influence of the composite character of components.

Many other parameters may influence the behaviour of the tested composite columns : beam depth / columns depth ratio, material properties, connection design details, value of axial force  $N_{sd}$  coupled to applied bending moment, etc ...and the original test programme has been modified several times following the progressive developments of analysis.

The final test program may be summarised into 2 tables.

Table 3-1. Characteristics of the specimens of the Liege experimental programme

phase	Design	Strong/weak axis section	R.C.	COMPOSITE			
				long anchorage (C1)		short anchorage (C2)	
				with stiffeners	without stiffeners	with stiffeners	without stiffeners
PHASE 1	Static	strong axis	RCL1	COL1	COL2	COL3	COL4
PHASE 2	DCL*	strong axis	RCL3	COL5	COL6	COL7	COL8
PHASE 3	DCM**	strong axis	RCL5	COL9	COL10	COL11	COL12
PHASE 4	Static	weak axis	RCL2			COL13	
	DCL*	weak axis	RCL4	COL14			

Table 3-2. Characteristics of the specimens of the Trento experimental programme

phase	Design	Strong/weak axis section	R.C.	COMPOSITE			
				long profile (C1)		short profile (C3)	
				with stiffeners	without stiffeners	with stiffeners	without stiffeners
PHASE 1	DCL*	strong axis	RCT3	COT5	COT6	COT7	COT8
PHASE 2	DCM**	strong axis	RCT5	COT9	COT10	COT11	COT12
PHASE 3	Static	strong axis	RCT1	COT1	COT2	COT3	COT4
PHASE 4	Static	weak axis	RCT2	COT13			
	DCL*	weak axis	RCT4	COT14			

\* = Ductility Class LOW

\*\* = Ductility Class MEDIUM

A set of 128 A4 drawings presenting all details of test set up, steel components, reinforced concrete elements, composite steel concrete elements has been produced for the fabrication of the specimens.

### 3.3. Test set up and testing procedure.

Slightly different test set up have been designed for the University of Trento and the University of Liège, due to differences in infrastructures and due to the two different aims of the tests:

-the test set up at Trento is designed to test "strong beams-weak columns" situations in order to provide data necessary for the understanding of the behaviour of the composite "panel zone" (beam-column intersection zone).

-the test set up in Liège aims at reproducing a "weak beam-strong columns" situation, necessary to create more difficult situation of anchorage of the encased steel profile ; the effect of infills is simulated by presence of two stiffened steel plate (in yellow at Figure 3-5).

Both test set up allow the application of a constant axial force in the column up to 1000 kN together with the application of a horizontal variable force up to 1000 kN (positive and negative) with a displacement range up to 2000 mm (+-). Drawings are presented hereafter.

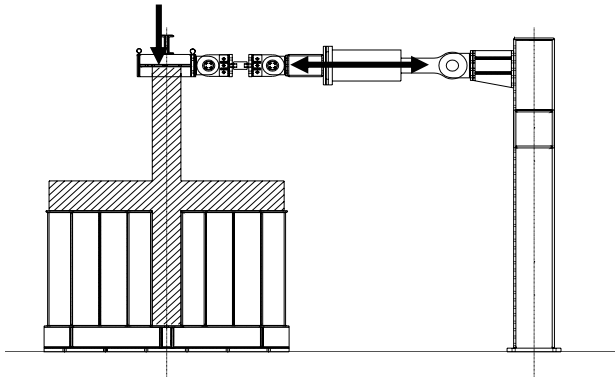


Figure 3-5. Test configuration adopted at the University of Liege (masonry “infills” are in yellow).

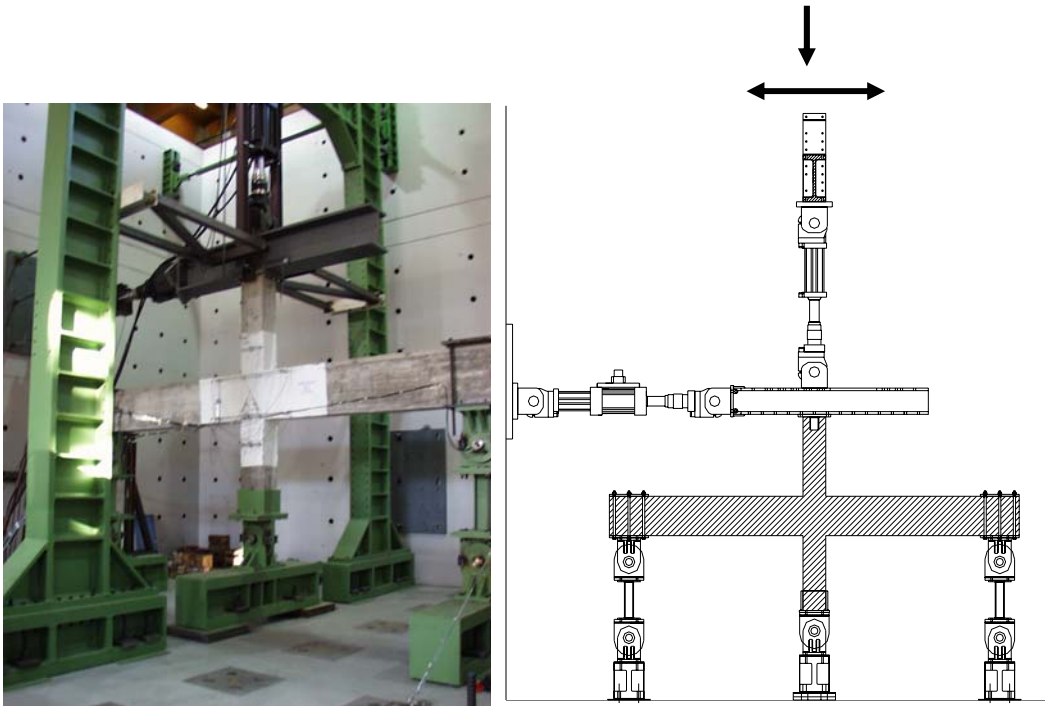


Figure 3-6.: Test configuration adopted at the University of Trento (no masonry infills).

The choice of a testing programme and the associated loading history depends on the purpose of the experiment, type of specimen and expected failure mode. The ECCS Procedure [1986] has been chosen, indeed, to verify the relationship between a pseudo-static horizontal force and a specified ductility factor given by Codes and Recommendations (ECCS Recommendations for Steel Structures in Seismic Areas).

In the present studies, a vertical constant load  $N$  is applied to the column before starting the cyclic application of horizontal loads. A horizontal load is applied to the column at a distance representing the mid height of the storey (1750mm from the beam axis). This load is displacement controlled and applied cyclically in positive and negative value by a 1000 kN actuator. The loading history follows the ECCS Procedure (1986) with a reference "yield displacement"  $\delta_y$  value determined as an absolute value defined a priori and kept for all specimens in order to make a direct comparison possible. For composite

columns, it has been estimated that the interstorey drift angle  $\theta_y$  at yield is  $0,5\% = 5 \text{ mrad}$ . The drift angle in the test set-up is the displacement at the actuator divided by the height of column which is free to deform, so that, in Trento:  $\delta_y = \theta_y \times 3500 = 17,5 \text{ mm}$  and in Liege:  $\delta_y = \theta_y \times 1750 = 8,75 \text{ mm}$  is the yield displacement at the actuator. Then the plastic cycles are applied as defined in the ECCS Procedure - 3 cycles at intervals  $\pm(2+2n) \delta_y$  with  $n=0,1,2,3,\dots$ , etc.

### 3.4. Plastic hinges in columns as dissipative mechanism.

#### 3.4.1. Specific features of the test set up.

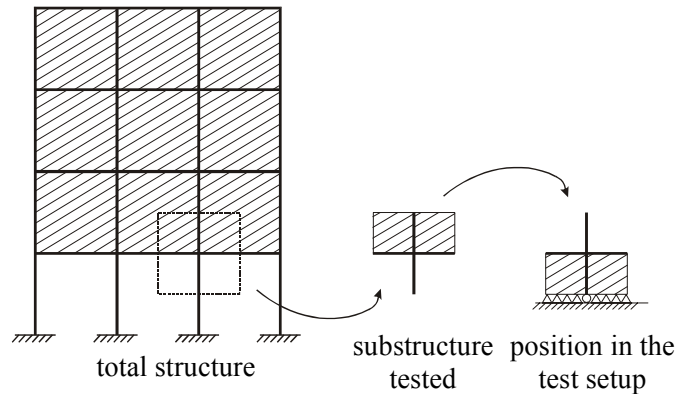


Figure 3-7.: Link between the reference structure and the local substructure to be tested.

The test set-up corresponds to a subassemblage zone of a real structure. The link between the real structure and the test set-up is shown on Fig. 3-7. The infills in the test set-up are represented by rigid steel stiffened plates (see Fig. 3-5 and 3-8).

The applied vertical load  $N$  corresponds to a compression rate of  $0.17 N_{Rd,R.C.}$ ,  $N_{Rd,R.C.}$  being computed referring to the R.C. section alone and the real properties of the materials.

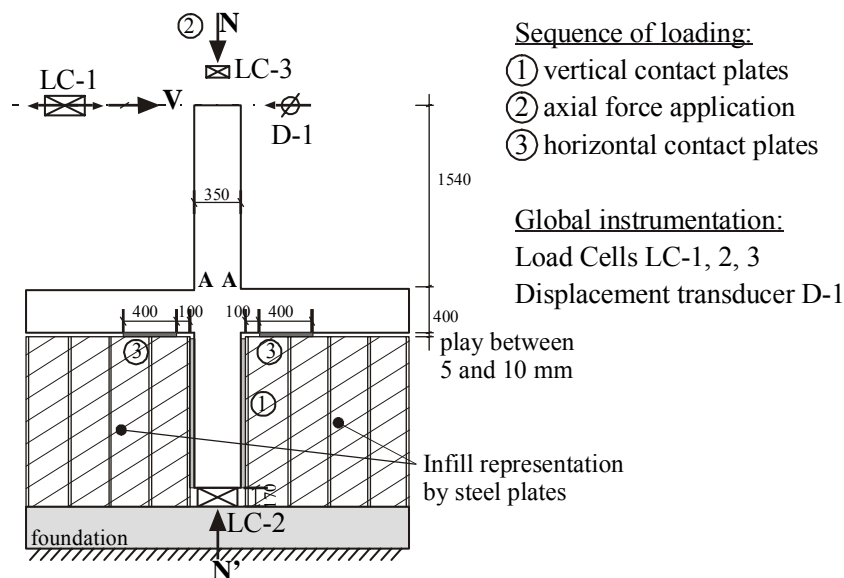


Figure 3- 8 : Addition of plates in the test set-up to ensure the contact and global instrumentation

The chosen test configuration intends to reproduce as accurately as possible the boundary conditions of a column in a soft storey. Nonetheless it has the drawback that the determination of the action effects in the beam and in the portion of the column between the infills cannot be directly deduced from external load. A specific load cell LC-2 is needed to determine the axial load  $N'$  in the column and to deduce the part of the load passing through the infills when the horizontal load is applied (see Fig.3-8). The in fills in the real structure are built after the hardening of the concrete frame. They are not aimed to transmit

vertical forces induced by vertical loads. If they do, it is accidental and due to problems of excessive deformations of the beams. To ensure that the infills do not transmit vertical loads in the test set-up, a “play” ensuring no contact has been provided between beams and infills during vertical loading (see Fig. 3-8). Horizontal contact plates have been placed after the application of the axial load.

### 3.4.2. Global behaviour of the tests specimens.

The failure modes of the composite columns of the strong axis phases are shown in Fig. 3-9.

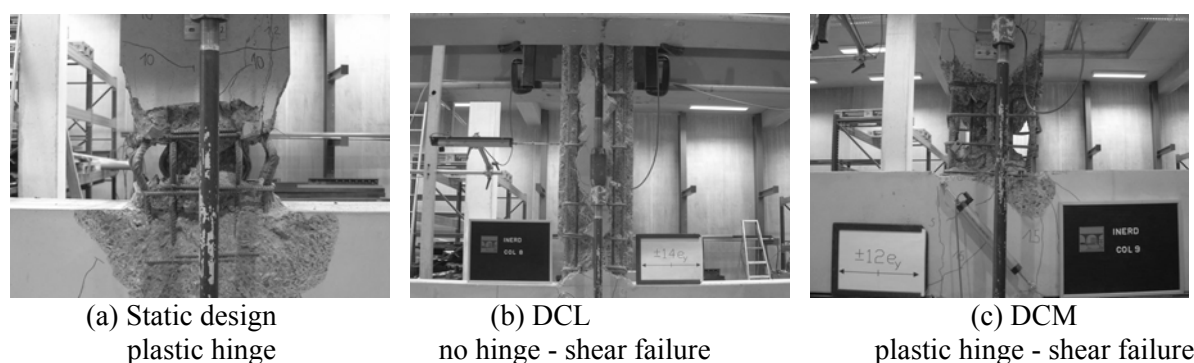


Figure3-9: Failure of the composite columns

All the tests results are not graphically presented here. Only some significant moment-rotation ( $M-\theta$ ) diagrams are given hereafter (see Fig. 3-10 to 3-14). The ( $M-\theta$ ) envelope curves are traced on Fig. 3-15 to 3-19 and allow the direct comparison between specimens.

$M$  and  $\theta$  are defined as follows:

-  $M$  is the bending moment in the section which should yield first – section A-A on Fig.8.

$$M = V(\text{measured at LC-1}).1,5 \text{ m} \quad [3-5]$$

-  $\theta$  is the global rotation:

$$\theta = D1/1,5 \text{ m} \quad [3-6]$$

The moment should also include a parasitical moment due to the system used to apply the axial force to the column. This additional moment is proportional to the horizontal top displacement. This means that it does not influence very much the maximal moment which corresponds to relatively small top displacement (moment increase of maximum 4 % when  $N$  is equal to 1000 kN). Its influence is greater on the degradation part of the curve. It has not been taken into account in this analysis and does not modify the conclusions.

The moment-rotation curve of the reference R.C. specimen RCL1 of Phase 1 is presented on Fig. 3-10(a). The maximum resistance is obtained for  $\theta_y = 21$  mrad, followed immediately by a sharp resistance decrease. The conventional failure (resistance reduced to 80% of maximum resistance) of the specimen is reached for  $\theta_{80\%} = 40$  mrad. The ductility is  $\theta_{80\%}/\theta_y=1,9$ . It may be estimated that the total loss of resistance corresponds to  $\theta$  around 60 mrad.

The cyclic moment-rotation curve of the composite specimen COL2 is presented on Fig. 3-10(b). The maximum resistance is obtained for  $\theta_y = 25$  mrad, followed by a rather ductile behaviour up to  $\theta_{80\%} = 67$  mrad, which is approximately the rotation corresponding to conventional failure. The ductility  $\theta_{80\%}/\theta_y=2,7$ . The maximum resistance is higher than the one of the reference R.C. specimen by a factor of 1,4 approximately. It may be estimated that the total loss of resistance corresponds to  $\theta$  around 100 mrad. That is 66% more than the reference R.C. specimen.

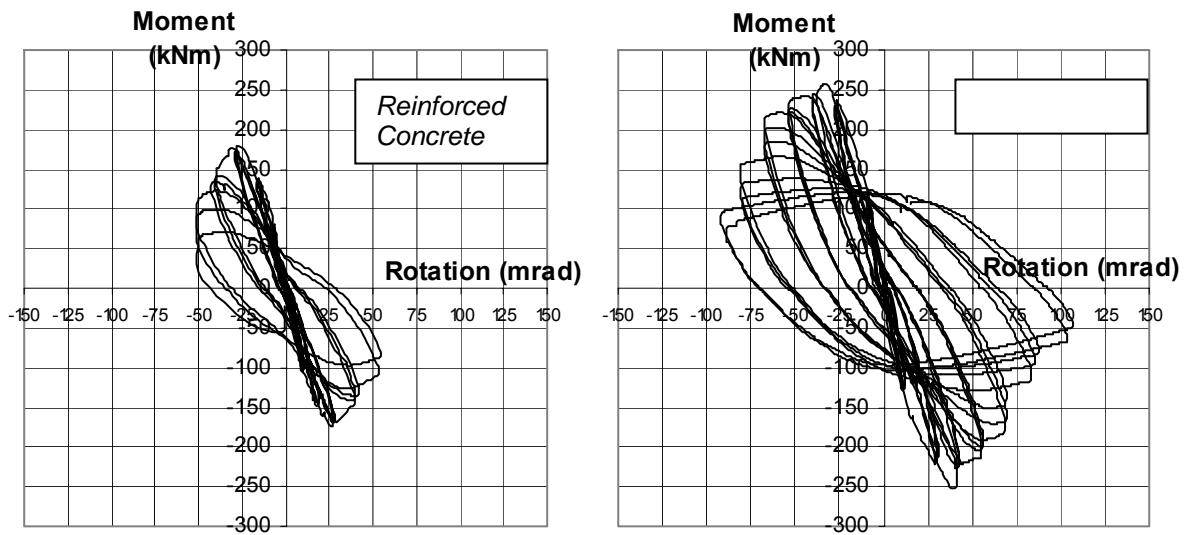


Figure 3-10 : Moment-Rotation curves for specimens RCL1 and COL2 (static design – strong axis)

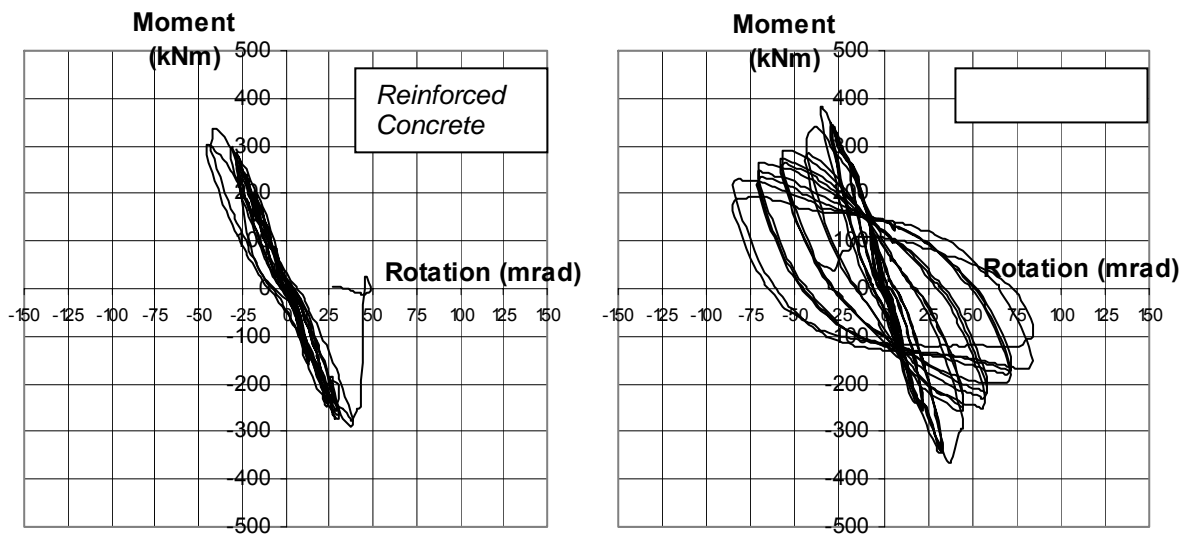


Figure 3-11: Moment-Rotation curves for specimens RCL3 and COL6 (low ductility design)

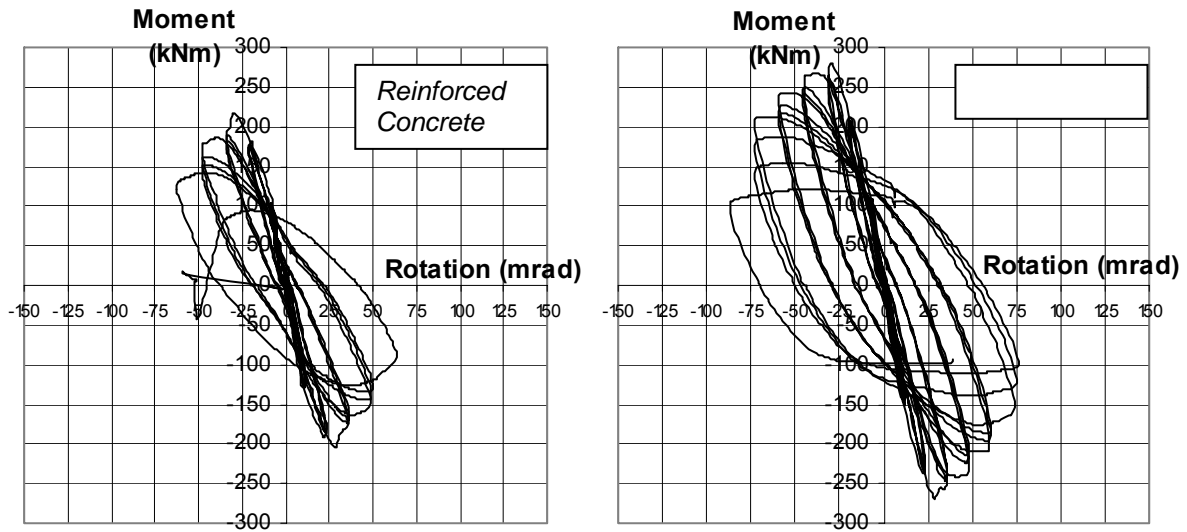


Figure 3-12 : Moment-Rotation curves for specimens RCL5 and COL10 (medium ductility design)

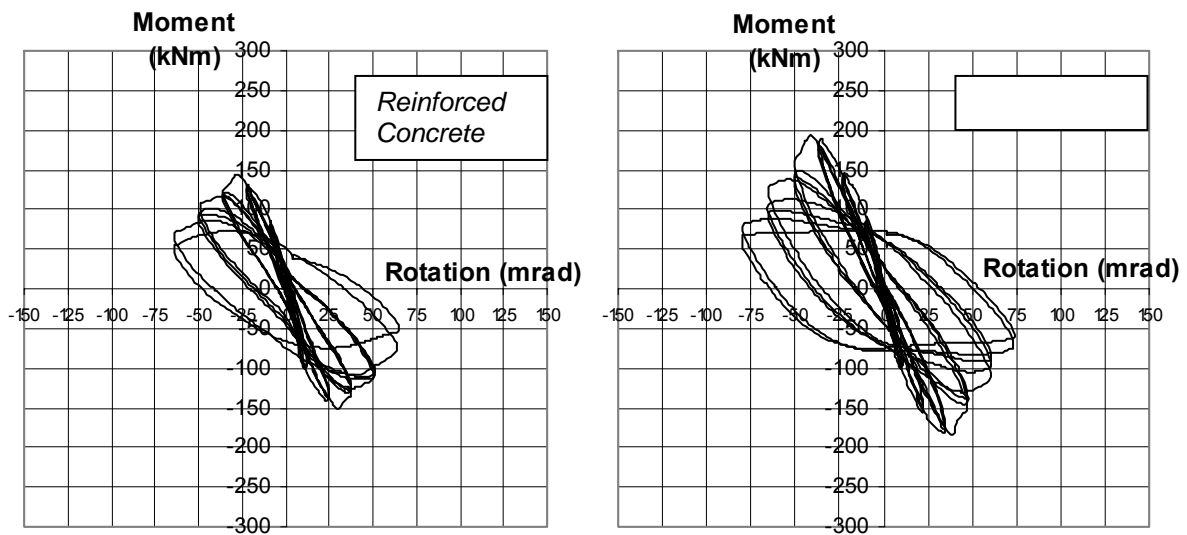


Figure 3-13 : Moment-Rotation curves for specimens RCL2 and COL13 (static design- weak axis)



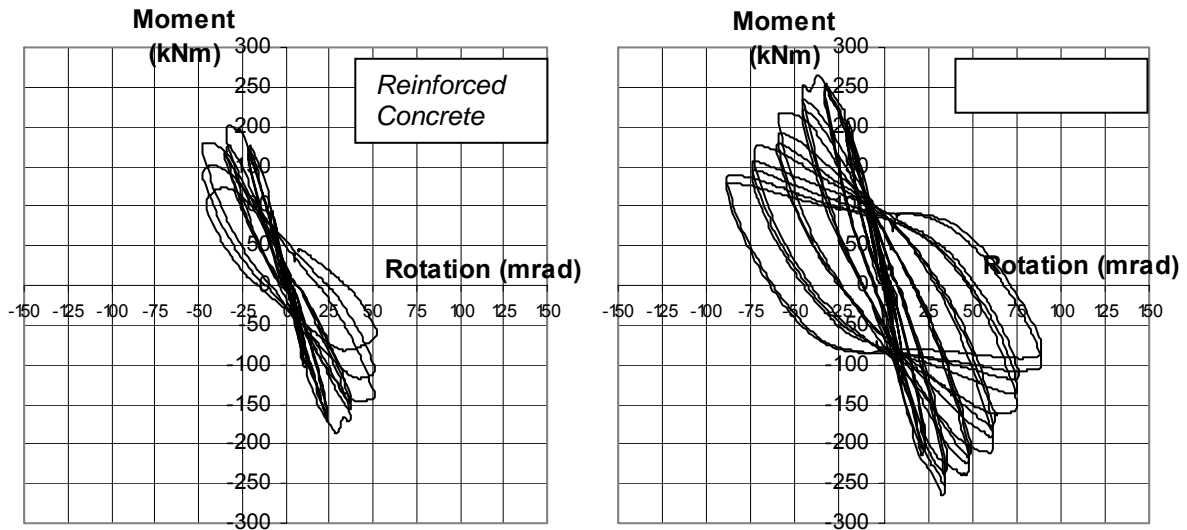


Figure 3-14: Moment-Rotation curves for specimens RCL4 and COL14  
(low ductility design – weak axis)

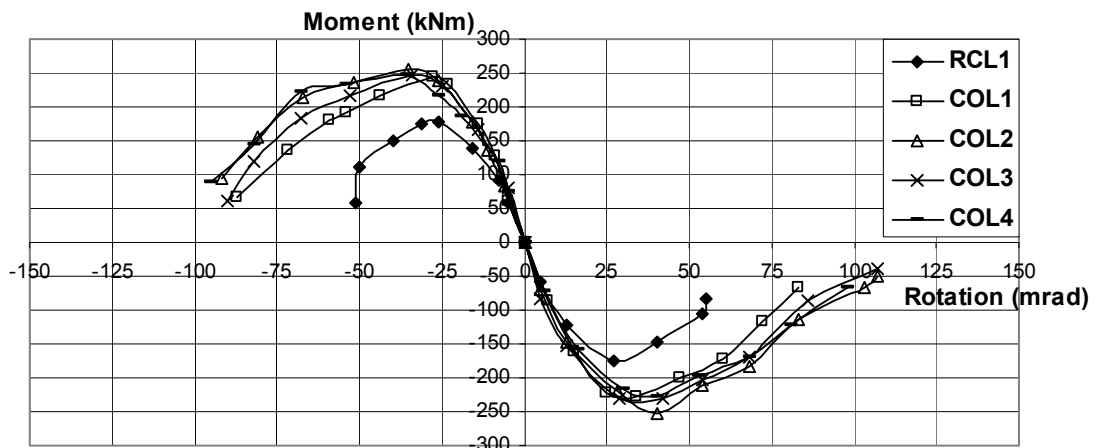


Figure 3-15: Envelope curves for all the specimens of phase 1.

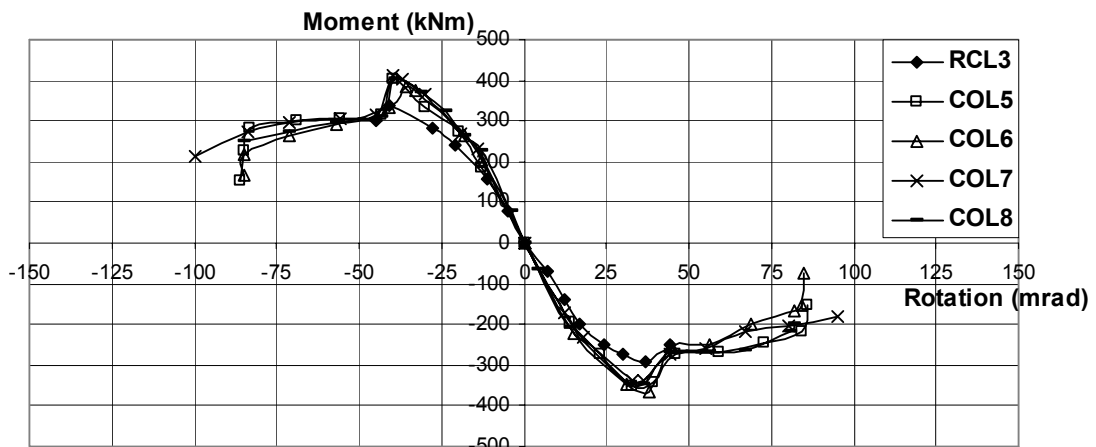


Figure 3-16: Envelope curves for all the specimens of phase 2.

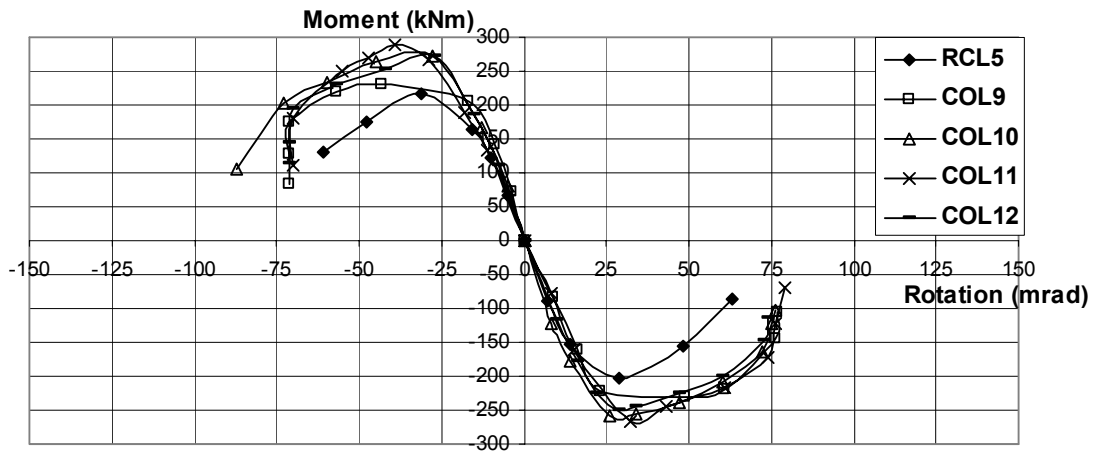


Figure 3-17 : Envelope curves for all the specimens of phase 3.

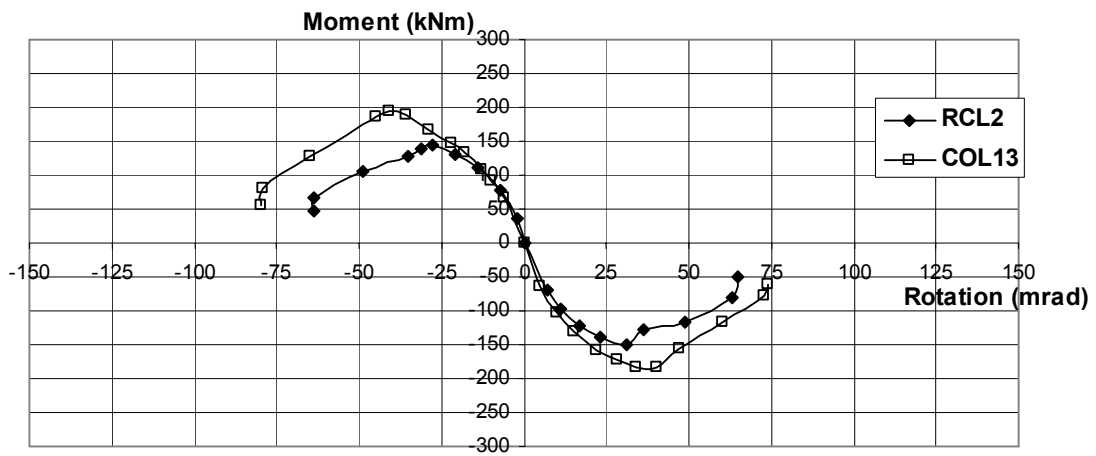


Figure 3-18: Envelope curves for some specimens of phase 4 (static design).

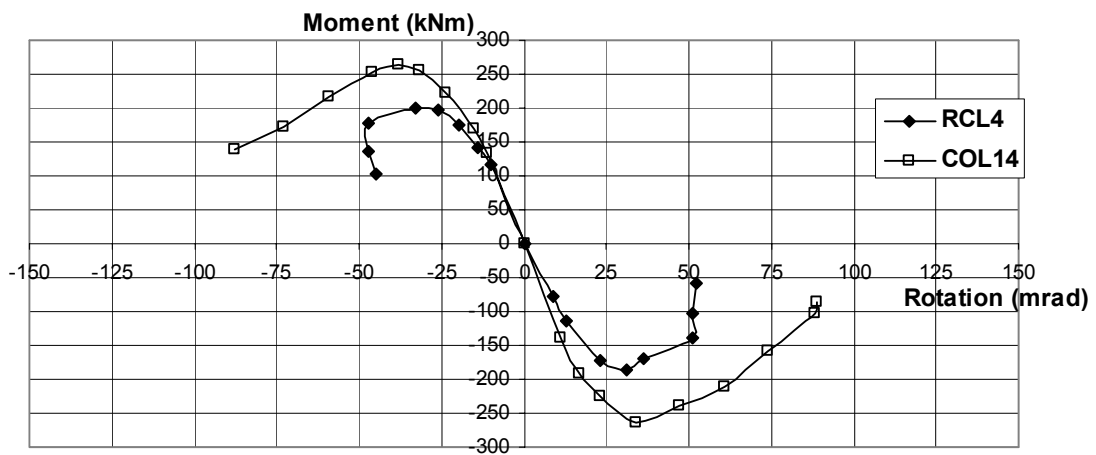


Figure 3-19: Envelope curves for some specimens of phase 4 (low ductility design).

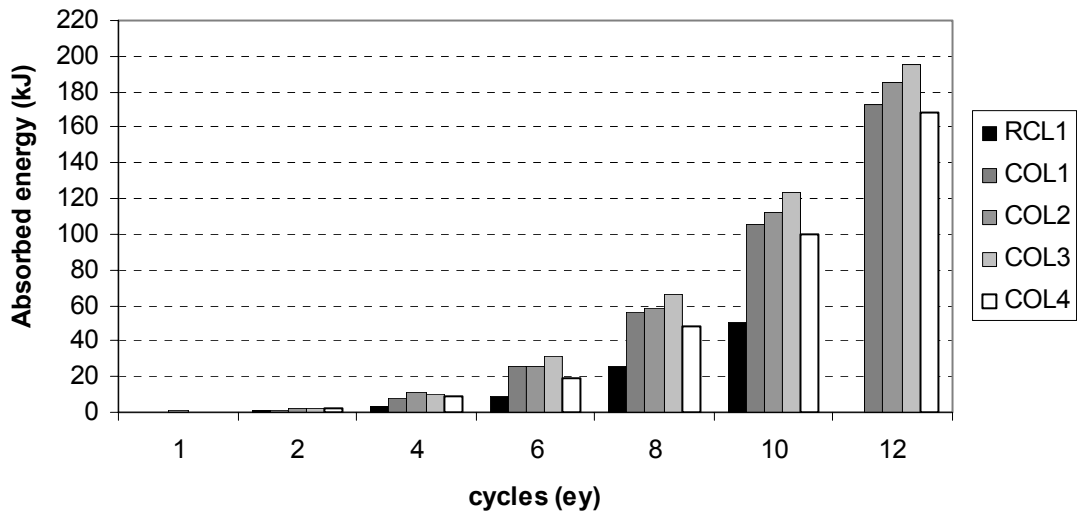


Figure 3-20 : Absorbed energy in function of the cycles for all the specimens of phase 1.

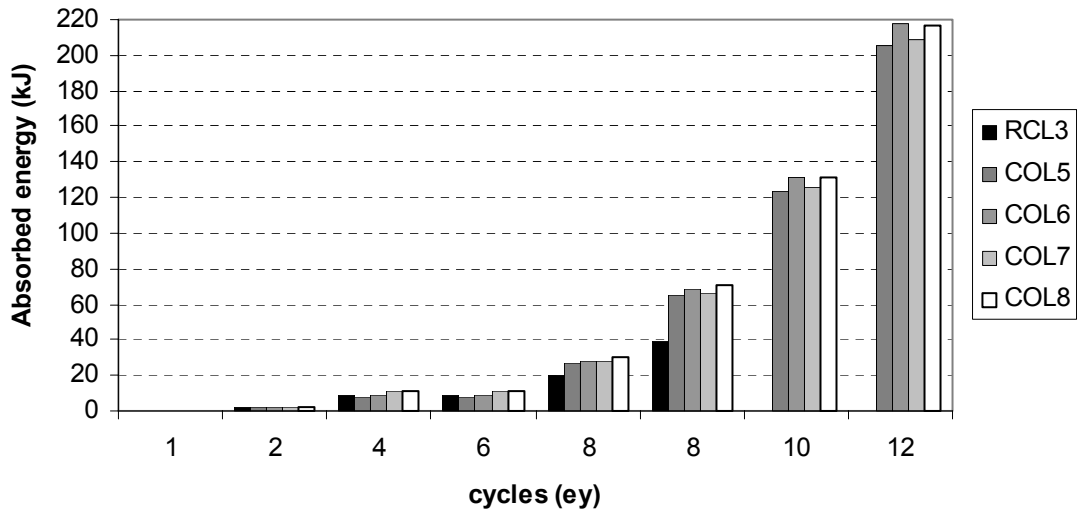


Figure 3-21 : Absorbed energy in function of the cycles for all the specimens of phase 2.

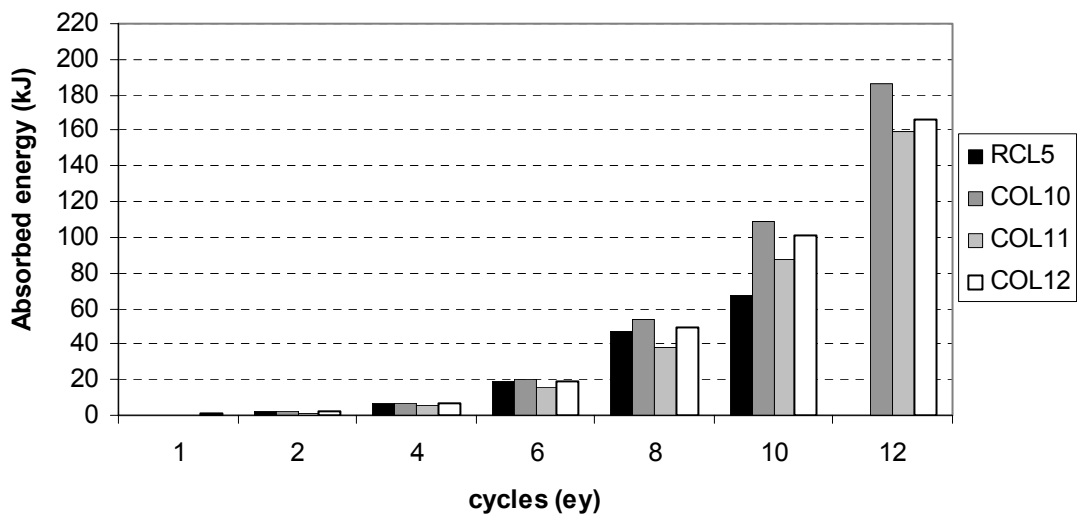


Figure 3-22: Absorbed energy in function of the cycles for all the specimens of phase 3.

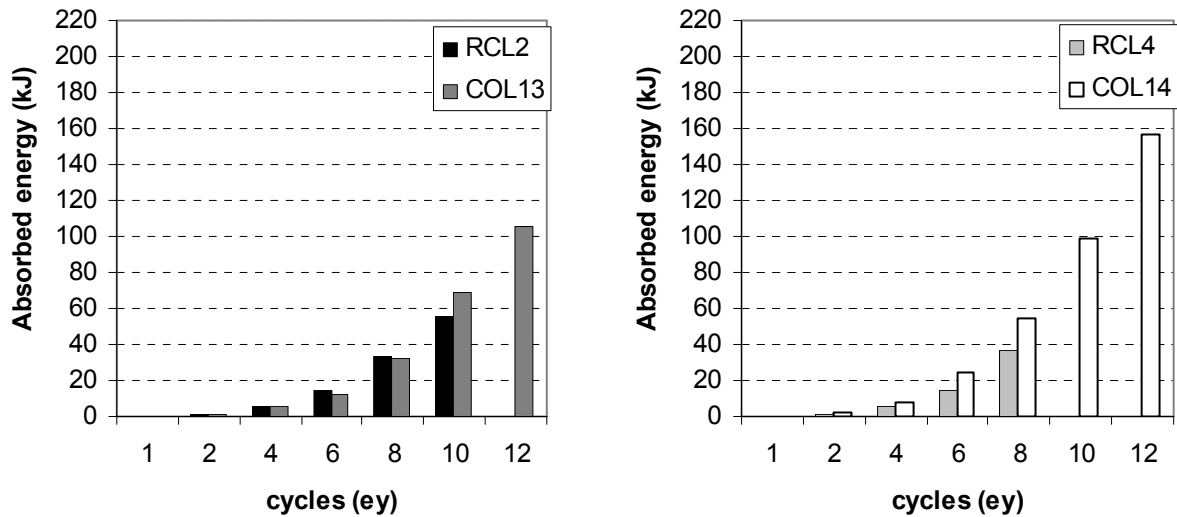


Figure 3-23: Absorbed energy in function of the cycles for all the specimens of phase 4.

Table 3-3 provides comparison data between the test specimens of all the phases. The parameters in the table are defined as follows:

- $\delta_y$  (mm): yield displacement defined as in ATC24 procedure (ATC, 1992). Fig. 3-24 presents the calculation of the yield displacement  $\delta_y$  (mm) in function of the horizontal force applied  $V$  ( $V_{max}$  is the maximum horizontal force reached).

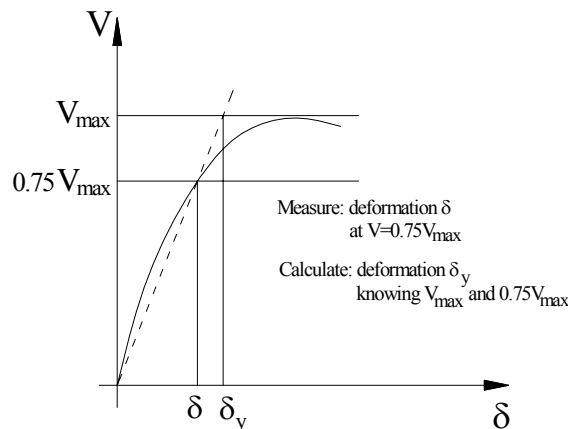


Figure 3-24: Assessment of the experimental yield displacement  $\delta_y$

- $\theta_y$  is the rotation (mrad) at yield obtained by geometrical consideration  
 $\theta_y(\text{mrad}) = \delta_y(\text{mm}) \cdot 1000 / 1500(\text{mm})$
- $\theta_{80\%}$  is the rotation (mrad) at which the specimen has lost 20% of its resistance ;
- $\theta_{50\%}$  is the rotation (mrad) at which the specimen has lost 50% of its resistance ;
- $M_{pl,exp}$  is the plastic moment of the column obtained experimentally ;
- $M_{pl,th}$  is the plastic moment of the column obtained from calculations ;
- $\theta_{comp}$  is the rotation (mrad) of the composite specimen corresponding to the maximum moment reached by the R.C. specimen of the same phase;
- $\theta_{R.C.}$  is the rotation (mrad) of the R.C. specimen corresponding to maximum moment reached by the specimen.  $\theta_{R.C.}$ ;

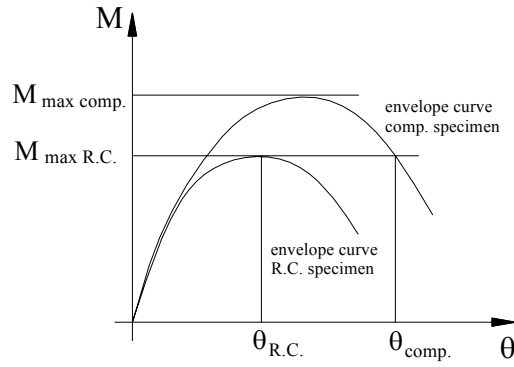


Figure 3-25. Rotation  $\theta_{R.C.}$  and  $\theta_{comp.}$ .

- $E_{total,50\%resist}$  is the energy dissipated until the specimen has lost 50% of its resistance. It is calculated as the hysteretic area of the force (measured at LC-1) - displacement (measured at D-1) diagram.
- $cycles_{50\%resist. n_f}$  is the number of cycles to failure

Table 3-3. Comparison between experimental and computed results.

Specimen	$\theta_y$ (mrad)	$\theta_{80\%}$ (mrad)	$\theta_{50\%}$ (mrad)	$M_{pl,exp.}$ (kNm)	$M_{pl,th.}$ (kNm)	$\theta_{comp.}/\theta_{R.C.}$ (ductility ratio)	$\theta_{80\%}/\theta_y$ (ductility)	$E_{total,50\%resist.}$ (kJ)	$cycles_{50\%resist.}$ ( $n_f$ )
RCL1	21	40	51	180	175	1.0	1.9	40	18
COL1	20	51	70	240	235	2.0	2.6	137	24
COL2	25	67	81	255	245	2.4	2.7	149	24
COL3	23	54	77	249	235	2.4	2.3	-	23
COL4	25	68	83	240	245	2.5	2.7	134	23
RCL5	22	48	61	216	195	1.0	2.2	55	18
COL9	18	68	71	231	250	1.8	3.8	-	21
COL10	26	59	73	276	260	1.9	2.3	174	23
COL11	29	56	70	290	250	1.8	1.9	124	22
COL12	22	58	70	272	260	1.9	2.6	138	22
RCL3	30	technical problem		335	285	1.0	-	38	16
COL5	35	43	85	400	415	1.0	1.2	258	25
COL6	31	43	83	385	415	1.0	1.4	269	24
COL7	31	43	100	411	415	1.0	1.4	298	26
COL8	30	43	84	400	415	1.0	1.4	259	24
RCL2	20	38	63	150	150	1.0	1.9	38	18
COL13	31	51	65	190	190	1.8	1.6	75	21
RCL4	21	47	45	195	230	1.0	2.2	33	16
COL14	26	59	87	265	300	1.8	2.3	168	24

### 3.4.3. Conclusions from the tests.

The following detailed conclusions can be made:

- Additional stiffeners in the steel profile do not significantly influence the resistance of the composite column. It can be concluded that they are not useful.
- There is no significant difference in the resistance of specimens with long and short anchorage length of the steel profile. At this stage it can be concluded that short anchorage is effective.
- For each strong axis specimens phases, the reinforced concrete specimen and the specimens with encased steel profile have almost equal yield rotations.

- For each strong axis specimen's phases, the stiffness of the reinforced concrete specimen and the composite specimens are similar, showing that the steel profile does not affect the stiffness of the R.C. column. This conclusion does not apply to the weak axis specimens showing the difficulty to ensure the neutrality of the encased steel profile for the stiffness simultaneously in both directions.
- The specimens with encased profile allow much greater rotation before they loose 20% resistance (see  $\theta_{80\%}$  in Table 3-3).
- The specimens with an encased steel profile have greater resistance than the reference R.C. specimen by a factor of about 1,20 to 1,37. This is favourable to achieve a weak beam-strong column mechanism. It can be seen from Table 3-3 that the full composite plastic moment is developed, since  $M_{pl,exp} = M_{pl,th}$ .
- The shear resistance of a composite column is the shear resistance of the web of the encased steel profile. In this case theory of composite columns meets quite well with tests.
- The rotation capacity  $\theta_{comp}$  of the composite specimen corresponding to the maximum resistance of the R.C. specimen is on the average 2 times greater than the deformation  $\theta_{R.C.}$  of the reinforced concrete specimen.
- The specimens with an encased steel profile can resist many more cycles till the end of the test (50% drop in resistance) – on the average 1,5 times more.
- The specimens with an encased profile have much greater capacity to dissipate energy before the end of the test. Composite specimens dissipate on the average 3 times more energy than the corresponding R.C. specimen. This is very favourable for earthquake resistance in high seismicity zones where the earthquake duration involves that structural components may undergo many plastic cycles.

#### **3.4.4. Effect of discrepancies between the concrete design resistance and actual resistance.**

In the test program, there is a big difference between the real concrete resistance and its design resistance. This influences the conclusions.

For a C25/30 concrete, a resistance of 14,17 N/mm<sup>2</sup> ( $\alpha f_{ck}/\gamma_c = 0,85f_{ck}/1,5$ ) was considered in the calculations. Finally, the concrete resistance was between 45 and 55 N/mm<sup>2</sup>. This means that the axial resistance and the bending resistance of the RC section were finally far higher than expected. This means that the design formulas used to determine the sections of the additional steel profile are not respected anymore. This means also that the improvement of the RC section characteristics by the steel profile are not as spectacular as expected.

In Table 3-26 and 3-27, the resistance of the steel profile and the reinforced concrete section are calculated with the design resistance and with the real properties of the materials for the specimens of phase 3. The cases with and without axial force are considered. Without axial force, the influence of a better concrete than expected is not too bad. The steel section is not sufficient to come in replacement of the concrete section, but the ratio is still ok ( $M_{Rd,conc} / M_{Rd,steel} = 1,31$ ). However with the axial force, the influence of the compression on the sections resistances is very different in the steel and in the reinforced concrete. If at the design stage,  $M_{Rd,conc} / M_{Rd,steel}$  is equal to 2, with the real material properties, the compression rate of the reinforced concrete section decreases to 15 %, the resisting bending moment of the R.C. section doubles and  $M_{Rd,conc} / M_{Rd,steel}$  becomes 4,63!! With such a strong R.C. section, the improvement of the behaviour by the composite section is clearly not as high as expected.

Figure 3-26. Assessment of the steel and R.C column resistance of phase 3 specimens with no axial load ( $N_{Sd} = 0$ )

	$f_y$ [N/mm <sup>2</sup> ]	$\alpha f_c$ [N/mm <sup>2</sup> ]	$f_s$ [N/mm <sup>2</sup> ]	$M_{Rd,steel}$ [kNm]	$M_{Rd,conc}$ [kNm]	$M_{Rd,conc} / M_{Rd,steel}$	$N_{Rd,steel}$ [kN]	$N_{Rd,conc}$ [kN]	$N_{Rd,conc} / N_{Rd,steel}$
At design stage	323	14,17	435	79	74	0,94	1386	2603	1,88
With the real material properties	310	44,6	560	78	102	1,31	1370	4968	3,63

Figure 3-27. Assessment of the steel and R.C column resistance of phase 3 specimens with experimental axial load ( $N_{Sd} = 750$  kN)

	$f_y$ [N/mm <sup>2</sup> ]	$\alpha f_c$ [N/mm <sup>2</sup> ]	$f_s$ [N/mm <sup>2</sup> ]	$N_{Sd} / N_{Rd,steel}$	$M_{Rd,steel}$ [kNm]	$N_{Sd} / N_{Rd,conc}$	$M_{Rd,conc}$ [kNm]	$M_{Rd,conc} / M_{Rd,steel}$
At design stage	323	14,17	435	0,54	41	0,29	85	2,07
With the real material properties	310	44,6	560	0,55	41	0,15	190	4,63

To have an idea of what would have happened with the design concrete (worse than the real one),

- the experimental curve of the RC specimen RCL5 is multiplied by  $M_{Rd,conc}^{design} / M_{Rd,conc}^{real}$  (with  $N=750$  kN) =  $85/190 = 0,45$
- the experimental curve of the composite specimen COL10 is multiplied by  $M_{Rd,comp}^{design} / M_{Rd,comp}^{real} = 190/285=0.70$

If the concrete behaved as expected, the specimens with an encased steel profile would have had greater resistance than the reference R.C. specimen by a factor of about 2 (see Fig. 3-28 and 3-29)

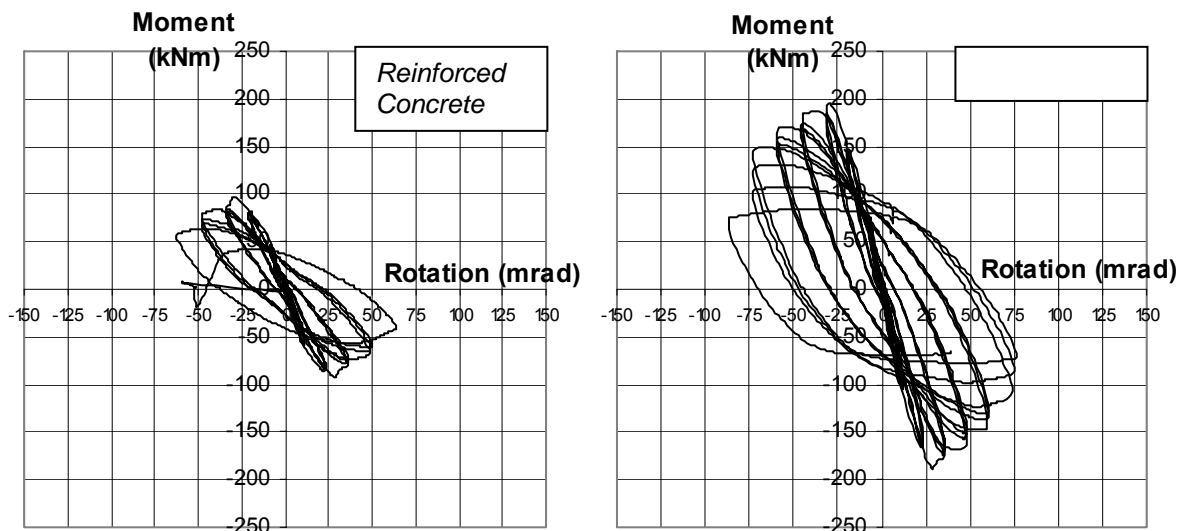


Figure 3-28: Moment-Rotation curves for specimens RCL5 and COL10 (medium ductility design) with the assumption of design concrete resistance (14,17 N/mm<sup>2</sup>)

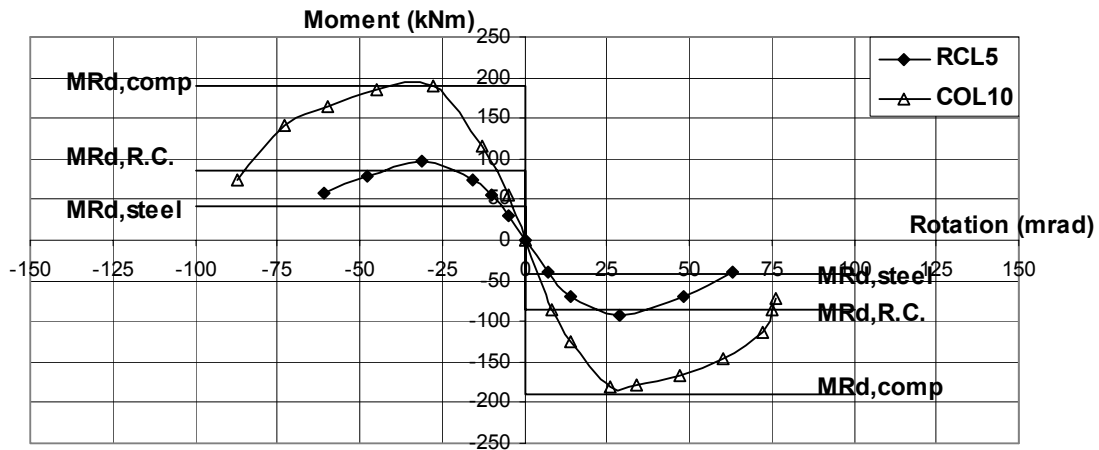


Figure 3-29: Envelope curves for specimens RCL5 and COL10 of phase 3. with the assumption of design concrete resistance ( $14,17 \text{ N/mm}^2$ )

### 3.4.5. Design resistance of potential local failure mechanisms.

A tentative of developments of design formulas has been done to quantify the potential local failure mechanisms in Liege specimens.

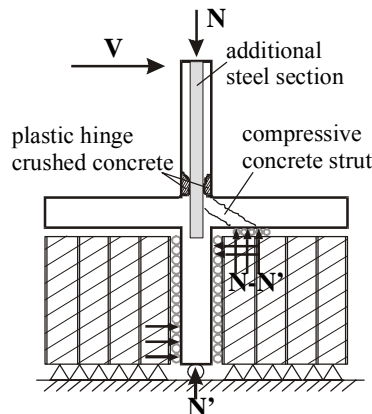


Figure 3-30. Global equilibrium of the specimen when contact between beam and infill is possible

The formation of the compressive strut in the beam is conditioned by local equilibrium in the node, implying steel ties in tension and concrete struts in compression, as shown in Fig. 3-31. As it was shown previously, the applied compression force  $N$  at the top of the column is necessary to anchor the tension induced in the steel profile by the horizontal load.

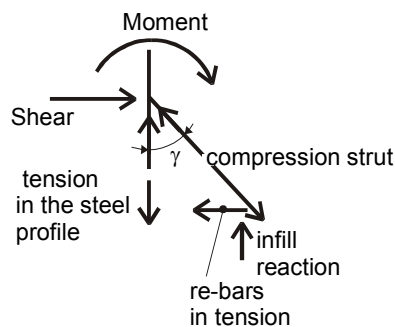


Figure 3-31. Global equilibrium of the steel profile



The tension in the steel profile is counterbalanced by the applied axial compression. As it can be shown by global equilibrium considerations, the applied compression is always greater than the tension in the steel profile induced by the horizontal loads. The steel profile applies a compression directly equilibrated by the concrete of the column (see Fig. 3-32).

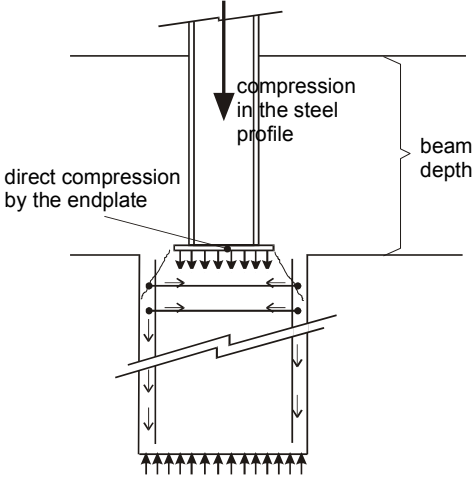


Figure 3-32. Equilibrium of steel profile in compression

The compression strut force (1) in Fig. 3-33 is equilibrated at both ends by compression perpendicular to contact surface (steel profile at one end, infill at the other end (2)) and by tension in re-bars of column and beam (3). The tension in the beam re-bar is also equilibrated by a compressed strut bearing on the vertical side of the infill.

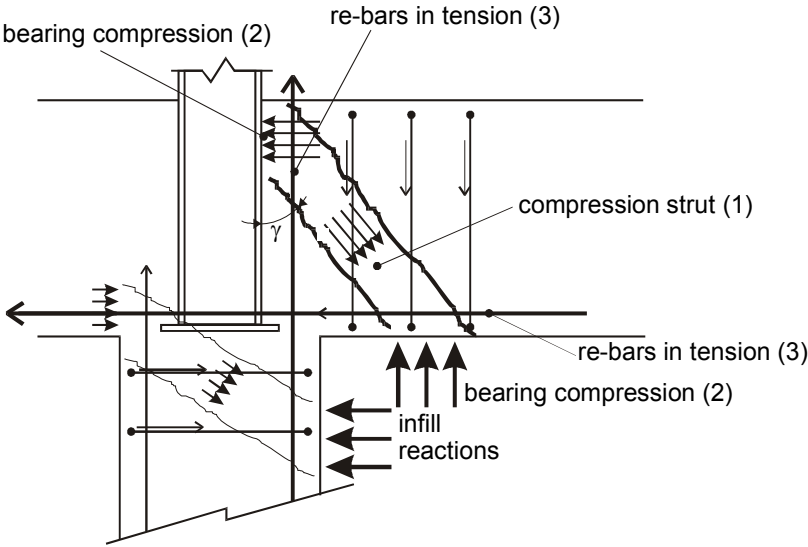


Figure 3-33. Equilibrium of one compressed concrete strut

The steel profile in tension is equilibrated by the additional compression coming from the applied vertical load, and also superposed and equilibrated by the compressed strut in the beam. No mechanism is independent. But the estimations of resistance will be done separately because the different mechanisms here are beneficial for each other. So, it is secure to work partly independently.

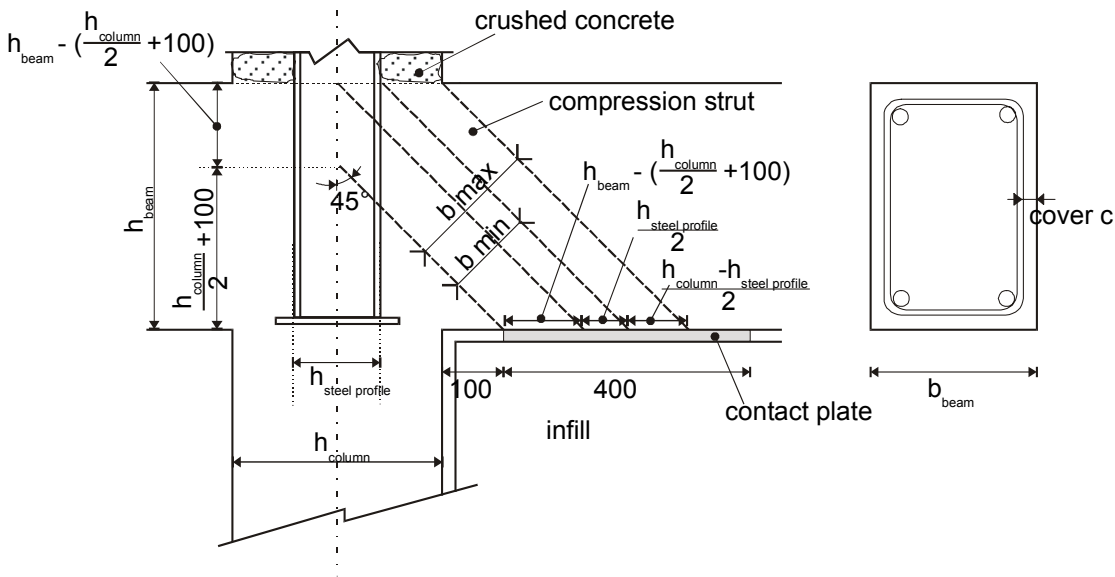
The basic compression resistance of concrete is the resistance obtained by the compression tests on cubes and translated in cylinder resistance  $f_c$

The confinement of the concrete (confined by stirrups) may be estimated on the basis of the critical reinforcing section of stirrups. On the basis of Mander's model (see [Paulay and Priestley]), the increase of resistance of the confined concrete may be assessed as:

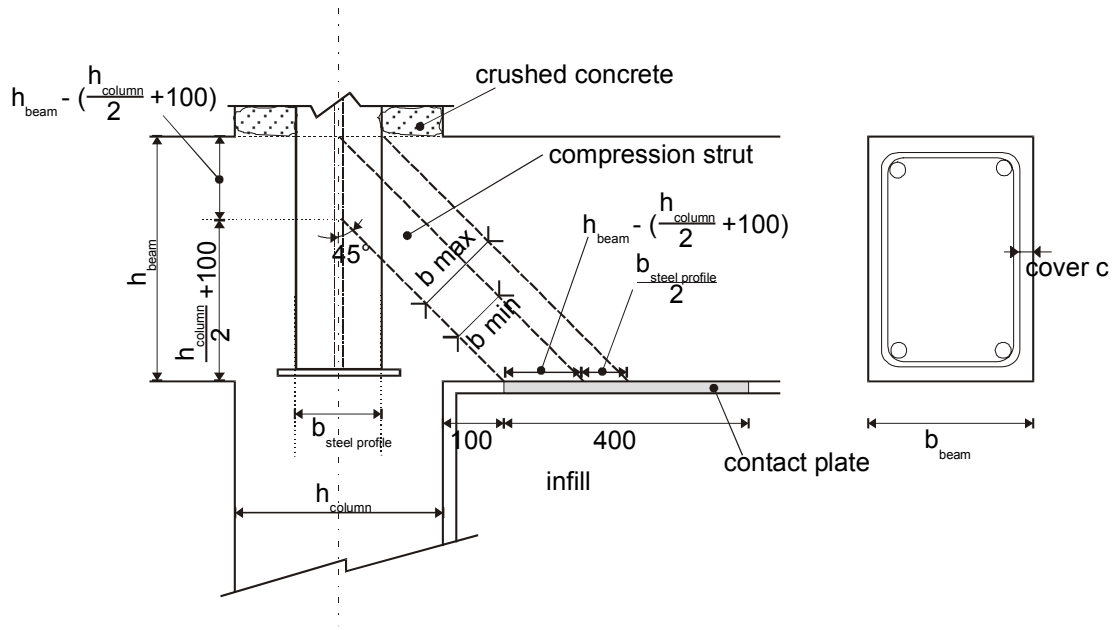
Columns	-for the static and medium ductility specimens,	$f_{cc} = 1.5 f_c$
	-for the low ductility specimens,	$f_{cc} = 1.35 f_c$
Beams	-for the static specimens,	$f_{cc} = 1.75 f_c$
	-for the low ductility specimens,	$f_{cc} = 1.80 f_c$
	-for the medium ductility specimens,	$f_{cc} = 2.00 f_c$

The resistance of concrete in struts is reduced because the compressed struts are not under pure compression, but are also crossed by stirrups in tension.

$$v f_c = 0.6 f_c$$



(a) strong axis specimen



(b) weak axis specimen

Figure 3-34. Notations to define the dimensions of the compressed strut

The dimensions of the compressed strut (1) are represented on Figure 3-34 with the assumption of a 45° slope for the compressed strut. Their resistance are calculated in function of minimum and maximum widths given in the following equations.

Width of the compressed strut for the strong axis specimens

$$b_{\text{strut min}} = \frac{\sqrt{2}}{2} \left( h_{\text{beam}} - \left( \frac{h_{\text{column}}}{2} + 100 \right) + \frac{h_{\text{steel profile}}}{2} \right) \quad [\text{mm}] \quad [3-7]$$

$$b_{\text{strut max}} = \frac{\sqrt{2}}{2} (h_{\text{beam}} - 100) \quad [\text{mm}] \quad [3-8]$$

Width of the compressed strut for the weak axis specimens

$$b_{\text{strut min}} = \frac{\sqrt{2}}{2} \left( h_{\text{beam}} - \left( \frac{h_{\text{column}}}{2} + 100 \right) \right) \quad [3-9]$$

$$b_{\text{strut max}} = \frac{\sqrt{2}}{2} \left( h_{\text{beam}} - \left( \frac{h_{\text{column}}}{2} + 100 \right) + \frac{b_{\text{steel profile}}}{2} \right) \quad [3-10]$$

Thickness of the compressed strut

$$t_{\text{strut}} = b_{\text{beam}} - 2 c_{\text{cover}} - \phi_{\text{stirrup}} \quad [3-11]$$

Resistance

$$N_{\text{Rd strut}} = v f_c b_{\text{strut}} t_{\text{strut}} \quad [3-12]$$

Table 3-4. Geometrical data for the estimation of the resistance of the compressed strut

specimens		$h_{\text{beam}}$ [mm]	$b_{\text{beam}}$ [mm]	$h_{\text{column}}$ [mm]	$h(b)_{\text{steel profile}}$ [mm]	$c_{\text{cover}}$ [mm]	$\phi_{\text{stirrup}}$ [mm]	$b_{\text{strut min}}$ [mm]	$b_{\text{strut max}}$ [mm]	$t_{\text{strut}}$ [mm]
strong axis	static	400	270	350	140	36	12	138	212	186
	low duct	400	270	350	180	53	12	152	212	152
	med. duct	400	270	350	140	39	12	138	212	180
weak axis	static	400	270	270	140	36	12	116.7	166.2	186
	low duct	400	270	270	180	53	12	116.7	180.3	152

The bearing compression of the concrete of the strut on the steel profile (2) is also estimated for both strong and weak axis specimens.

For the strong axis specimens, the bearing compression of the concrete is located on the flanges of the steel profile. The resistance to the bearing compression is calculated as follows:

$$h_{\text{bearing}} = b_{\text{strut min}} \sqrt{2} = h_{\text{beam}} - \left( \frac{h_{\text{column}}}{2} + 100 \right) + \frac{h_{\text{steel profile}}}{2} \quad [3-13]$$

$$W_{\text{bearing}} = b_{\text{steel profile}} \quad [3-14]$$

$$\text{Resistance} = N_{\text{Rd bearing}} = f_c h_{\text{bearing}} b_{\text{steel profile}} \quad [3-15]$$

For the weak axis specimens, the bearing compression is located on the web of steel profile instead of on the flanges. The resistance to the bearing compression is calculated as follows:

$$h_{\text{bearing}} = b_{\text{strut min}} = h_{\text{beam}} - \left( \frac{h_{\text{column}}}{2} + 100 \right) \quad [3-16]$$

$$W_{\text{bearing}} = h_{\text{steel profile}} - 2 t_{\text{flanges steel profile}} \quad [3-17]$$

$$\text{Resistance} = N_{\text{Rd bearing}} = f_c h_{\text{bearing}} (h_{\text{steel profile}} - 2 t_{\text{flanges steel profile}}) \quad [3-18]$$

The tension in the re-bars of the beam (3) is limited by the equation:

$$N_{\text{Rd re-bars}} = A_{\text{re-bars}} f_y \quad [3-19]$$

These assumed resistances were compared with the measured maximal actions, that is, the vertical reaction on the infills, translated in axial action in the re-bars, in the compressive strut or on the bearing section (see Fig. 3-35). Table 3-5 summarises this comparison with the hypothesis of a 45° slope of the compressed strut and without taking into account any confinement of the concrete.

$$N_{\text{strut}} = R_{\text{infill}} / \cos\beta \quad [3-20]$$

$$N_{\text{rebars}} = R_{\text{infill}} / \text{tg}\beta \quad [3-21]$$

$$N_{\text{bearing}} = R_{\text{infill}} \quad [3-22]$$

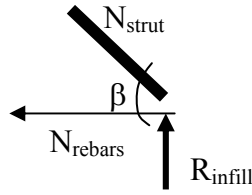


Figure 3-35. Link between the infill reaction and the action forces in the strut and tie mechanism.  
Definition of the angle  $\beta$ , slope of the compressive strut

Table 3-5. Comparison between proposed design resistance  $R_d$  and action effect  $S_d$  deduced from the measurements

Specimens	vertical infill reaction $S_d$	Bearing $R_d$	$S_d/R_d$	Max Strut $R_d/\sqrt{2}$	$S_d/R_d$	Min Strut $R_d/\sqrt{2}$	$S_d/R_d$	Beam rebars $R_d$	$S_d/R_d$
	[kN]	[kN]		[kN]		[kN]		[kN]	
RCL1	238	1213.0	0.20	743.4	0.32	483.8	0.49	225.1	<u>1.06</u>
COL1	357	1218.3	0.29	746.6	0.48	486.0	0.73	225.1	<u>1.59</u>
COL2	357	1250.0	0.29	766.0	0.47	498.6	0.72	225.1	<u>1.59</u>
COL3	373	1262.1	0.30	773.5	0.48	503.4	0.74	225.1	<u>1.66</u>
COL4	385	1225.1	0.31	750.8	0.51	488.7	0.79	225.1	<u>1.71</u>
RCL3	453	1727.0	0.26	609.7	0.74	437.4	<u>1.04</u>	689.6	0.66
COL5	585	1820.2	0.32	642.5	0.91	461.0	<u>1.27</u>	689.6	0.85
COL6	571	1751.7	0.33	618.3	0.92	443.6	<u>1.29</u>	689.6	0.83
COL7	657	1804.1	0.36	636.9	<u>1.03</u>	456.9	<u>1.44</u>	689.6	0.95
COL8	586	1810.6	0.32	639.1	0.92	458.5	<u>1.28</u>	689.6	0.85
RCL5	308	1278.7	0.24	757.8	0.41	493.5	0.62	549.7	0.56
COL9	395	1283.3	0.31	760.5	0.52	495.2	0.80	549.7	0.72
COL10	416	1271.9	0.33	753.8	0.55	490.9	0.85	549.7	0.76
COL11	420	1322.5	0.32	783.8	0.54	510.4	0.82	549.7	0.76
COL12	397	1273.4	0.31	754.7	0.53	491.5	0.81	549.7	0.72
RCL2	224	1032.1	0.22	707.2	0.32	496.6	0.45	225.1	1.00
COL13	326	990.8	0.33	678.9	0.48	476.7	0.68	225.1	<u>1.45</u>
RCL4	309	1364.2	0.23	632.5	0.49	409.5	0.75	689.6	0.45
COL14	440	1314.9	0.33	609.6	0.72	394.7	1.11	689.6	0.64

Table 3-5 shows that

- There is no problem of bearing resistance of concrete. The action to resistance ratios are always smaller than 0,40.
- The crushing of the compressed concrete struts does not seem to be a problem. With the assumption of mobilising the minimal width of the strut, the action to resistance ratios of the “low ductility design” specimens reaches 1 (max 1,44). But during the tests, no crushing is observed in the strut. Two possible reasons are that more than the minimum width is mobilised and that confinement exist and increase the resistance of the concrete.
- The weak point could be the yielding of the beam reinforcing bars, especially in case of the static design specimens. But no big cracks were observed. With the assumption of 60° for the slope of the struts, the action in the re-bars could be divided by 1,73.

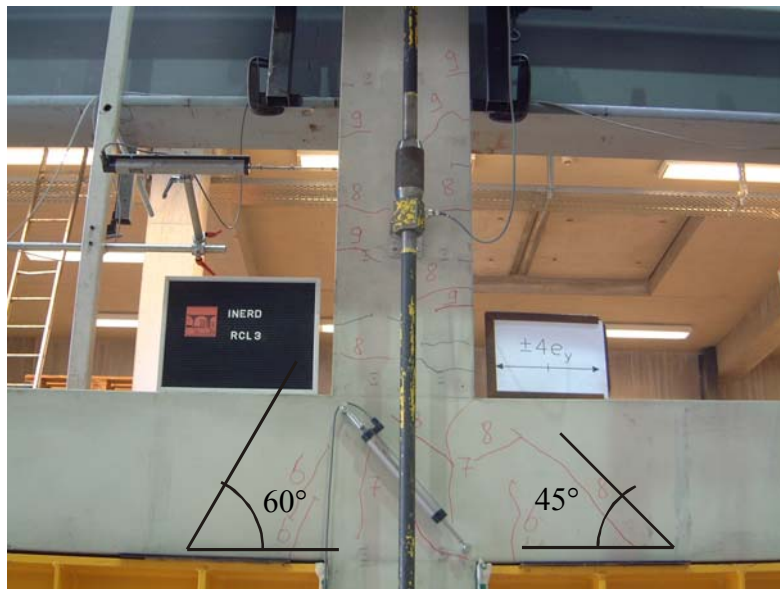


Figure 3-36. Visual inspection of the cracks in specimen RCL3

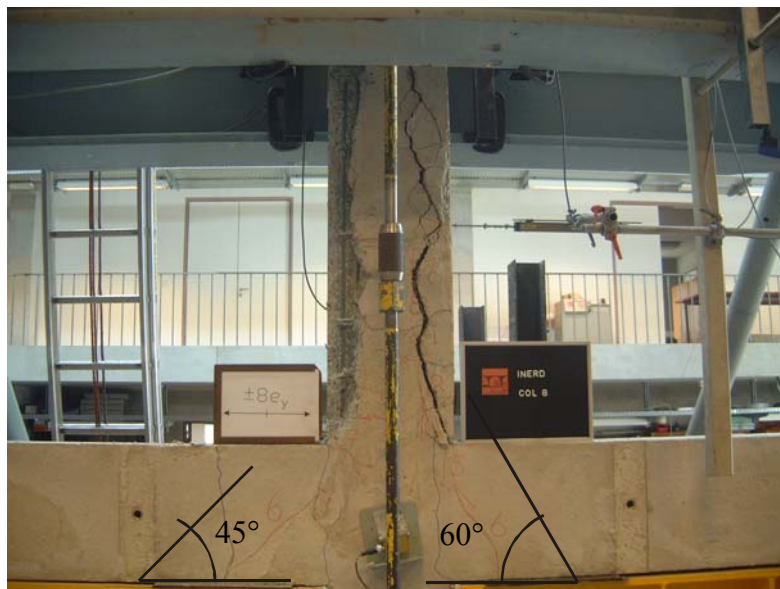


Figure 3-37. Visual inspection of the cracks in specimen COL8

An additional visual inspection (see Fig. 3-34 and 3-35) shows that the cracks in the beam have a slope between  $45^\circ$  and  $60^\circ$ . Measurements on the re-bars were made (see strain gauges SG6-7-8-9 on Fig. 3-38), axial loads in the re-bars were deduced and compared with the vertical reaction on the infills. Figures 3-37, 3-38 and 3-39 give the slope of the compressive struts in function of the column shear. It can be seen that the slope vary with the shear. The maximum slope corresponds to the maximum shear and can vary from  $45^\circ$  to  $70^\circ$ .

Table 3-6 compares the stresses in the beam re-bars. The global ones are obtained from global measurements ( $R_{infill}$  – see equation [3-21]) with the assumptions of struts of  $60^\circ$  and  $45^\circ$  and the local ones are obtained from direct local measurements. The conclusions are that

- the model with  $45^\circ$  struts gives calculated stresses closer to the measured ones, and
- in terms of design, the model with  $45^\circ$  struts is on the safe side.

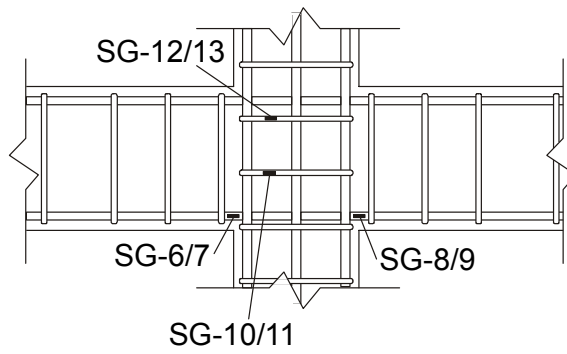


Figure 3-38. Strain gauges on reinforcing bars

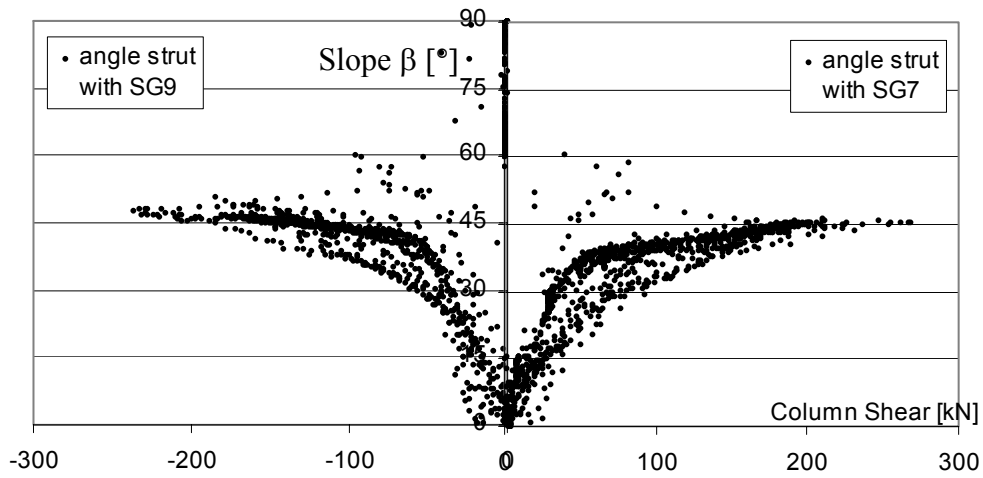


Figure 3-39. Assessment of the slope of the compressive struts in function of the column shear for COL5 composite specimen

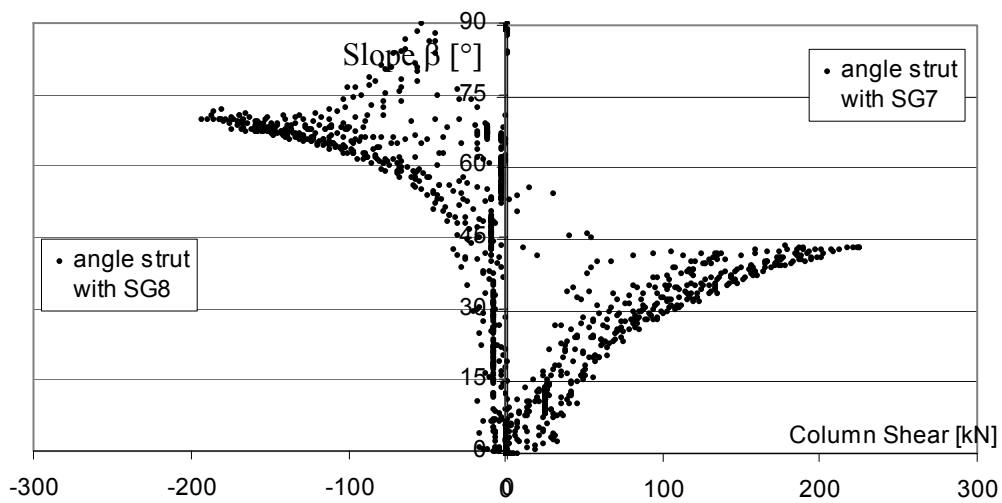


Figure 3-40. Assessment of the slope of the compressive struts in function of the column shear for RCL3 reinforced concrete specimen

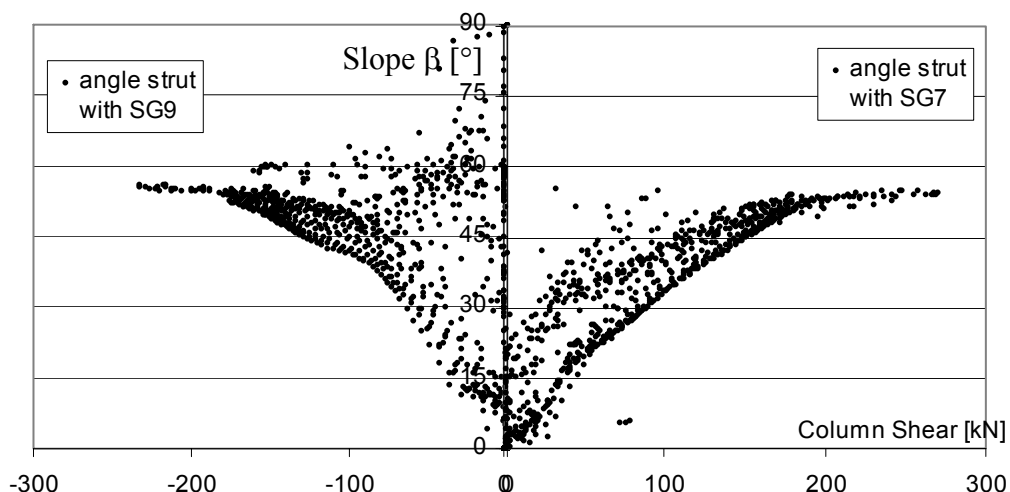


Figure 3-41. Assessment of the slope of the compressive struts in function of the column shear for COL8 composite specimen

Table 3-6. Stresses in the beam re-bars

specimens	maximal stresses $\sigma_{rebars}$ [N/mm <sup>2</sup> ]			Comparison	
	From global measurements		From local measurements on the rebars	$\sigma_{local}/\sigma_{global}$	
	$\sigma_{global} = R_{infill}/tg\beta / A_{rebars}$			$\beta = 45^\circ$	$\beta = 60^\circ$
	$\beta = 45^\circ$	$\beta = 60^\circ$	$\sigma_{local}$		
RCL3	370	214	422	1,14	1,97
COL5	476	275	488	1,03	1,77
COL6	465	269	467	1,00	1,74
COL7	532	308	516	0,97	1,68
COL8	476	275	340	0,71	1,24

### 3.5. Composite panel zone as dissipative mechanism.

#### 3.5.1. Forces acting at the beam-to-column joint

The behaviour of the beam-to-column joints under cyclic loading is characterised by an interaction of different resistant mechanisms for which considerable uncertainties exist, especially when the response is well beyond the first yield excursion. This should explain the significant differences that still exist among Seismic Codes, not only with regard to the shear transfer mechanisms adopted to establish the provisions necessary to the joint reinforcement, but even with regard to the forces to be taken into account for the joint core design.

In Eurocode 8, the beam-to-column joints in moment frames are required to have a high enough moment resistance  $M_{j,Rd}$  in order to enhance the ductile capacity of the columns and to avoid the local formation of plastic hinges in the column panel zone. Provided that, at the design stage, the plastic hinge formation in the beams is envisaged, it is necessary in any case to take into account the increase in the beam moment values in order to derive the joint design forces. This matter considers two aspects: *i*) the possibility to have a yield strength of the re-bars present in the beam higher than the value indicated in the guidelines and, *ii*) the possible increase in stress of the beam longitudinal re-bars due to the strain hardening. Thus, it is of crucial importance to respect the following:

$$M_{j,Rd} \geq 1,3 \cdot \sum M_{Rd,beam} \quad [3-23]$$



That means:

$$M'_{j,Rd} \geq \sum M_{Rd,beam} = M_{j,Sd} \quad [3-24]$$

with 
$$M'_{j,Rd} = \frac{M_{j,Rd}}{1,3} \quad [3-25]$$

The design resisting moment of the joint takes into account the Capacity Design Principle.

Focusing on the behaviour of an internal beam-to-column joint belonging to a frame free to deform in plane and subjected both to gravitational and seismic loads, as depicted in Figure 3-42, it is possible to define the following relations for the bending moments acting on the left and on the right of the joint.

$$M_{left} = M_{s,left} + M_{g,left} \quad [3-26]$$

$$M_{right} = M_{s,right} - M_{g,right} \quad [3-27]$$

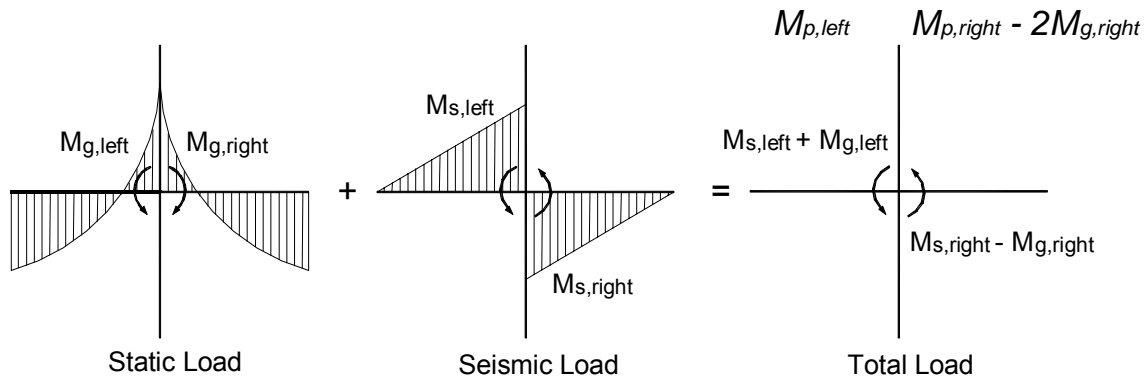


Figure 3-42. Gravitational and seismic bending moments acting at the connection

If it is assumed that during a seismic event the left bending moment of the beam reaches the value accorded to the plastic bending moment, as a consequence:

$$M_{p,left} = M_{s,left} + M_{g,left} \quad [3-28]$$

If the same allowances for the beam bending moment acting on the right side are made, it is that:

$$M_{p,right} = M_{s,right} + M_{g,right} \quad [3-29]$$

Hence, combining Equations [3.27] and [3.29], it is easy to obtain that the bending moment acting on the right side of the joint is equal to:

$$M_{right} = M_{s,right} - M_{g,right} = M_{p,right} - 2M_{g,right} \quad [3-30]$$

This equation underlines that the gravitational loads reduce the effects of the seismic action in terms of bending moment acting at the joint. The beneficial effect of the gravitational loads is not included in the Eurocode prescriptions. Nevertheless, the AISC provisions [1997] approximately account for it by means of a reduction coefficient equal to 0,8 applied to  $M_{p,right}$ .

Besides, it is to be noted that the longitudinal column shear reduces the total shear action at the beam-to-column joint position, as illustrated in Figure 3-43, where the seismic configuration of internal forces affecting the joint is represented:

In accordance with the preceding assumptions for the seismic load combinations, it is to check that:

$$V_{j,Rd} \geq V_{j,Sd} = 0,8 \cdot \frac{\sum M_{Rd,beam}}{d_s} - V_{col,wp,u} \quad [3-31]$$

with

$$\sum M_{Rd,beam} = M_{Rd,beam,right} + M_{Rd,beam,left} \quad [3-32]$$

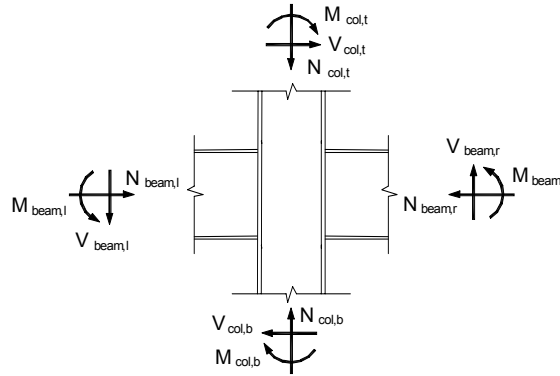


Figure 3-43. Possible seismic actions on an internal structural joint

Referring to Figure 3-43,  $V_{col,wp,u}$  is the average shear force  $(V_{column,top} + V_{column,bottom})/2$  in the column web at the joint when collapse is incipient and also equal to:

$$V_{col,wp,u} = \frac{M_{Rd,col,top} + M_{Rd,col,bottom}}{L_{col} - d_s} \quad [3-33]$$

With  $L_{col}$  and  $d_s$  as indicated in Figure 3-44. It is assumed that the zero-moment inflexion points are located in the middle of the column length and that the equilibrium condition:

$$\sum M_{Sd,beam} = \sum M_{Sd,col} \text{ is satisfied.}$$

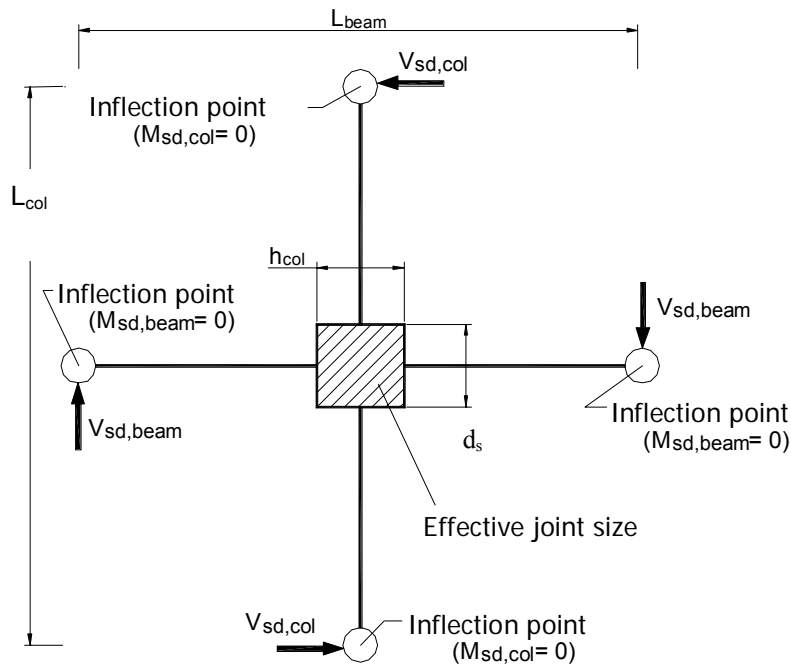


Figure 3-44. Points of inflection at mid length of the beams and columns

### 3.5.2. Analytical procedure for an effective composite joint design

It has to be noticed that the topics listed above deal with some problems for which research studies were needed due to a lack of information in the European Design Codes. Up to now the European code has not clarified yet the behaviour of the composite beam-to-column joints. In fact, the issues tied with the contribution in dissipative zones of the concrete parts of composite members in computing the overall shear resistance are not entirely probed. One of the purposes of the INERD Project is to validate experimentally the joint mechanisms providing their shear resistance. Hence, once the presumed joint formulation was derived, it had to be validated through the experimental data obtained from the testing procedure.

The investigation of the interior properties of some beam-to-column joints found in literature was important in order to understand the force transfer mechanisms activated at the U.L.S. in the joint typology under study when it undergoes seismic forces. For this purpose, it was taken into account other research studies of composite frames, tested under monotonic and cyclic loading, and investigating the joint resistance and collapse mechanisms. Nonetheless, it was required to re-adjust the mechanical models considered to fit best the study case under evaluation, see Figure3-45.

The analytical models taken into account were those of:

- R. Kanno and G. G. Deierlein [2000];
- C.-C. Chou and C.-M. Uang [2002].

The analyses illustrated in Kanno-Deierlein [2000] and Chuo-Uang [2002] were readapted to the survey of the Innovative Beam-to-Column Composite Joint (IBCC Joint) on the basis of the guidelines deduced from the Eurocodes.

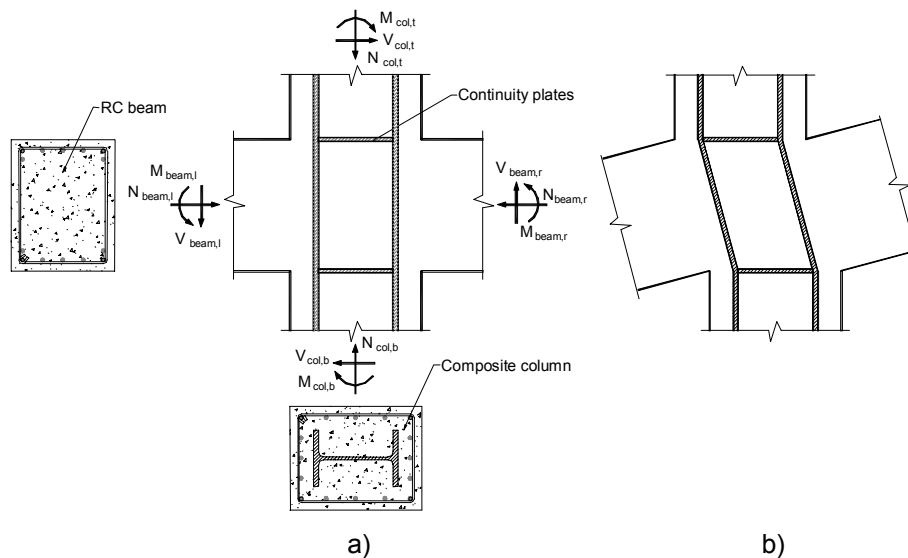


Figure 3-45. (a) Forces acting at the connection, (b) joint deformation

The main type of failures occurring at the joint location are in the form of those indicated in Figure 3-46a), panel shear failure, and Figure 3-46b), bearing failure.

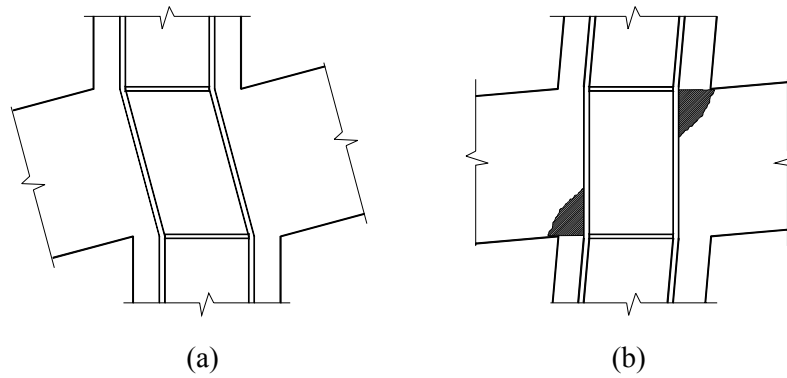


Figure 3-46. a) Panel shear failure, b) bearing failure

These possible behaviours which develop in the beam-to-column joint area are tied to the resistance mechanisms reacting to the forces stressing the area under consideration. These mechanisms and their envisaged resistances are now illustrated.

### Panel Zone Resistance

This resisting mechanism has been studied following the indications contained in prEN 1994-1-1: 2001, 3<sup>rd</sup> draft, paragraph 8.3.3.2. The panel zone shear resistance is obtained from the summation of the column steel web panel resistance  $V_{j,swp}$  and of the concrete compression strut resistance  $V_{j,ccs}$  generated between the continuity plates (stiffeners) and the steel profile flanges.

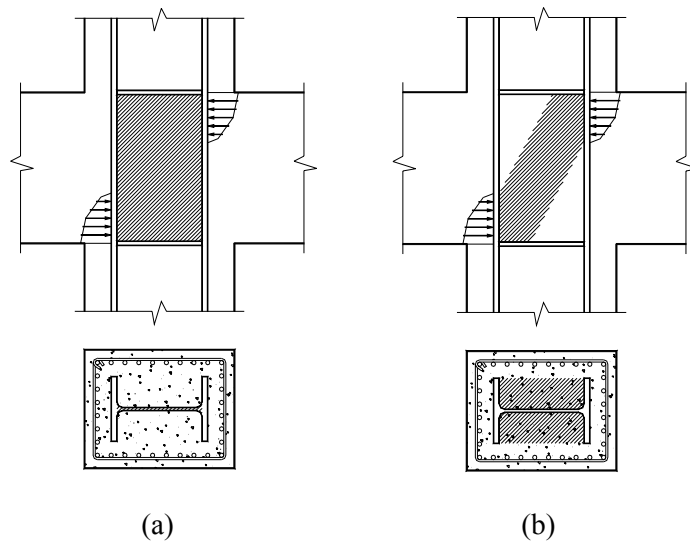


Figure 3-47. a) Steel web panel mechanism, b) concrete compression strut mechanism

The design shear resistance and the design moment resistance for the steel-column web panel are calculated as follows:

$$V_{j,wps} = 0,7 \cdot \left( \frac{f_{ym,d,cw}}{\sqrt{3}} \cdot \min(A_v; t_{cw} \cdot d_s) + \Delta V_{j,swp} \right) \quad [3-34]$$

$$M'_{j,Rd,swp} = V_{j,swp} \cdot (1 \cdot d_s) \quad \text{if } A_v < t_{cw} \cdot d_s \quad [3-35]$$

$$M'_{j,Rd,swp} = V_{j,swp} \cdot (h_c - t_{cf}) \quad \text{if } A_v > t_{cw} \cdot d_s \quad [3-36]$$

Following the prescriptions of Eurocode 2, for a double-sided joint in which the beam depths are similar, the design shear and moment resistances of the concrete strut should be calculated as follows:

$$V_{j,ccs} = \frac{1}{1,3} \cdot \nu \cdot 0,85 \cdot f_{cd} \cdot A_{cs} \cdot \sin \theta \quad [3-37]$$

$$M'_{j,Rd,ccs} = V_{j,ccs} \cdot (0,9d_s) \quad [3-38]$$

### Horizontal Bearing Resistance

In order to evaluate this type of resistance it is important to be able to guarantee an adequate confinement (by inserting a proper quantity of hoops), which enhances the concrete performance. The shear resistance given by the concrete horizontally compressed inside the column,  $V_{j,hbf}$ , is determined by a stress block model similar to that used for the flexural strength of the RC members.

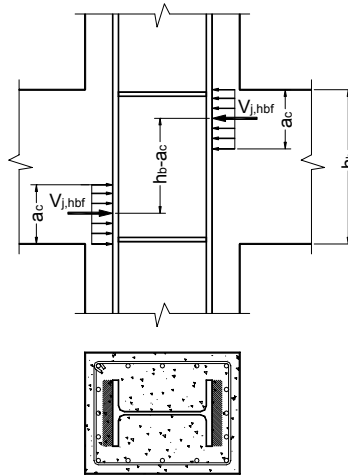


Figure 3-48. Horizontal bearing mechanism

Accounting for the Eurocode 2 indications, the shear resistance becomes:

$$V_{j,hbf} = \frac{1}{1,3} \cdot \left( 0,85 \cdot \frac{f_{ck,c}}{\gamma_c} \right) \cdot a_c \cdot b_{cf} \quad [3-39]$$

$$M'_{j,Rd,hbf} = V_{j,hbf} \cdot (h_b - a_c) \quad [3-40]$$

## Concrete Compression Field Resistance

The concrete compression field mechanism  $V_{\text{joint,ccf}}$  shown in Figure 3-49, consists of several compression struts that act with the horizontal reinforcement to form a truss mechanism (often used for modelling shear in reinforced concrete beams). Shear is transferred horizontally from the beam into the compression field by the concrete bearing against the embedded steel column.

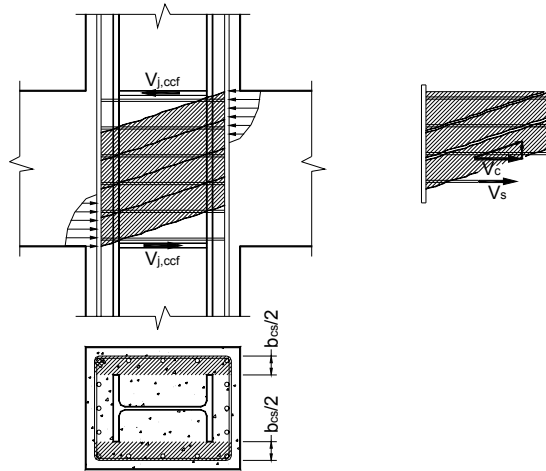


Figure 3-49. Concrete compression field mechanism

The shear resistance, considering the Eurocode 2 prescriptions, becomes:

$$V_{j,ccf} = \frac{1}{1,3} \cdot \min(V_c; V_s) \quad [3-41]$$

with

$$V_c = \alpha_c \cdot \nu \cdot f_{cd} \cdot b_{cs} \cdot 0,9 \cdot d \cdot \frac{1}{(\cot \theta + \tan \theta)}$$

$$V_s = \frac{A_{s,tie}}{S_{tie}} \cdot f_{yd,w} \cdot 0,9 \cdot d \cdot \cot \theta$$

$$M'_{j,Rd,ccf} = V_{j,ccf} \cdot 1,1 \cdot d_s \quad [3-42]$$

## Bond Shear Resistance

An idealisation of the bond resistance  $V_{\text{joint,bf}}$ , provided by the longitudinal re-bars acting in friction with concrete, is shown in Figure 3-50. The bond failure occurs if the compression and tension forces compatible with the moment equilibrium (along with the forces mobilised in the concrete compression field) are greater than the bond strength provided by one set of longitudinal reinforcing bars embedded in the outer most joint region. Thus if,  $T_{cb} + T_{tb} = T_{mb}$  with  $T_{mb}$  the bond mechanism strength at failure.

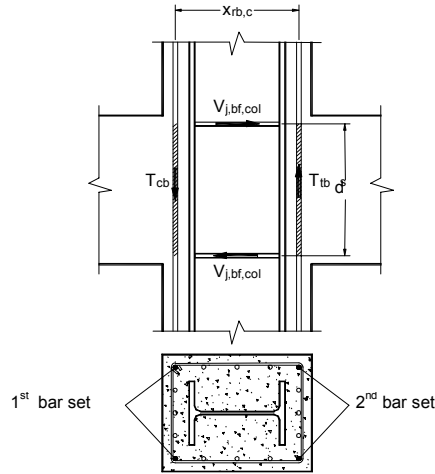


Figure 3-50. Bond mechanism due to the friction between steel and concrete

In order to determine the friction forces, the procedure in prEN 1992-1, Final Draft, Chapter 8.4.2, has been followed. Considering the moment equilibrium given by the forces acting on the two sets of longitudinal re-bars and reducing the shear strength of the value derived from Eurocode 8, it is immediate to derive the shear resistance:

$$V_{j,bf,col} = \frac{1}{1,3} \cdot f_{bd} \cdot \phi_b \cdot x_{rb,c} \quad [3-43]$$

$$M'_{j,Rd,bf,col} = V_{j,bf,col} \cdot d_s \quad [3-44]$$

The following equations, obtained from equilibrium of forces, have to be used in order to calculate the shear resistance of the whole joint region considering the contribution of each single mechanism :

$$M'_{j,Rd,inner} = \min \left\{ M'_{j,Rd,swp} + M'_{j,Rd,ccs}; M'_{j,Rd,hbf} \right\} \quad [3-45]$$

$$M'_{j,Rd,outer} = \min \left\{ M'_{j,Rd,ccf}; M'_{j,Rd,bf,col} \right\} \quad [3-46]$$

$$M'_{j,Rd} = M'_{j,Rd,inner} + M'_{j,Rd,outer} \quad [3-47]$$

$$V_{j,Rd} = \frac{M'_{j,Rd}}{d_s} \quad [3-48]$$

### 3.5.3. Conclusions from the tests.

An abridgement of the results obtained from testing are hereafter illustrated along with some comments. The F - Δ curves of five specimens belonging to the same study case are represented. The test conducted on the specimen RC-T (sample without steel profile) is used as test control and reference for the other tests of the same category. In fact, the behaviour of this specimen relies only on the resistance and ductility of a reinforced concrete section.

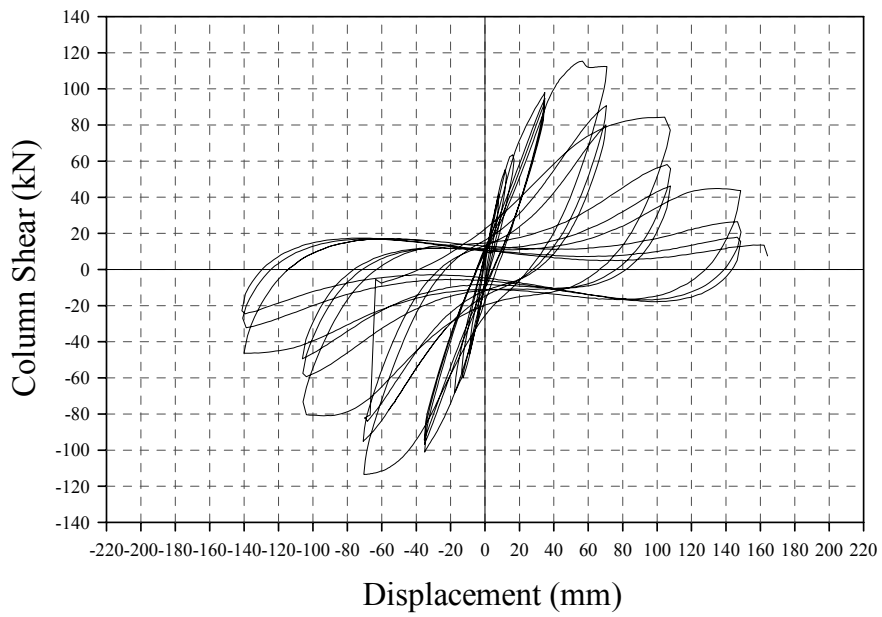


Figure 3-51. Graph of the RC-T specimen for comparison

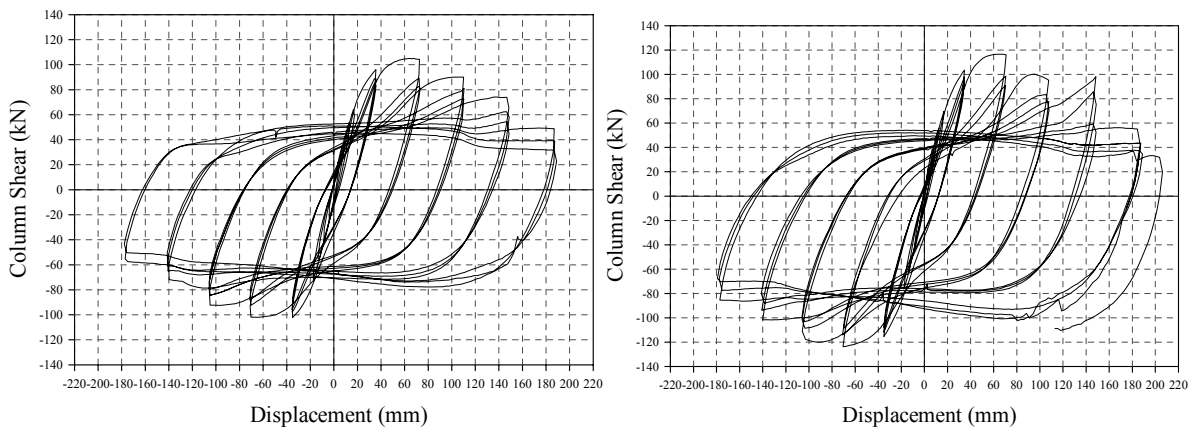


Figure 3-52. F-Δ curves for CO-Ts in the C1 configuration

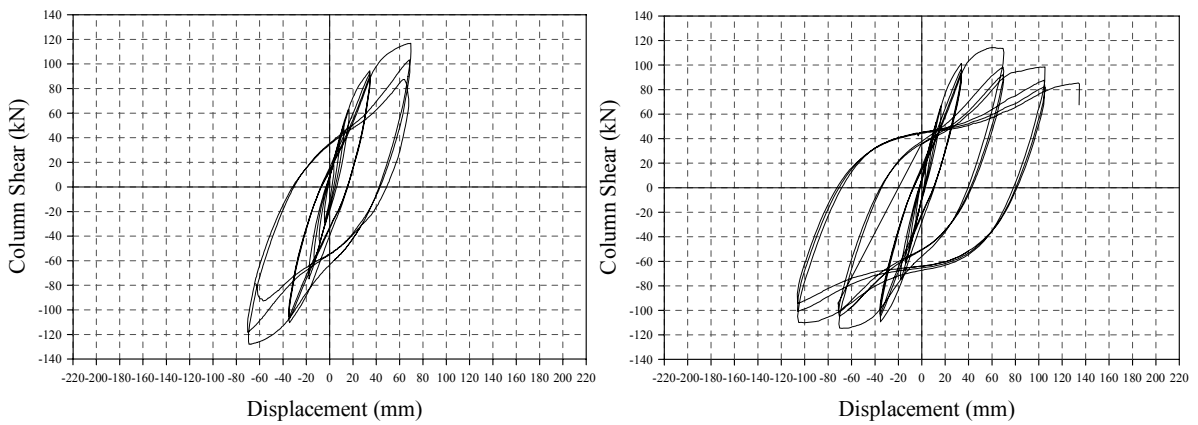


Figure 3-53. F-Δ curves for CO-Ts in the C3 configuration



Figure 3-51 highlights the typical performance of a RC column with regular stiffness and resistance up to a  $4e_y$  displacement from which it loses the mechanical properties very quickly. In fact, at the subsequent  $6e_y$  and  $8e_y$  cycles the sample reacts to the imposed top displacement with an average force equal to 35% of the maximum reached level ( $\approx 120\text{kN}$ ). The failure occurred at the beginning of  $10e_y$  with a reaction force of approximately  $15\text{kN}$ . The joint region was rather deteriorated. For the CO-T samples in the C1 configuration at large displacements the loss of the concrete mechanical properties is compensated by those of the steel section. The shear force goes from  $\approx 110\text{kN}$  at  $4e_y$  to  $\approx 30\text{kN}$  at the end of the three  $10e_y$  cycles. Up to  $4e_y$  the resistance and stiffness of the composite concrete-steel column prevails whereas for the other cycles the only effective part of the cross section is that of the steel profile, i.e. large hysteresis cycles with constant level of stiffness and a modest loss in resistance. The trials were stopped after reaching very large displacements ( $11e_y$ ) with a quite strong deterioration of the joint panel.



Figure 3-54. Pictures of the CO-Ts joint deterioration

The samples CO-T in the C3 configuration (with a short steel profile stump encased in the joint region) showed the same monitored resistance values of the aforementioned samples (C1 configuration). Nonetheless, those in the C3 configuration displayed a lesser amount of ductility noticing that the collapse took place some cycles before  $10e_y$ . The collapses occurred far from the joint region.

Thus, no great difference in term of strength and stiffness seems to exist between the four classes embedding the steel profiles. From the graphs, for the CO-Ts in the C1 configuration, the capacity to maintain a certain strength also after the  $6e_y$  cycles is evident. Besides, they can derive a greater amount in terms of ductility thus avoiding the problem with the anticipated ruptures far from the joint region. The difference in terms of strength between the CO-T and the RC-T specimens after the  $4e_y$  cycles is evident.

For the specimens belonging to the same category of studies the experimental outcomes have been also summarised in charts, which permit a direct comparison of the results in terms of force, displacement and energy, see Figure 3-55 and 3-56.

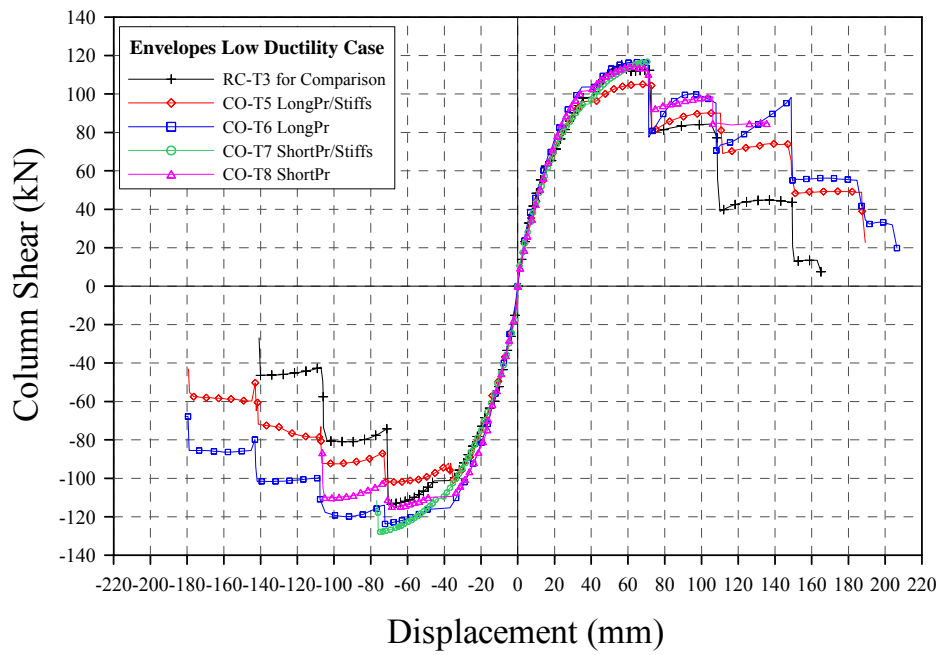


Figure 3-55. Comparison chart in terms of resistance and ductility

In terms of absorbed energy, the different behaviour between the RC-T specimen and the CO-T specimens is to be evidenced. This chart shows that, for the RC-T sample, the absorbed energy after the  $4e_y$  cycles increases at a much lower rate than that belonging to the other samples.

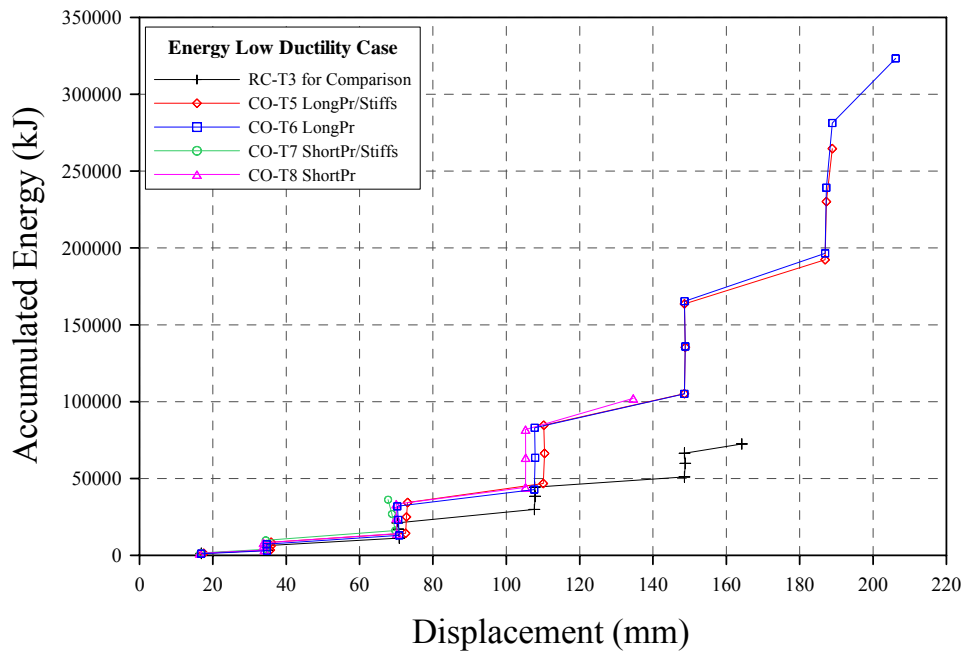


Figure 3-56. Accumulated energy chart

### 3.5.4. Experimental and numerical validation of the analytical formulas.

In this section, the effectiveness of the anticipated analytical formulas necessary to evaluate the resistance in shear of the Innovative Beam-to-Column Composite Joint is shown. On the basis of a numerical modelling carried out using the finite element ABAQUS Code (2003), the activation of the single mechanism contributing to the resistance has been monitored. Thereby, the 3D-FE model has been calibrated and the joint stress-strain state has been simulated in the monotonic displacement regime. The model has been also verified by comparing the experimental cyclic response of the specimens with the predicted monotonic response, as illustrated in Figure 3-57.

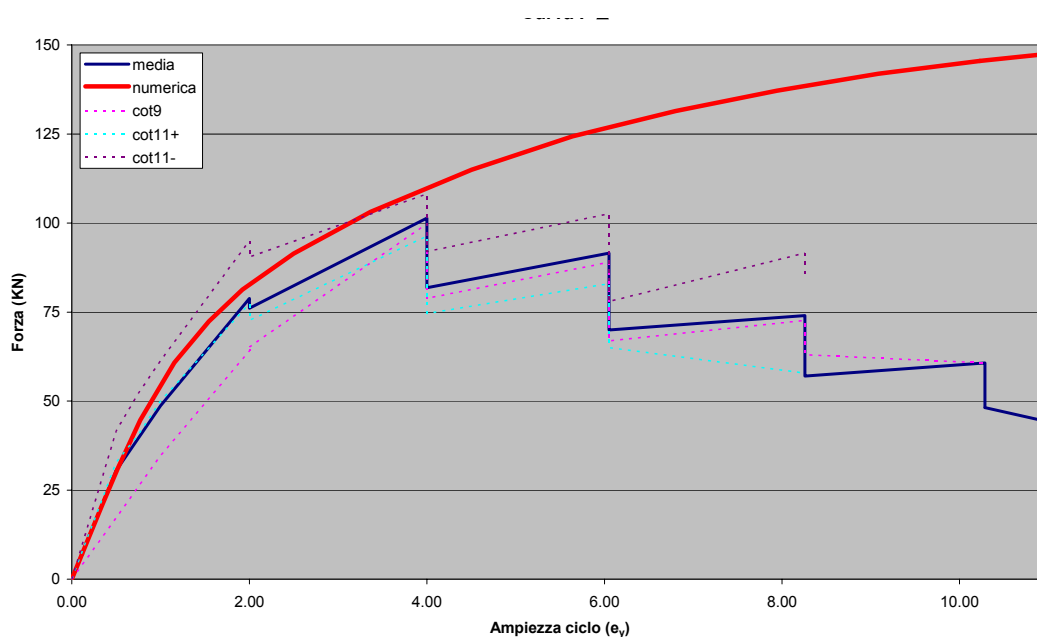


Figure 3-57. Predicted and numerical response of the specimen CO-T

A model reproduction is reported in Figure 3-58 and represents a CO-T specimen endowed with a HEB 140 steel profile. It is characterised by a reduced integration eight-node solid-elements. In fact, elastic and inelastic convergence studies have been conducted to evaluate the final mesh to be adopted. Surface-to-surface contact elements have been used to model the surface interaction. The FE analyses account for the material non-linearity through the classical plasticity theory based on the Von Mises yield criterion.

Even if the model is not able to capture the loss of resistance and stiffness due to the crushing of the concrete after a certain level of the imposed displacement, the experimental data are in good agreement with the numerical simulation. The elaboration of the numerical evidences has led to the modification of some geometrical parameters related to the formulae and it has permitted to better figure out the experimental response of the joint subjected to shear loading. Also the measurements obtained from the local instrumentation by means of strain gauges helped in the understanding of the activation and evolution of the mechanisms while testing.

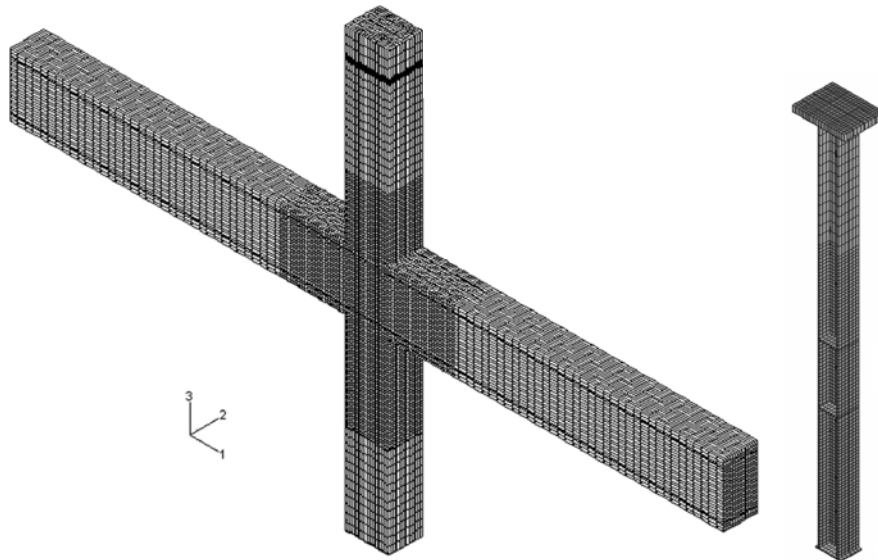


Figure 3-58. 3D numerical model of a CO-T specimen

As formerly introduced, the panel zone shear resistance is given by the summation of the panel web resistance  $V_{j,swp}$  and the compression strut resistance  $V_{j,ccs}$ . The graphs below, deduced from the experimental data (strain gauges), give explanation of the shear mechanisms activated in the steel web, steel flanges and stiffeners. As depicted in Figure 3-59, the measured web strains increase uniformly up to a displacement equal to  $4e_y \div 6e_y$  when it exceeds the steel yield strain. It is the central zone of the panel that deforms most. It can be imagined the web stresses increasing during the test until the panel zone yields uniformly for a top displacement equal to  $6e_y$ . From this point on, concentration of stresses shifts to the four corners of the steel web panel in correspondence of the stiffeners, and the resistance of the panel zone is given by the contribution of these four local plastic hinges.

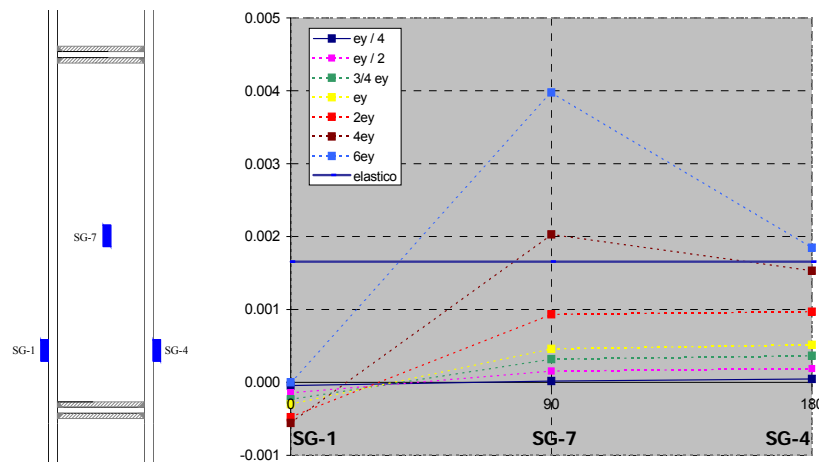


Figure 3-59. Evolution of the measured shear strain in the web panel of the steel profile

In fact, by the elaboration of the values of the strain gauges positioned on the flange of the steel profile it was possible to evidence that the deformation in the zone of the stiffeners is greater than that along the flange. High plastic deformations, intended as local plastic hinges, are well localised in these points where part of the shear forces are transmitted, see Figure 3-60.

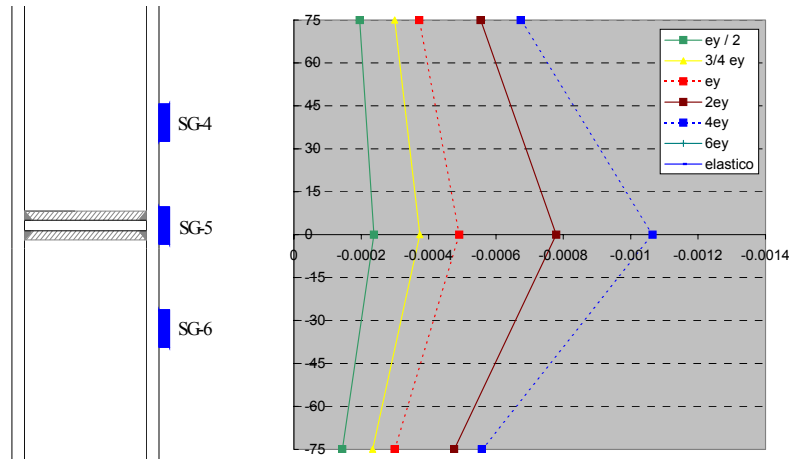


Figure 3-60. Evolution of the measured strains in the flange of the steel profile

Nevertheless, it is of primary importance to point out that this behaviour was encountered also in the specimens without the horizontal steel plates. Therefore, the plastic hinges form at the four joint corners where the shear forces have to be transferred, regardless of the presence of the stiffeners.

Where the steel column web is encased in the concrete, the design shear resistance of the panel may be increased with the contribution of the inner concrete strut  $V_{ccs}$  that is the design shear resistance of the concrete encasement of the web panel. In composite connections, the concrete compression strut may be mobilised in resisting the shear either due to the presence of the horizontal plates welded to the column or simply due to friction and flexural forces acting in the steel column flanges.

Through the numerical FE model (ABAQUS, 2003), it was possible to monitor the evolution of the principal stresses of compression for different imposed top displacement. By increasing the displacement imposed at the top of the column, high stresses of compression are mobilised in the concrete strut. For a displacement equal to  $6e_y$ , all the concrete in the zone reached the value of 40MPa that represents the maximum allowed compression strength implemented in the model on the basis of the concrete cube tests. At an imposed displacement equal to  $10e_y$ , as depicted in Figure 3-61, the concrete in the internal zone and around the joint crushed. Nonetheless, the confinement effects (due to the presence of the steel profile and of the stiffeners) would permit, in practice, to attain greater values than the 40MPa implemented in this model for what concerns the concrete compressive strength.

The shear resistance given by the concrete horizontally compressed by the elements inside the column  $V_{j,hbf}$ , is determined through a standard Stress Block model. For a good development of the Horizontal Bearing Mechanism it is important to provide a sufficient concrete confinement. The provided amount of stirrups in the tested specimens seems to be adequate to this aim.

The Concrete Compression Field Mechanism  $V_{j,ccf}$ , consists of several compression struts that act with the horizontal reinforcement to form a truss mechanism. The activation of the concrete compression field was verified by means of the strain gauges positioned on the stirrups.

As evidenced in Figure 3-62, with the increase of the imposed top displacement the stirrups were mobilised to transfer the shear forces into the joint. At elevated displacements  $8e_y \div 10e_y$ , the transversal re-bars are subjected to high tensile stresses that should equilibrate the compression struts in the outer concrete part of the joint.

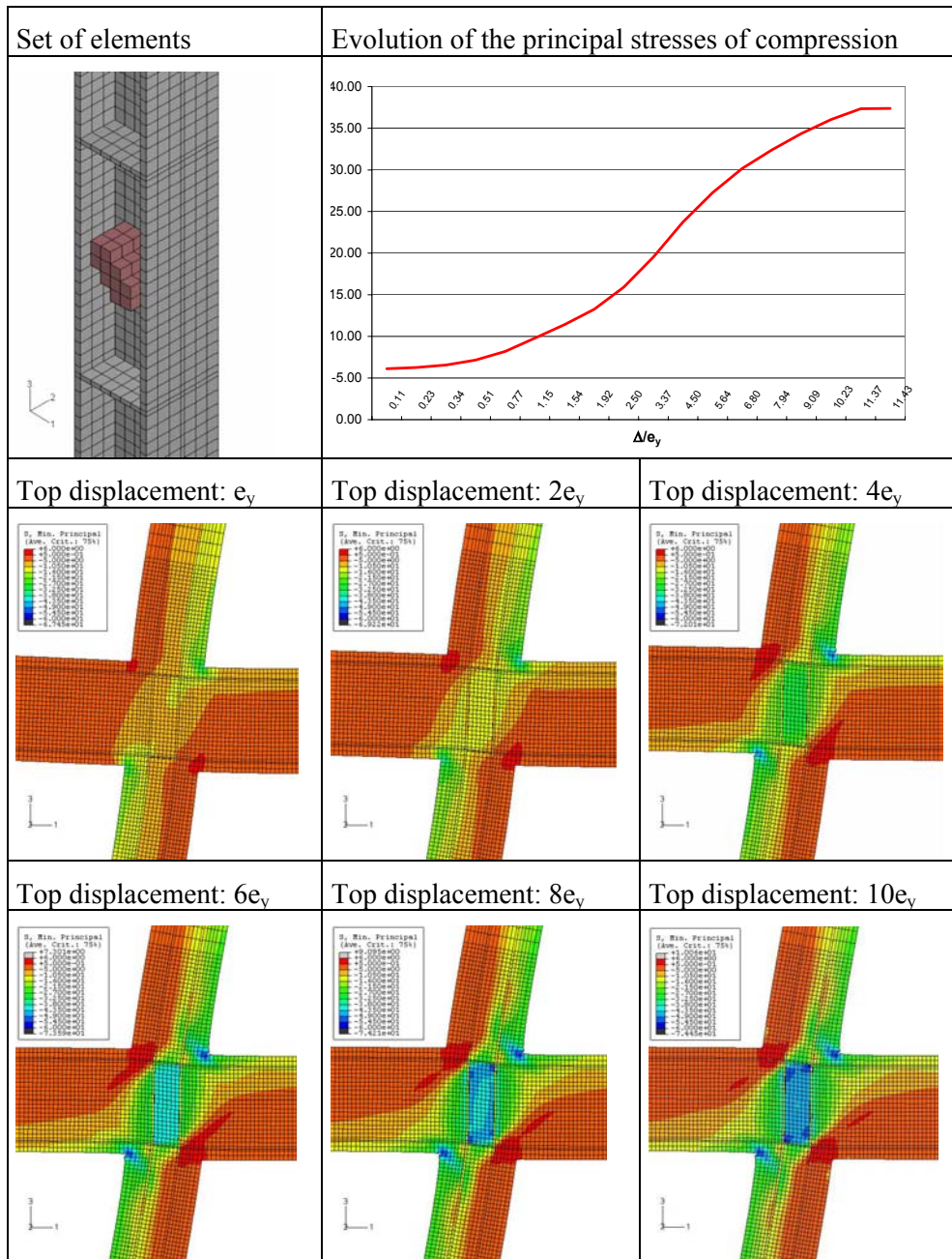


Figure 3-61. Concrete compression strut mechanism –  $\sigma_{\min,prin}$  stresses

The equilibrium of forces results satisfied by the tension and compression stresses in the longitudinal re-bars which transfer the relative component of the compression strut into the column. The evolution of the tensile and compressive stresses in the column was obtained through the elaboration of the Abaqus numerical results. It is also possible to underline that, at elevated imposed top displacements, the deformations of the longitudinal re-bars in the panel zone increase due to the tensile and to the compressive forces transmitted by the concrete.



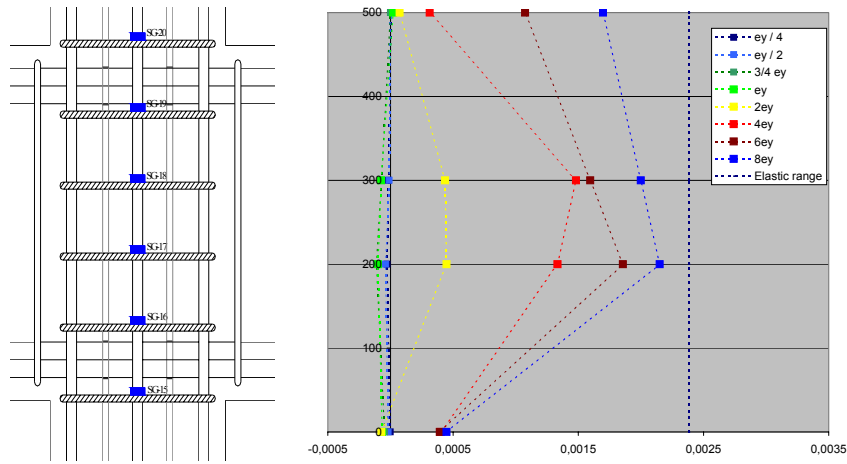


Figure 3-62. Evolution of the measured strain in the stirrups of the column

The Bond Resistance  $V_{j,bf,col}$  is provided by the longitudinal reinforcing bars acting in friction with concrete and embedded in the outer joint region. The bond failure occurs in the outer elements if the compression and tension forces (due to moment equilibrium), along with the forces mobilised in the concrete compression field, are greater than the strength of the bond mechanism of a set of main longitudinal re-bars.

In Figure 3-63, the strain values measured by means of the strain gauges stuck on the longitudinal re-bars of the column are reported. The augmentation of the strains tied to the increase of the top displacement can be noted.

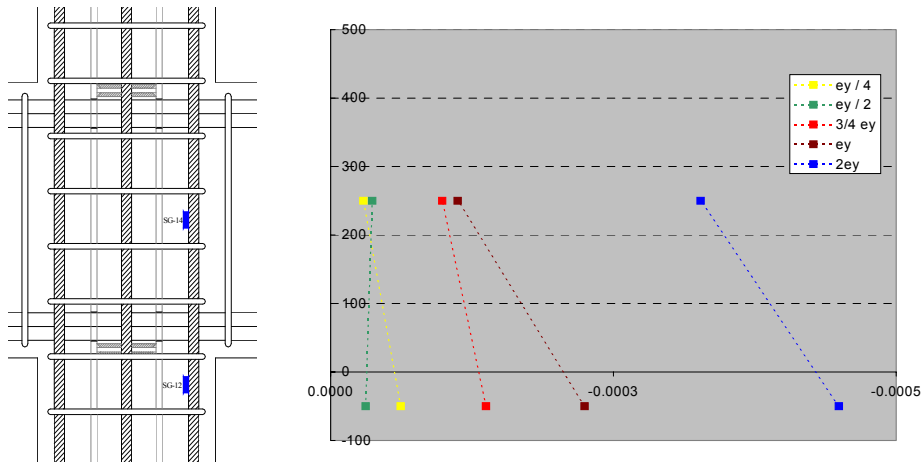


Figure 3-63. Strains of the longitudinal re-bars of the column

The differences between the analytical model, i.e. the equations previously illustrated necessary to determine the single joint mechanism resistance, and the experimental values obtained from the tests in terms of maximum average shear force resisted at the joint region are introduced in the following Table 3-7. The analytical values obtained from the previous equations well agree with the joint shear resistances obtained from the experimental tests in the case that an increase in the shear resistance of the steel web panel (when subjected to high cyclic strains) is allowed. Hence, in equation [3-34], the factor  $\left(\frac{1}{\sqrt{3}}\right)$  is substituted by a value equal to unity:

$$V_{j,wps} = 0,7 \cdot \left( \frac{f_{ym,d,cw}}{1} \cdot \min(A_v; t_{cw} \cdot d_s) + \Delta V_{j,swp} \right) \quad [3-49]$$

It can be noticed that, in this analysis, the single mechanism resistance evaluated by means of the analytical model, does not take into account the partial safety factor value equal to 1.3 as prescribed by the Capacity Design principle. Furthermore, the resistance values are determined considering the real material strengths obtained from specific tests conducted on concrete and steel samples. In fact, it is intended to make a direct comparison to establish the precision of the proposed analytical equations. Of course, at the design stage, it is necessary to account for all the relevant safety factors as already foreseen in the equations previously presented.

Table 3-7. Comparison of analytical and experimental data regarding the shear joint resistance

ANALYTICAL PROCEDURE					
Inner Resistance			Outer Resistance		
Mechanism	$V_{j,Rd}$ [kN]	$M_{j,Rd}$ [kNm]	$M_{j,Rd}$ [kNm]	$V_{j,Rd}$ [kN]	Mechanism
PANEL ZONE	583	230	66	52	CONCRETE COMPRESSION FIELD
CONCRETE COMPRESSION STRUT	134	47			
HORIZONTAL BEARING	1231	437	77	194	BOND
	$M_{j,Rd,MINIMUM}$		$M_{j,Rd,MINIMUM}$		
	277		66		
	$\Sigma M_{j,Rd,MINIMUM}$ [kNm]				
	344				
	$V_{j,Rd}$ [kN]				
Analytical Value	871				
Experimental Value	915				
Difference	-4,8%				



### **3.6. Conclusions on composite columns.**

As a global conclusion of the research it can be stated that the proposed constructional measure, by which a steel profile would be encased in all bottom storey columns of R.C. buildings, can substantially increase the ability of R.C. buildings to resist an earthquake, even in case a soft storey mechanism is possible, because this constructional measure provides a significant increase in the capacity to dissipate energy and a margin of safety on rotation capacity.

The demonstration of this effectiveness has been made for two potential critical zones of reinforced concrete moment resisting frames.

In the University of Liege, the stress in the research was put on a critical zone which is the column itself. Due to locking of deformations by uncontrolled use of infills, the column may become the most stressed zone and clearly reinforced concrete do not provide much ductility in such circumstances. A composite column does it.

In the University of Trento, the stress in the research was put on another critical zone: the beam column panel zone. It is submitted to high shear forces and post earthquake surveys have demonstrated that it is often another weak point in columns of reinforced concrete structures. Composite columns transform this weak zone into a composite shear panel and the tests have demonstrated that an increase in ductility is obtained in that way.

From this two fold approach has been derived the general recommendation to reinforce some strategic points of the building, such as the column of the lowest storey. In that way both potential bending or shear failure in the one storey span of the column and the beam column panel zone can be saved from a local failure and then the structure is protected against global collapse due to these localised brittle failures.

Both anchorage solutions of the steel profile studied in the research, with long and short steel anchorage length revealed to be effective in order to greatly improve the performance of the concrete members in terms of strength and ductility at large deformations. In fact, it can be stated that also the short steel profile stump is able to guarantee an adequate contribution to resistance and ductility in the joint critical region, even if some cracking occurred in the column length between the joint and the inflection point.

The continuity plates (stiffeners) welded to the steel column in the joint region do not seem to give a substantial contribution to the load transfer at the beam-to-column joint. Their use, which in addition is costly, is not necessary.

The mechanisms activated in the shear load transfer at the inside behaviour of the beam-to-column joints were determined. They are presented in 3.4.5 for University of Liege and in 3.5.4 for the University of Trento.

Globally, the proposed innovation brings unquestionable positive results and new concepts of interest for construction practice and for safety.

Further research and testing, both numerical and experimental, are needed to gain knowledge on the following aspects:

- The need of horizontal stirrups in beam-to-column connection zone should be assessed. In practice, these stirrups are difficult to put in place and sometimes omitted. The contribution of the steel profile to shear resistance in the node may be sufficient without stirrups.
- The results given above indicate that short anchorage is as effective as long anchorage of the steel profile. However, this result may be due to the good quality of the concrete in the tests. The anchorage behaviour with low quality concrete has also to be assessed.
- Exploration of a wider range of axial force  $N$  in the column, combined with bending moment  $M$ , is needed to fully assess the proposed construction measure.



## **4. RESEARCH REPORT ON DISSIPATIVE CONNECTIONS FOR FRAMES WITH CONCENTRIC BRACINGS.**

### **4.1. Motivation for using dissipative connections in frames with concentric bracings.**

Seismic resistant steel structures are designed for stiffness, strength and ductility. Stiffness requirements are imposed in order to limit non-structural damage in case of minor to moderate earthquakes and limit instability effects, strength in order to ensure the capacity of the structure to resist safely the action effects and ductility in order to dissipate part of the seismic input energy through inelastic deformations and therefore reduce the action effects. Conventional frames, both unbraced and braced, have certain disadvantages in respect to the above design criteria (Table 4-1, columns 2 to 4).

In addition, braced frames that are widely applied in Europe, face following problems after unusually strong earthquakes that result in some degree of damage: a) for concentric braced frames, the need for strengthening or replacement of damaged and buckled braces which have a certain length and are difficult to handle, b) for eccentric braced frames, the need for strengthening and repair of the links or the beams that are part of the main system that supports gravity loading. Such works require therefore considerable skill and are associated with high material and labour costs.

Table 4-1: Structural typologies and main characteristics for Steel Frames

1	2	3	4	5
	Moment resisting Frames (MRF)	Concentric Braced Frames (CBF)	Eccentric Braced Frames (EBF)	CBF or EBF with dissipative INERD-connections
Stiffness	Low	High	Moderate	High
Ductility	High	Low	Moderate	High
Strength	As required	As required	As required	As required
Dissipative zones at	Beam-ends	Braces	Link beams	Connections

Table 4-1 shows that the dissipative zones in conventional frames are placed within the structural members. An alternative approach is to allow for energy dissipation in the connections rather than in the members. The introduction of flexible, partial strength connections is well known for moment resisting frames subjected to gravity loading. However, the application of semi-rigid connections in seismic resistant moment frames is associated with important problems. Indeed, moment resistant frames are generally flexible structural systems, so that lateral drift limitations at serviceability conditions are in many practical cases the prevailing design criteria. The introduction of semi-rigid connections enhances further the structural flexibility and would magnify the problems, which would not be solved by selection of heavier profiles for beams and columns.

For the above reasons, dissipative connections are better suitable for braced frames. Such frames are generally sufficiently stiff against lateral displacements, so that an introduction of flexible connections would not harm the overall behaviour. On the contrary, flexible connections may protect the braces from buckling and therefore increase the overall ductility. Additionally, any repair works after strong seismic events would concentrate within the connections and would be easier to handle.

In the frame of the INERD research project, dissipative (INERD) connections suitable for braced frames were developed. The advantages of braced frames with INERD-connections (Table 4-1, column 5) in comparison with conventional braced frames may be summarized as following:

- g) Better compliance with the seismic design criteria.
- h) Protection of compression braces against buckling.
- i) Activation of all braces, either in compression or in tension, even at large storey drifts.
- j) Limitation of inelastic action in small parts that may be easily replaced.
- k) Possibility for easy inexpensive repair after very strong earthquakes, if required.
- l) Reduction of overall structural costs for the same performance level.

#### 4.2. Description of the INERD connections and research approach.

Innovative dissipative (INERD) connections are used in seismic resistant braced steel frames for the connection of the braces to the adjacent members (columns or beams). After a brain storming in the initial phase of the project, two types of INERD connections were developed:

##### a) Pin connections

The pin connections consist of two external eye-bars welded or bolted to the adjacent member (column or beam), two internal eye-bars welded to the brace and a pin running through the eye-bars (Fig 4-1). In this type of connection the pin exhibits inelastic bending deformations and dissipates energy due to the fact that the eye-bars are placed at some distance between each other.

##### b) U-connections

The U-connections consist of one or two bent, U-shaped thick plates that connect the brace to the adjacent member (Fig. 4-2). Here again, energy dissipation takes place in the bent plate(s).

The advantage of these connections is that, by appropriate sizing, inelastic deformations are limited within exactly predetermined zones, the pins or the U-plates, whereas the adjacent parts remain elastic. Consequently, braces are protected from buckling and damage is restricted in the pins or the U-plates. These are small parts that may be easily replaced if they are largely deformed, after an unusually strong earthquake.

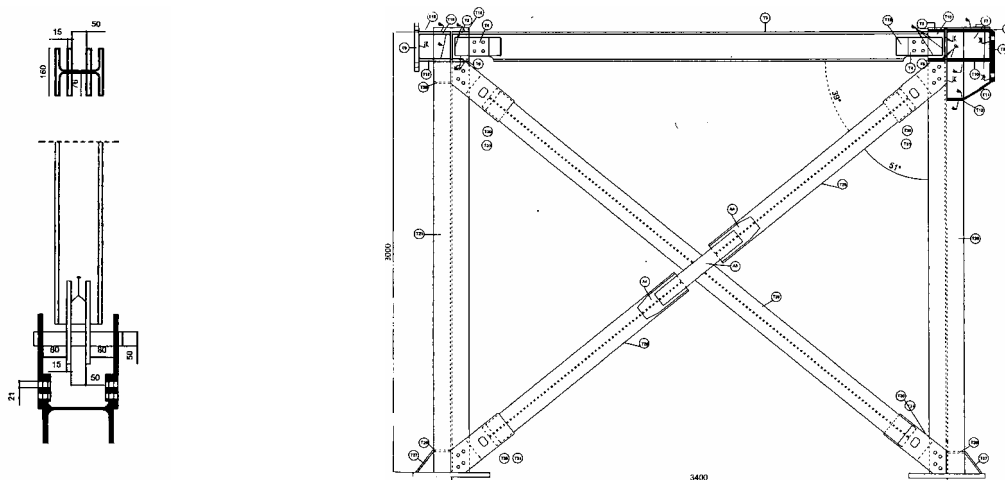


Figure 4- 1: INERD pin connections in the test frame at Milano.

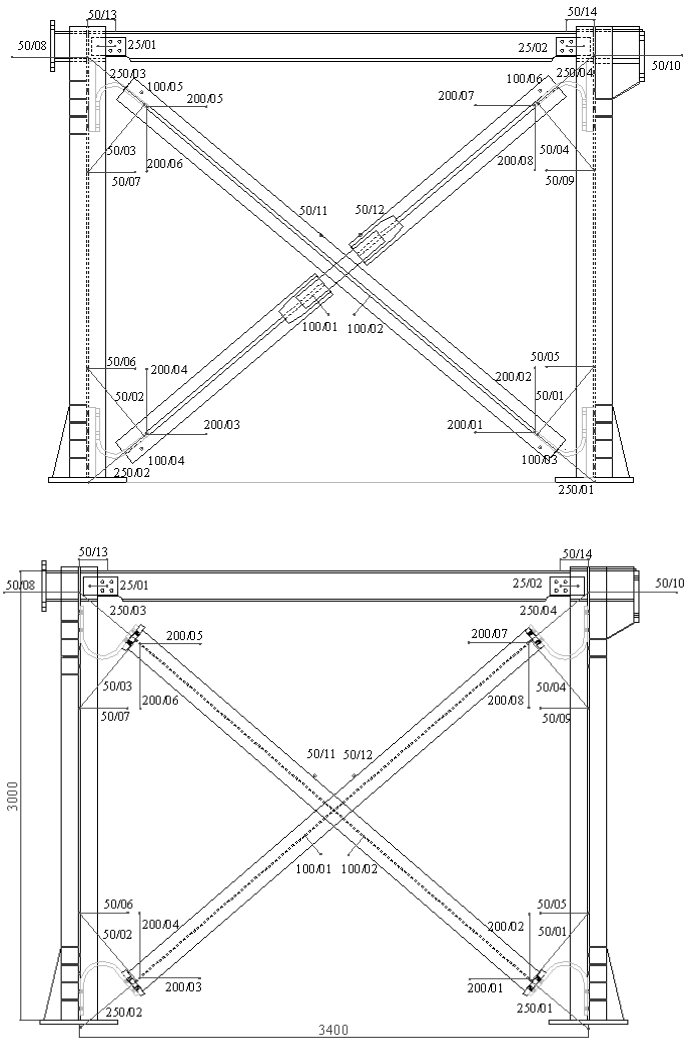


Figure 4- 2: INERD U-connections in the test frame at Milano.

The research work on connections took 3 logical steps:

- The behaviour of the connections considered alone and outside of any frame effect was studied in a horizontal test machine at IST Lisbon (see 4.3)
- The experimental response of frame with concentric bracing was studied in a dedicated set up at Politecnico di Milano (see 4.4)
- At the National Technical University of Athens, theoretical or numerical approaches of the behaviour of the connections and of the behaviour of representative frame structures using the INERD connections were made to assess the practicability of this new technology. (see 4.5).

### 4.3. Tests on single connections.

#### 4.3.1. Test setup and test programme.

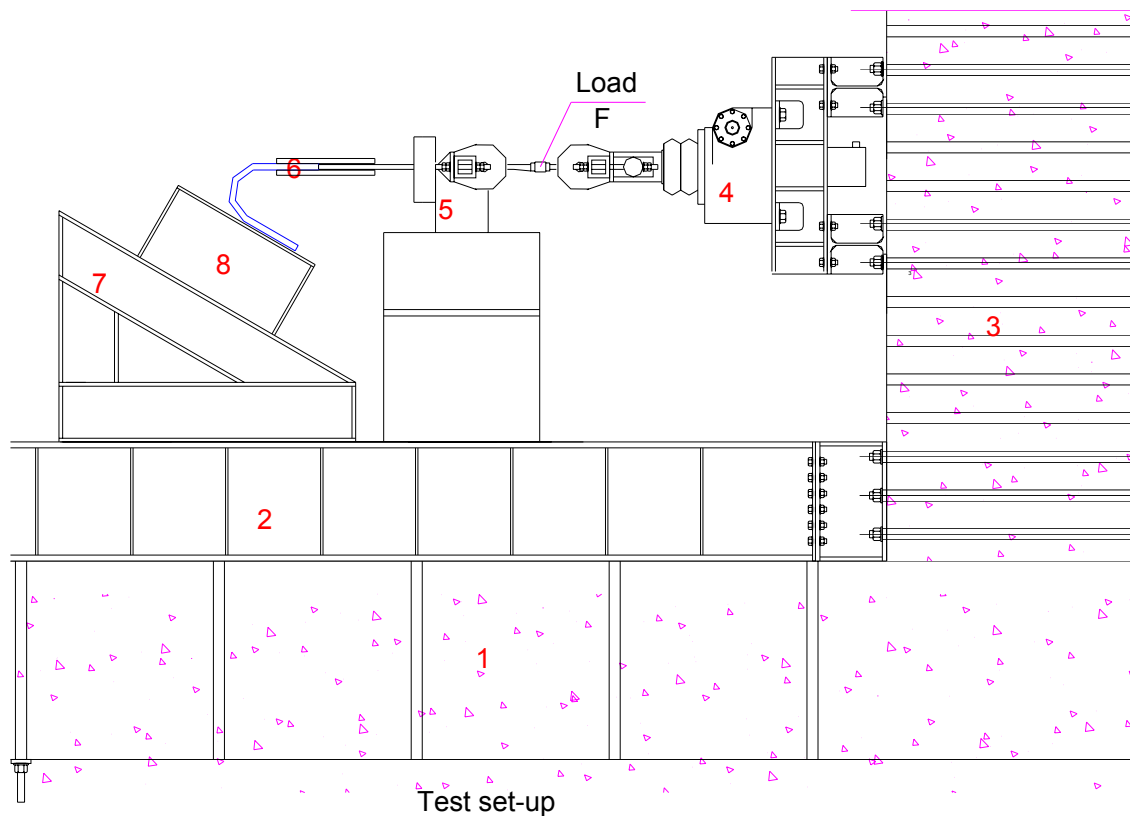


Figure 4.3. Test set up at IST Lisbon

The fixed equipment consists basically of 1) a foundation, 2) a beam of base 3) a reaction wall 4) an actuator 5) a trolley 6) a part of transition between device-actuator 7) a frame of reaction 8) pieces for Set-Up. Experimental tests on the cyclic behaviour of two types of dissipative devices were developed at Instituto Superior Técnico at Lisbon. These dissipative devices can be observed at Figure 4.4.

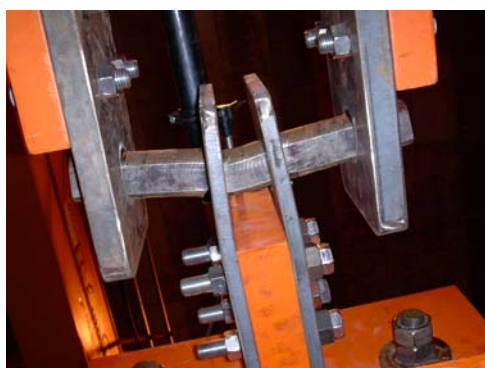


Figure 4-4. U-Devices



Pin devices

### Pin connections

The parameters analysed with Pins specimens are:

- distance between the eye-bar plates (50 mm or 70 mm);
- shape (rounded or rectangular).

Loading:

- monotonic tests (traction and compression);
- cyclic tests following the ECCS testing procedure
- cyclic tests with constant amplitude.

In the case of rectangular Pins amplitudes were always 30, 40, 50, 60 mm.

In the case of circular Pins amplitudes were always 40, 60 mm.

In every tests bolts M20 class 8.8 were utilized.

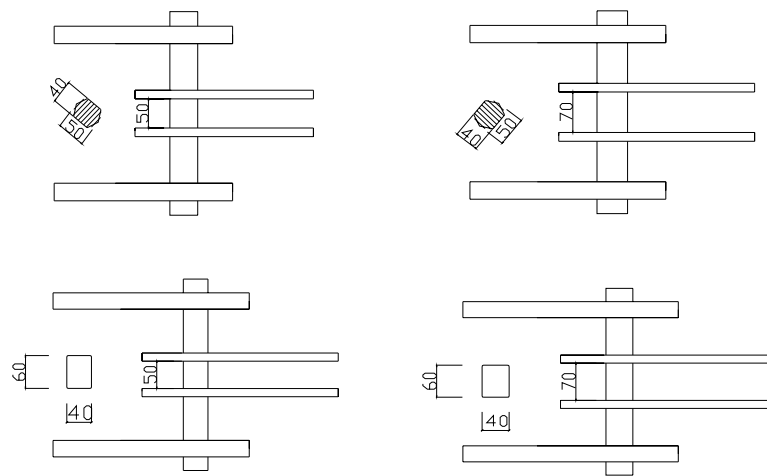


Figure 4.5. Pin specimens.

### U connections

The parameters analysed with U connections are:

- Type : number of factory
- R : radius
- B : Length of plate
- e : Thickness
- Position : load way

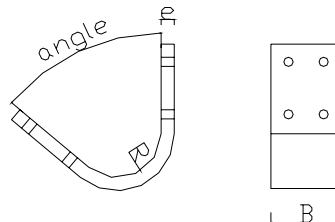
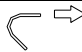
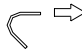
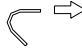
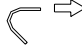
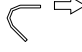
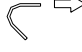
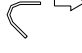






Figure 4.6. Definition of parameters for U connections

Table 4-2. Tests on U connections

type	R	B	e	angle	position
2	100	160	25	45	
3	100	160	25	50	
4	100	160	30	50	
5	125	160	30	50	
6	125	160	25	30	
7	125	160	25	45	
8	125	160	25	50	
9	125	160	25	30	
10	125	160	25	39	
11	125	160	25	45	
12	125	160	30	39	

Every U-Device was subjected to:

- monotonic tests (traction and compression);
- ECCS test;
- tests with constant amplitude.

The amplitudes were always 40, 80, 120, 160 mm. Only in the case of U-Device type 12, tests with constant amplitude of 120 mm have not been realized.

In most tests, bolts M20 class 8.8 were used. For U-Device type 10 and 12, bolts M24 class 12.9 were used.

#### Elaboration of Test Data

All test data were elaborated using specific softwares developed at IST. In the complete laboratory report, the following results are presented in detail:

- hysteresis loops of the frame response, in terms of the applied force (kN) vs. imposed interstorey drift;
- absorbed energy of the framed vs. n° cycles;
- cumulative absorbed energy of the frame vs. n° cycles;
- rigidity of the frame vs. n° cycles.
- maximum and minimum Force;
- maximum and minimum displacement;
- yield Force and yield displacement;
- Total number of cycles.



### 4.3.2. Results in terms of energy dissipation capacity

#### Pin connections.

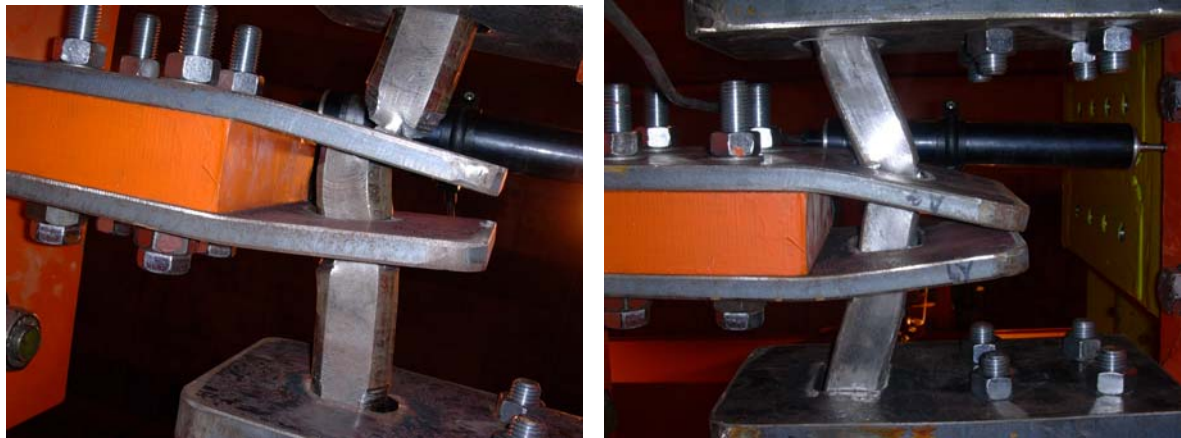


Figure 4.7. Deformed pin connections after test

The comparisons between pins have been made in function of the distance between plates (50 or 70 mm) and for a same distance, in function of the geometrical characteristics (circular Pin or rectangular Pin).

The comparison terms have been the number of cycles until the rupture and the absorbed total energy. In these terms the dissipative behaviour improves generally with increasing of the distance of the plates.

The dissipative behaviour of rectangular Pins is better than circular Pins, independently of the distance of plates. However the opposite result was obtained by ECCS tests in Milan. Therefore it should be useful to continue the investigation realizing ulterior tests in frames with constant amplitude loading history.

The better dissipative behaviour of rectangular Pins with respect to circular Pins can be justified by the greater inertia of rectangular Pin than circular one.



Figure 4.8.

Circular Section

Rectangular section

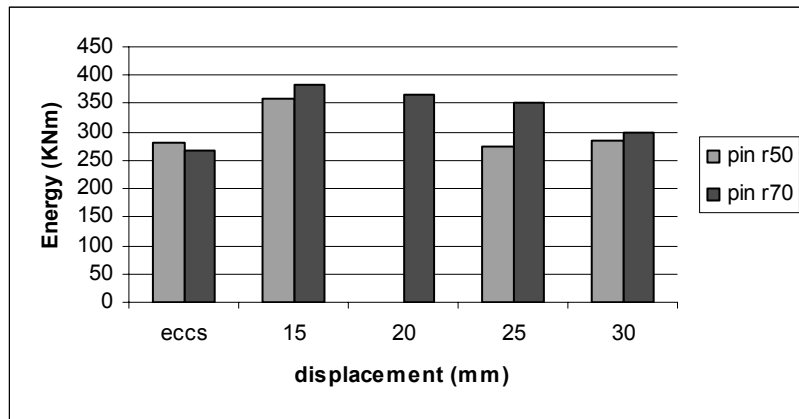


Figure 4.9. Rectangular Pins r50 (distance of plates 50mm) and r70 (distance of plates 70mm)

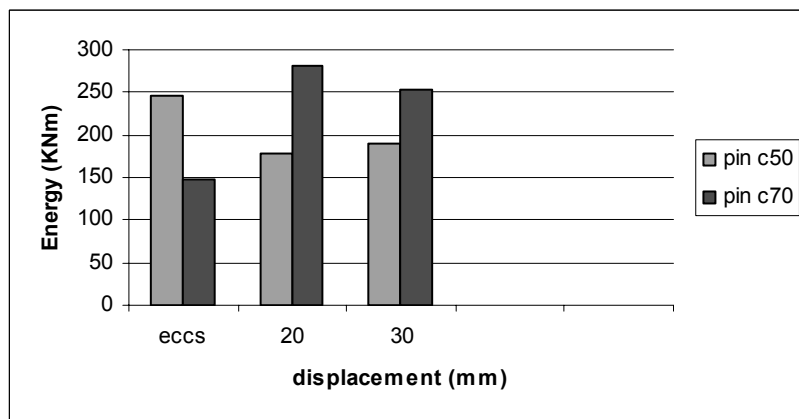


Figure 4.10. Circular Pin c50 (distance of plates 50mm) and c70 (distance of plates 70mm)

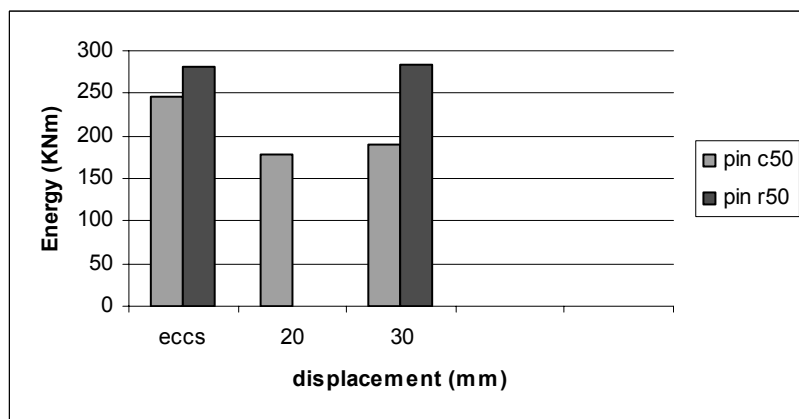


Figure 4.11. Distance of plates 50mm. Pin c50 (circular) and Pin r50 (rectangular)

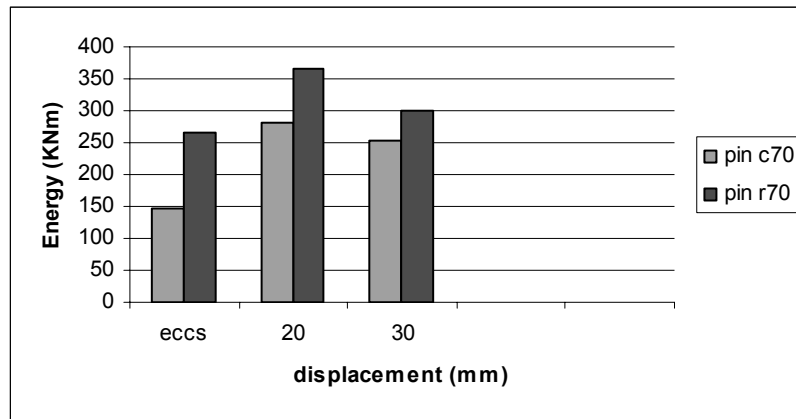


Figure 4.12. Distance of plates 70mm. Pin c70 (circular) and Pin r70 (rectangular)

U connections.

The behaviour of all U connections have first been compared in function of the position of application of the load (parallel or perpendicular to connecting plate). For the same position of load application, U-Devices have been compared in function of the angle, the thickness and the radius.

The comparison terms have been the number of cycles up to failure and the total energy absorbed. In terms of the dissipative behaviour, U-Devices loaded parallel to the connecting plate behave better than those loaded perpendicularly to connecting plate. A better dissipative behaviour of connections exists when the angle is different of 45°. The dissipative behaviour improves with decreasing of the thickness. The dissipative behaviour improves with increasing of the radius.

The U-Device with the best dissipative behaviour is characterised as follows:

- loading parallel to connecting plate
- e=25mm
- R=125 mm

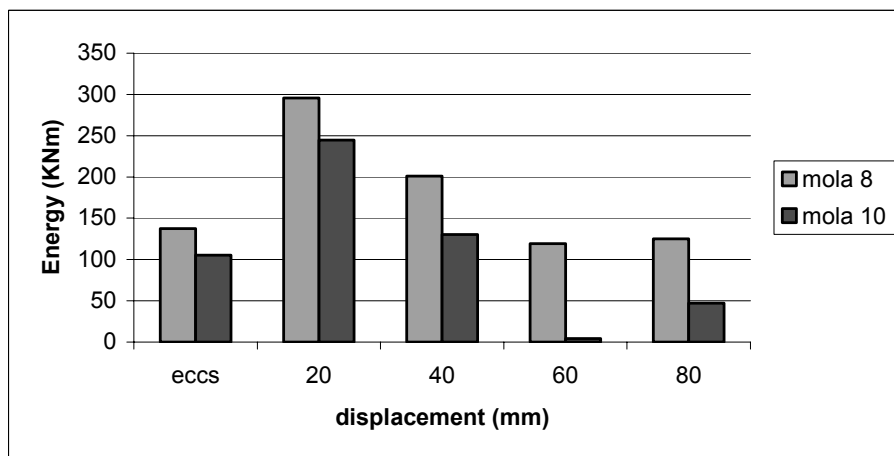


Figure 4.13. Parallel position (mola 8) vs. Perpendicular position (mola 10)

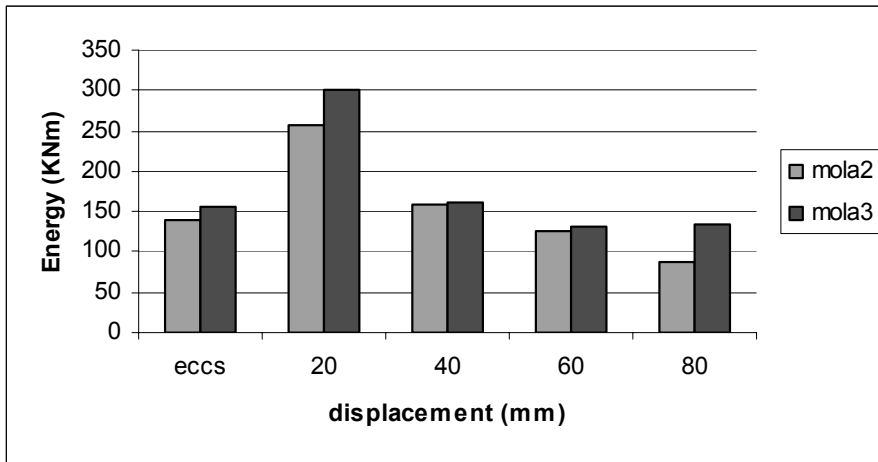


Figure 4.14. Angle: mola 2 ( $\alpha=45^\circ$ ); mola 3 ( $\alpha=50^\circ$ )

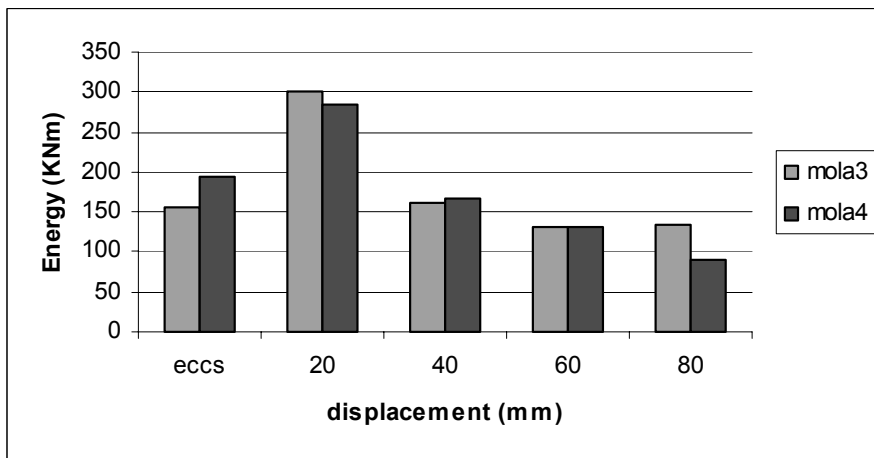


Figure 4.15. Thickness: mola 3 ( $e=25\text{mm}$ ); mola 4 ( $e=30\text{mm}$ )

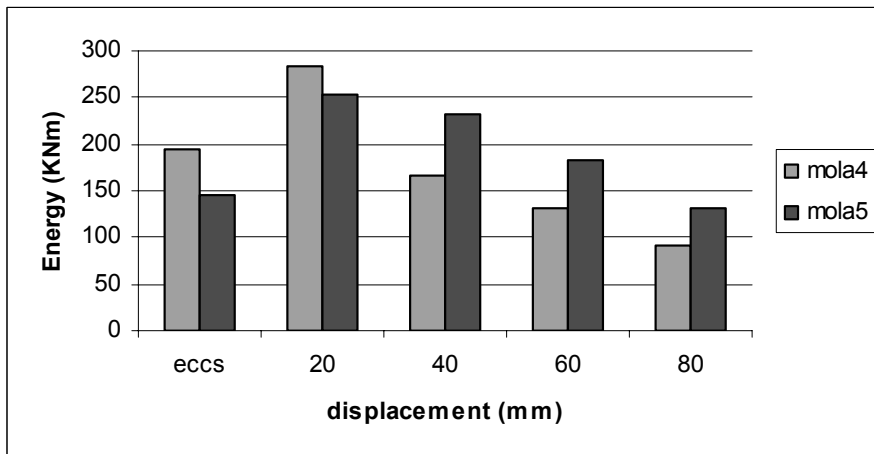


Figure 4.16. Radius: mola 4 ( $R=100\text{mm}$ ); mola 5 ( $R=125\text{mm}$ )

## Global comparisons

One of the most interesting results is the different behaviour of the Pin and the U-Devices.

Figure 4.17 shows that the force necessary to obtain a given displacement in Pins is higher when compared with the U-Devices.

Pins have a larger strength instead U-Devices allow larger deformation.

Pins dissipate more energy than U-Devices because Pins attain the plastic moment earlier than U-Devices.

It seems that the best dissipative connecting device for concentric bracings is Pin with a rectangular section and a large distance between the eye-bar plates.

In relation with U-Devices, the best performance can be obtained with parallel load type with radius 125 mm and thickness 25 mm.

However, the best performance for the U-Device can be obtained by decreasing the thickness and increasing the radius.

From a practical point of view Pins are easier to be put in place within the structure and to be removed than with U-Devices.

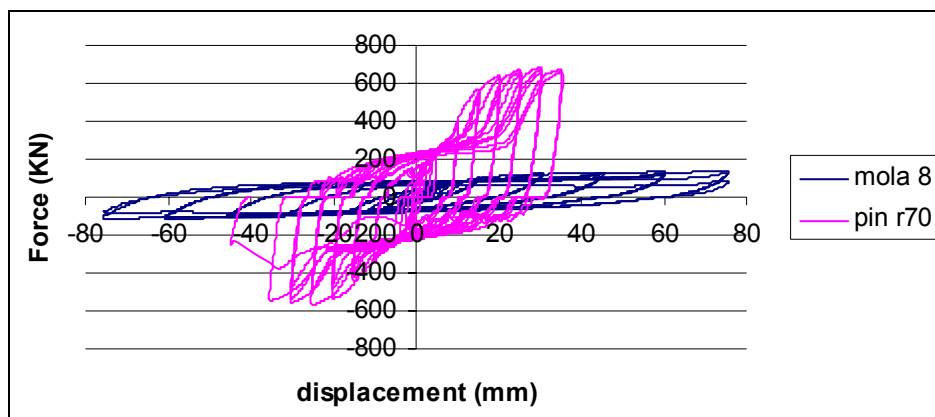


Figure 4.17. Comparison U-device vs. Pin

### 4.3.3. Results in terms of Fatigue

The method for re-elaboration of test data of devices under cyclic action is based on S-N line approach. Because of its simplicity, the S-N curve approach has been introduced into many fatigue design codes. As this approach allows to interpret correctly the phase of stable propagation of cracks, it is commonly adopted in civil engineering for the assessment of the fatigue strength. The fatigue resistance curves adopted in design Standards are built using a statistical analysis of constant amplitude fatigue test data. If variable amplitude (ECCS) loads are used, the direct assessment of the fatigue resistance is not possible and reference should be made to cycle-counting method (rainflow) and to a suitable damage accumulation rule. Usually the linear damage accumulation rule proposed by Miner is adopted for calculation of an effective value; in case of variable amplitudes, an equivalent amplitude  $S_{eq}$  is adopted instead of S as argument in the fatigue failure prediction.

All test data were elaborated using specific software developed at IST.

A first software called “**Rainflow**” permits to calculate  $S_{eq}$  in cases of cycles with variable amplitudes. In this software it is enough to enter the total number of plastic cycles ( $N_{tot}$ ) and the load history to obtain the  $S_{eq}$ .

The second software called “**S-N curves**” permits to calculate experimental and design data and to draw the experimental S-N line and the design S-N line. In this software it is enough to introduce the characteristics of connections (i.e., yield force, yield displacement, total number of plastic cycles and amplitude of cycles), to obtain the experimental S-N line and the design S-N line.

Fatigue of U connections. Comparisons

The parameters are : position of application of the load (parallel or perpendicular), angle, thickness and radius of the plate. The comparison terms have been the best fit lines, design curves, and EC3 lines. In terms of the fatigue behaviour, U-Devices loaded parallel behaves better than those loaded perpendicular. For the parallel load case it was observed:  
 A better fatigue behaviour of connections exists when the angle is different of 45°. The fatigue behaviour improves with decreasing of the thickness. The fatigue behaviour improves with increasing of the radius.

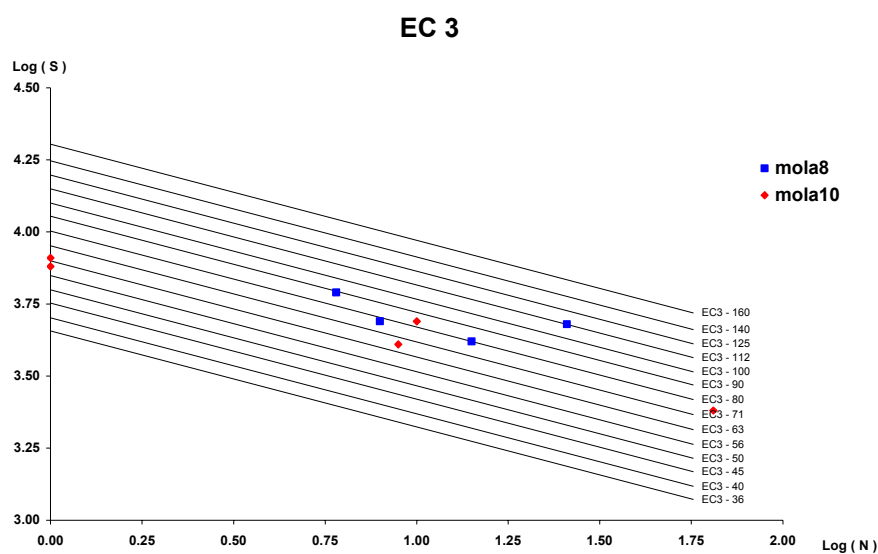


Figure 4.18. Parallel position (mola 8) vs. Perpendicular position (mola 10)

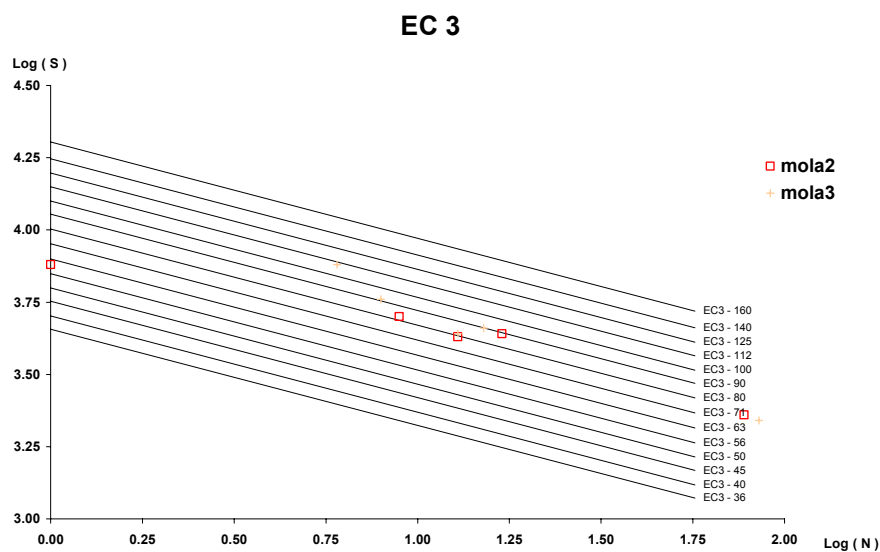


Figure 4.19. Angle: mola 2 ( $\alpha=45^\circ$ ); mola 3 ( $\alpha=50^\circ$ )

### EC 3

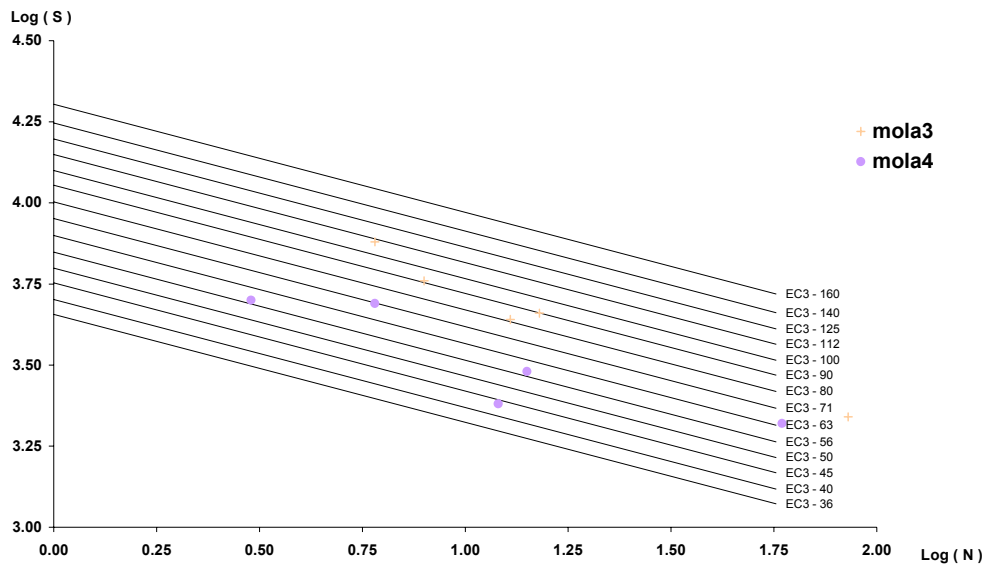


Figure 4.20. *Thickness*: mola 3 (e=25mm); mola 4 (e=30mm)

### EC 3

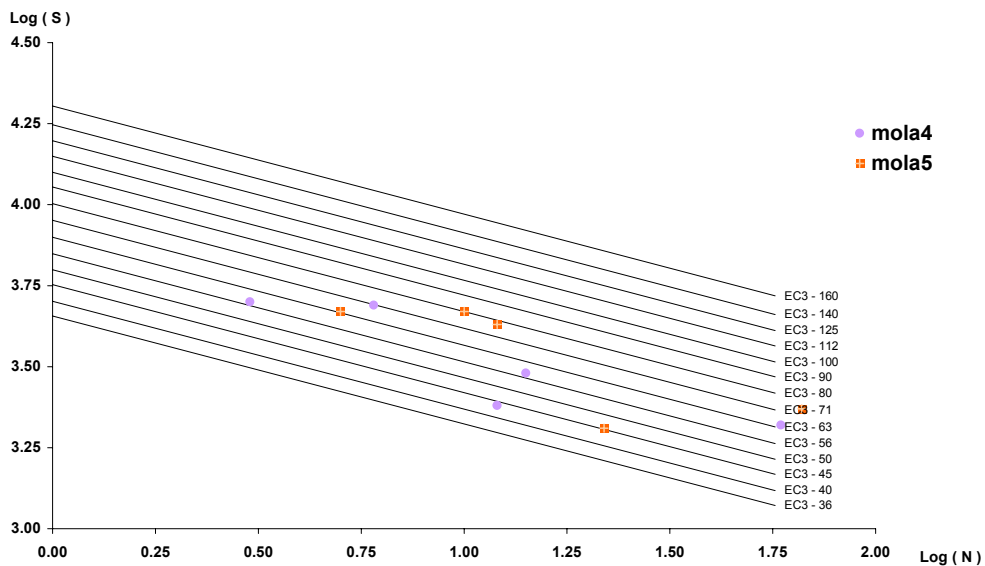


Figure 4.21. *Radius*: mola 4 (R=100mm); mola 5 (R=125mm)

#### Fatigue of Pin connections. Comparisons of the results.

The parameters are: distance between the plates (50 or 70 mm), geometrical characteristics (circular pin or rectangular pin). The comparison terms were made for the best-fit lines, design curves, and EC3 lines. The fatigue behaviour of circular Pin is better than the one of rectangular Pin, independently of the distance of plates.

The fatigue behaviour of circular Pin increases with decreasing of the distance of plates.

Fatigue behaviour of rectangular Pin increases with increasing of the distance of plates.

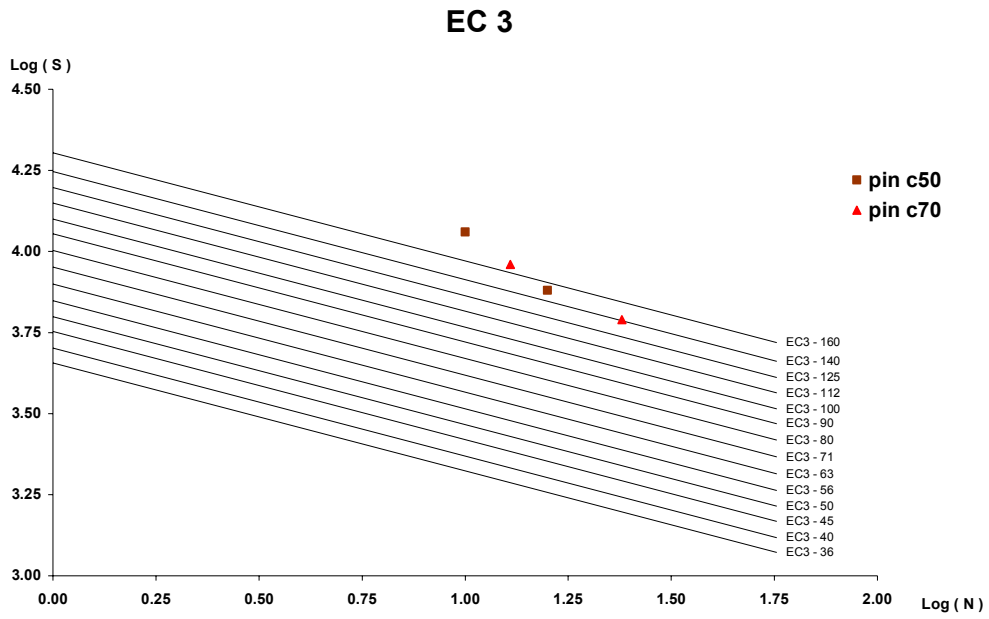


Figure 4.22. *Circular Pin*: Pin c50 (distance of plates 50mm); Pin c70 (distance of plates 70mm)

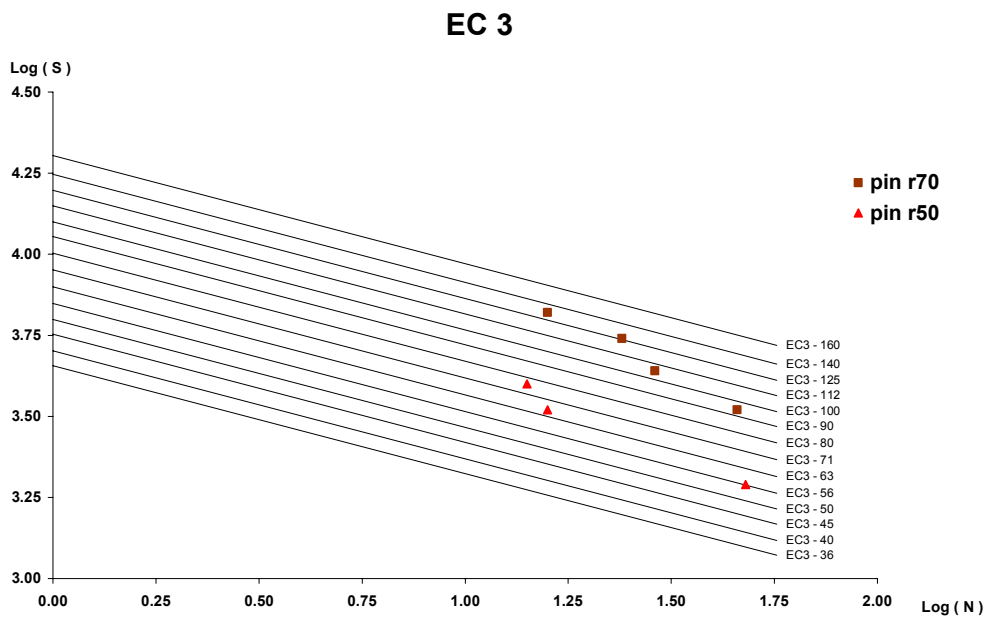


Figure 4.23. *Rectangular Pin*: Pin r50 (distance of plates 50mm); Pin r70 (distance of plates 70mm)



### EC 3

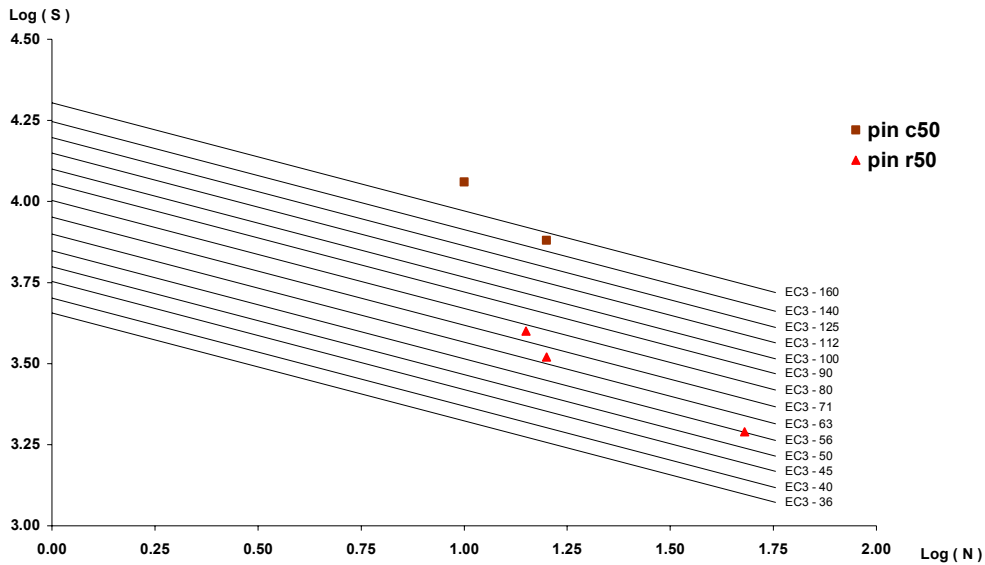


Figure 4.24. Distance of plates 50mm: Pin c50 (circular); Pin r50 (rectangular)

### EC 3

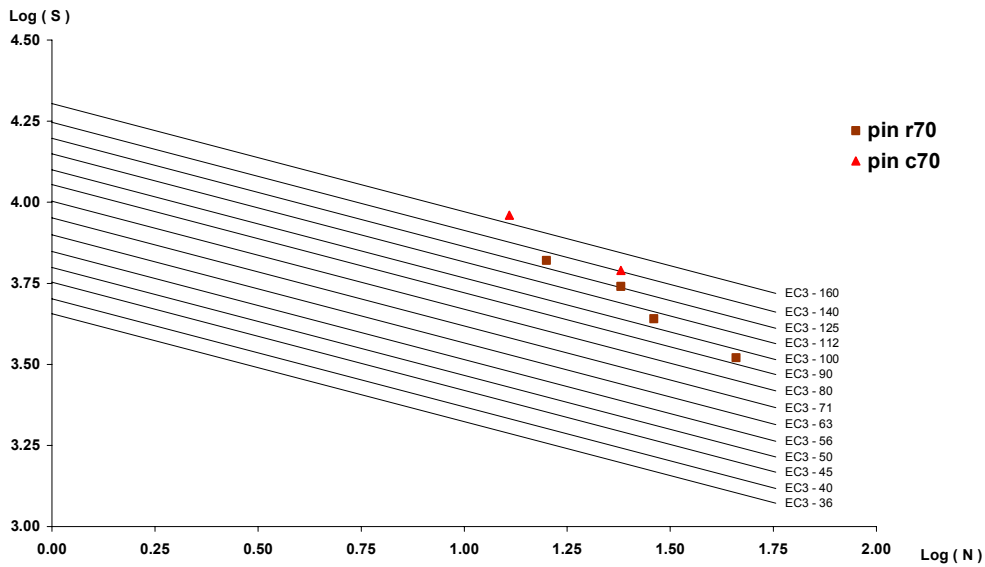


Figure 4.25. Distance of plates 70mm: Pin c70 (circular); Pin r70 (rectangular)

#### **4.4. Tests on frames with concentric bracings and dissipative connections.**

##### **4.4.1. Test set up and test programme.**

This activity performed at Politecnico di Milano consists in an experimental work on large scale frames made in order to characterise the global behaviour of frames in which connections are dissipative and belong to one of the two types developed in the INERD project.

In order to choose the device with best performance, the following constraints were considered:

- Sufficient elastic stiffness, in order to limit the interstorey drift
- $R_{\text{connection}} < N_{\text{bracing}} = \min(N_{\text{tension}} \text{ or } N_{\text{buckling}})$
- Significant deformation capacity to reach 3 % drift

in our case: (90 mm)       $\Delta_{\text{diagonal}} = 68 \text{ mm}$

$\Delta_{\text{connection}} = \Delta_{\text{diagonal}} / 2 = 34 \text{ mm} = 3 \% \text{ diagonal length}$

Specimens and details were designed and chosen taking into account the following criteria:

<u>CRITERIUM 1</u>	Same device specimens (both pins and U) for both: Lisbon tests (small scale for characterization of device behaviour) Milano tests (large scale for global behavior characterization)
Motivation	Better comparison and interpretation of test results
Consequences	In Lisbon a thorough parametric study will be performed, while in Milano only 4 + 4 geometries will be tested in full scale frame configuration
<u>CRITERIUM 2</u>	All test-frame members and connection plates should remain elastic while plastic deformations occur only in the devices and, eventually in the diagonals' connection plates (eye-bars) in bearing.
Motivation	Steel saving, as only two frames should be constructed
Consequences	Oversizing connection plates (for bearing) and welds (for fatigue)
<u>CRITERIUM 3</u>	Two different geometries for pin devices: Rectangular (original I.Vayas design) Circular sectioned (modified design)
Motivation	Avoid torsional stresses in the pin as well as stress concentrations in sharp edges of eye-bars
Consequences	2 pin geometries each one with 2 distances of eye-bars to be tested in frame configuration
Motivation	Explore possible situations recurring in practice
Consequences	2 geometries of diagonal members (HE 160 B or 2 UPN220) 2 geometries of U device, each one with 2 different thicknesses and radiuses of curvature

The experimental phase of the research carried out in Milan is performed on large size specimens. It is aimed at investigating the influence of two types of dissipative devices (connecting the bracing members to the frame) on the structural response.

Sixteen experimental cyclic quasi-static tests were performed on two typologies of connections: PIN and U-DEVICES. The tests results were re-analysed and compared, in order to assess the influence of the main geometric parameter on the response of the devices.

The test specimens were designed so that the beam and columns as well as the diagonal members remained elastic, while the plastic deformation was concentrated in the “dissipative devices” connecting the diagonals to the columns.

Tests may be divided in two different categories due to the different type of devices (PINS or U devices).

Concerning the first ones, we can distinguish four different configurations defined by the geometry of the pin section (rectangular or rounded) and the distance (d) between the eye bar plates on the diagonal (Figure 4.26 and Table 4.3).

Table 4.3 – Different pin tests

Test	Loading History	Pin Shape	d (mm)
INERD 01	ECCS	Rounded	50
INERD 02	ECCS	Rounded	70
INERD 03	SEISMIC	Rounded	50
INERD 04	SEISMIC	Rounded	70
INERD 05	ECCS	Rectangular	50
INERD 06	ECCS	Rectangular	70
INERD 07	SEISMIC	Rectangular	50
INERD 08	SEISMIC	Rectangular	70

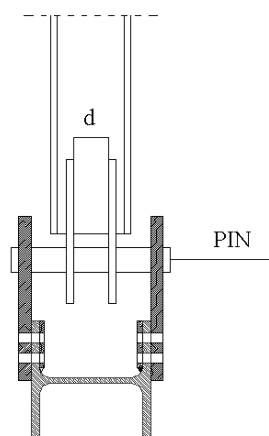
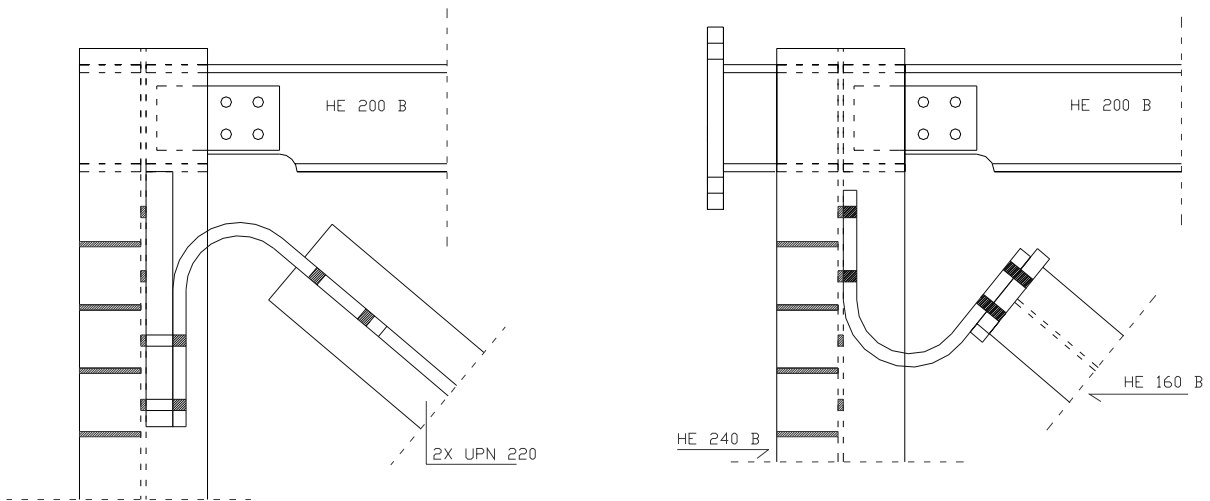


Figure 4.26 - Pin connection characteristics

For each of the four configurations two tests were carried out: a cyclic test performed according to the ECCS standard testing procedures and a seismic one.

The seismic test was performed imposing in a cyclic quasi-static way the displacement history obtained by NTUA by numerically simulating the response of a frame structure similar to the one under the test, subjected to the Thessaloniki earthquake. The numerical model adopted to obtain the displacement history to be imposed to each device was calibrated on the cyclic test results of similar geometry.

U-devices can be identified in terms of their thickness, radius and typology of the connection to the diagonal (Fig. 4.27).



U1 typology of connection

U2 typology of connection

Figure 4.27- U connections typologies

This last feature defines the operative aspects of assemblage of the specimens, as well as the “opening” angle  $\alpha$  of the U device, and the shape of the diagonal member (Figure 4.28 and Table 4.4).

For U-devices only cyclic tests were performed.

Table 4.4 - Different U connections

Test	$\alpha$	Radius (mm)	Thickness (mm)
INERD 09	50	125	25
INERD 10	50	100	25
INERD 11	50	125	30
INERD 12	50	100	30
INERD 13	40	100	30
INERD 14	40	100	25
INERD 15	40	125	30
INERD 16	40	125	25

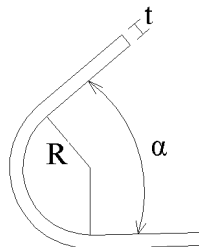


Figure 4.28- U-device characterization

## 4.2.2. Results

The permanent deformation of the pin, at the end of the test, and its eventual failure allow us to know which of the four pins was subjected to the largest ductility demand. In these tests, this was always the top right pin, the one placed in the joint connected to the jack.

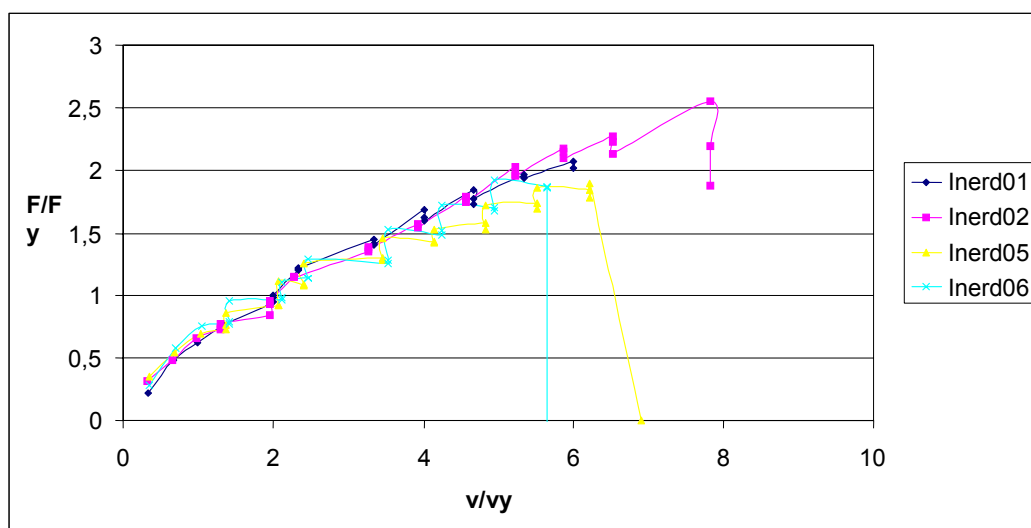
For tests on U1 type devices, the top right connection is the one that was subjected to the largest ductility demand

Instead, for U2 type, the highest deformation occurred in the bottom left device. Only in test 14, maximum damage cumulated in the bottom right spring.

### PINS

For the same distance between the eye-bar plates (both 50 mm and 70 mm) the rounded pins have a better performance than the rectangular ones, as they can sustain a larger force. For small cycles the rectangular section (with slightly larger inertia) are stronger, however for large deformations (large amplitude cycles) the rounded section seems to have a better performance, because the torsional effects are smaller.

The best performance can be obtained with the maximum distance between the eye-bar plates, maximizing the energy absorption capacity of the device.



**Figure 4.29. Pins**

According to the frame statics and kinematics, the following relationships are valid:

Relation between global frame lateral displacement and pin deflection :

$$\delta = \frac{\Delta \cdot \cos \phi}{2}$$

Relation between global frame lateral force P and pin axial force F:

$$F = \frac{P}{2 \cdot \cos \phi}$$

Taking into account that the slope of the braces in the tests was approximately 39 degrees, the following figures show a comparison between theoretical values and experimental results.

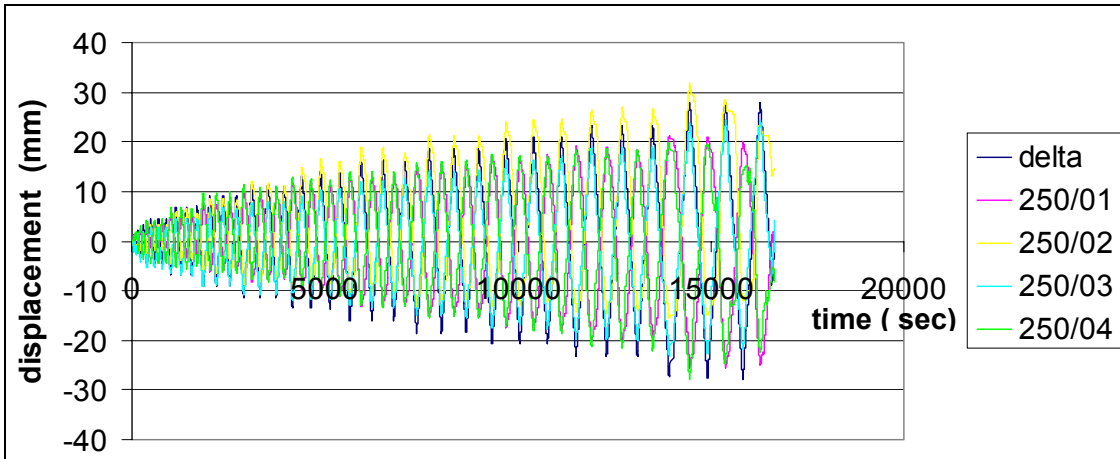


Figure 4.30. Comparison between theoretical value of  $\delta$  (delta) and the pin deflections measured in test 02. (circular  $d=70$  mm)

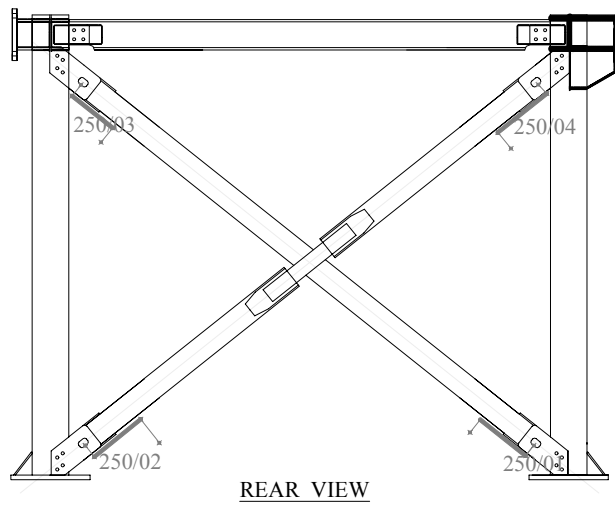


Figure 4.31. Position and name of the different pin connections in test 02

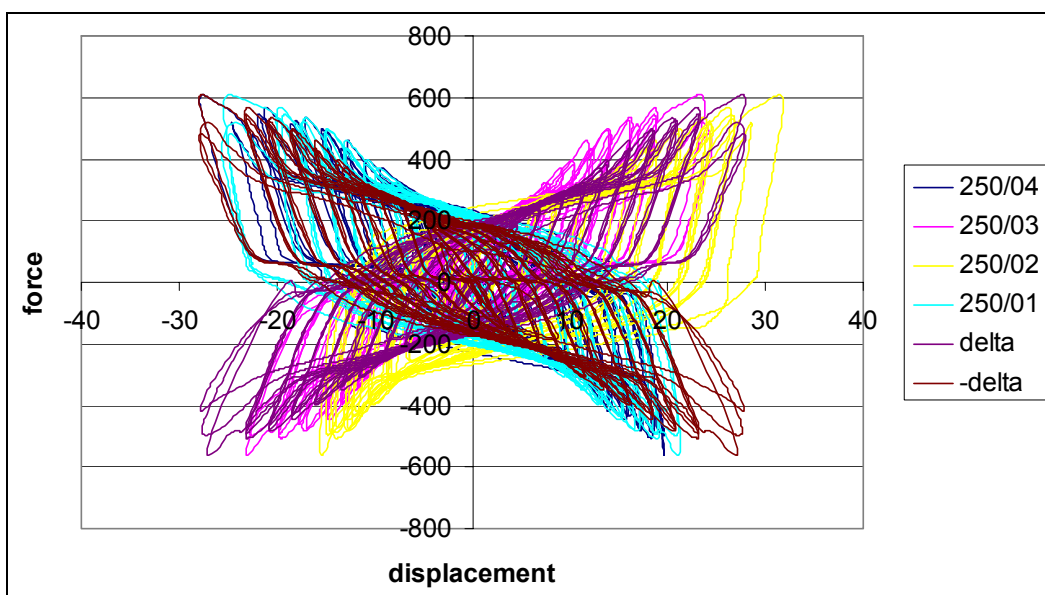


Figure 4.32. Comparison of the experimental and theoretical hysteresis loops in terms of Force in the diagonal (kN) and pin deflections  $\delta$  (mm) in test 02

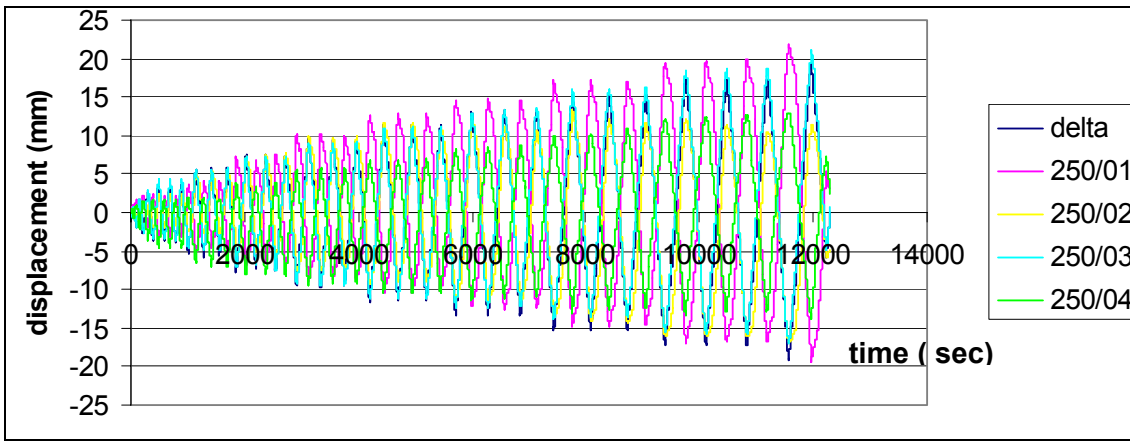


Figure 4.33. Comparison between theoretical value of  $\delta$  (delta) and the pin deflections measured in test 05. (rectangular  $d=50$  mm)

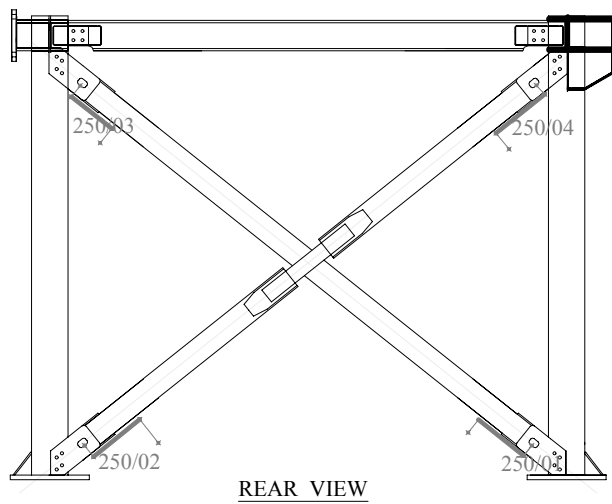


Figure 4.34. Position and name of the different pin connections in test 05

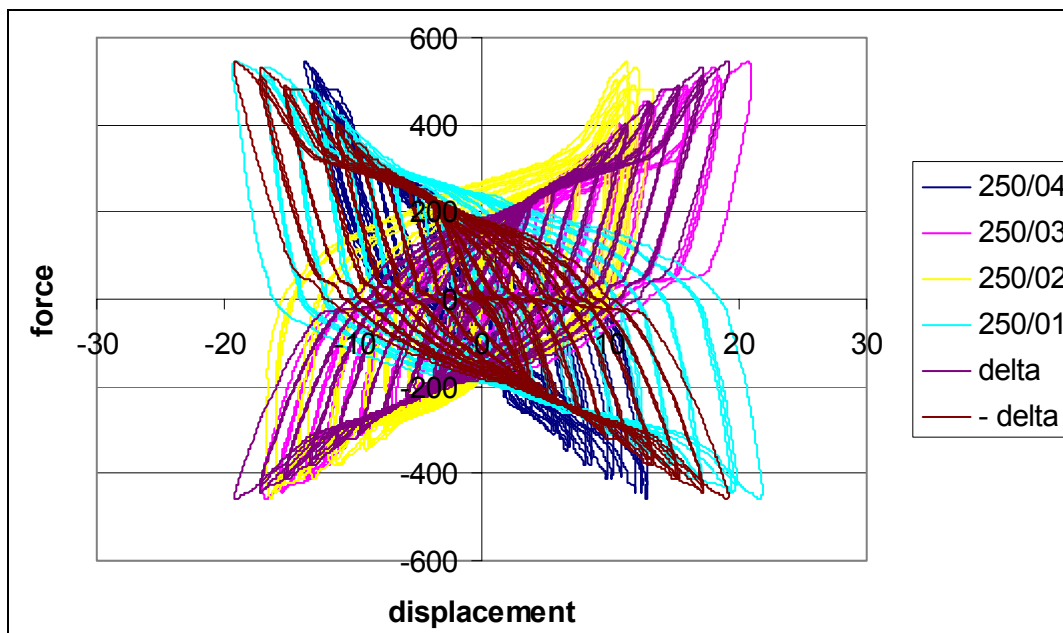


Figure 4.35. Comparison of the experimental and theoretical hysteresis loops in terms of Force in the diagonal (kN) and pin deflections  $\delta$  (mm) in test 05

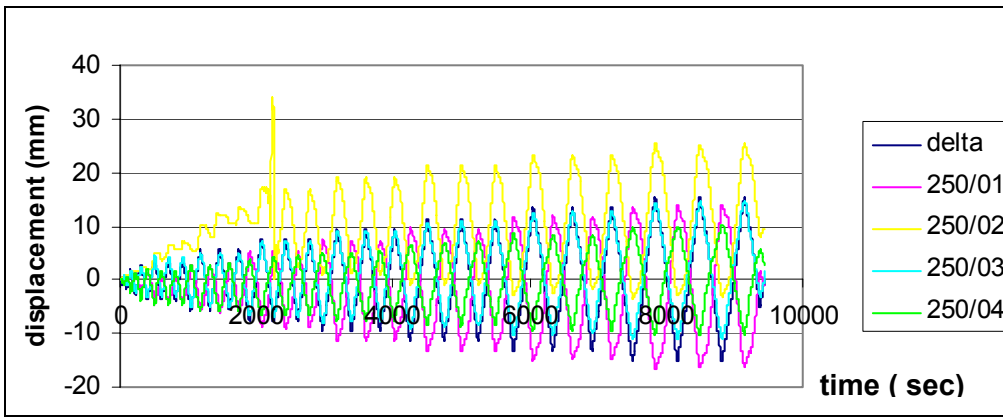


Figure 4.36. Comparison between theoretical value of  $\delta$  (delta) and the pin deflections measured in test 06. (rectangular  $d=70$  mm)

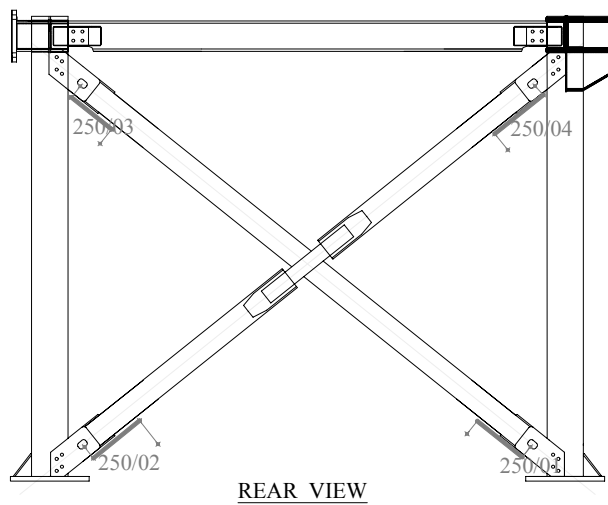


Figure 4.37. Position and name of the different pin connections in test 06

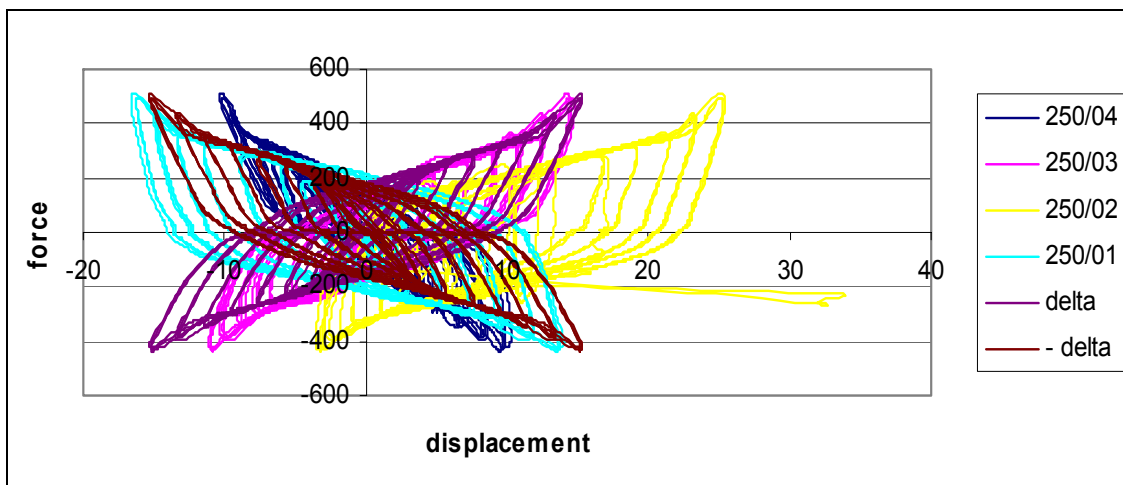


Figure 4.38. Comparison of the experimental and theoretical hysteresis loops in terms of Force in the diagonal (kN) and pin deflections  $\delta$  (mm) in test 06



## U-devices

In the case of U-Devices, a radius of 100 mm allows better energy dissipation than the radius of 125 mm, for the same thickness (both 25 mm and 30 mm), and device configuration (U1 or U2).

The best behaviour of U-Devices is obtained with a larger thickness (e.g. 30 mm) and a small radius (e.g. 100 mm). This is evident, because increasing the thickness and reducing the radius results in a larger bending stiffness of the device.

So, as a general conclusion we can state that the best performance of the U-Device can be obtained by increasing the thickness and decreasing the radius.

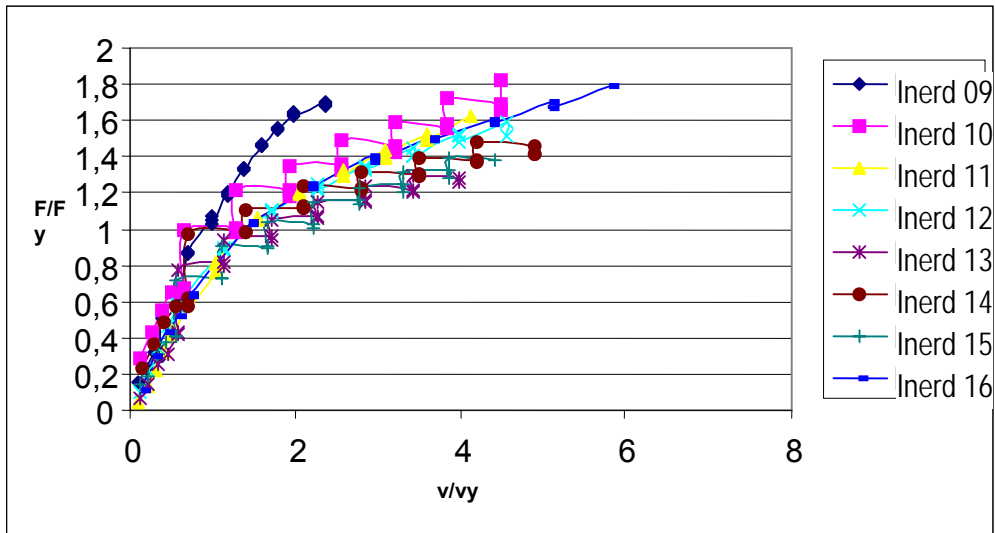


Figure 4.39. U-Devices

## Global comparisons

The analysis of graphic 1 reveals that the force necessary to obtain a given displacements, in the pins is double than for the U-Device.

Pins have a larger strength while U-Devices allow larger deformation.

In fact, the maximum displacement that could be safely imposed to the structure with the U-devices was 120 mm while for the pins devices it was 60 mm.

The second test is peculiar, because the maximum displacement was 72 mm and the pin A suffered a complete failure.

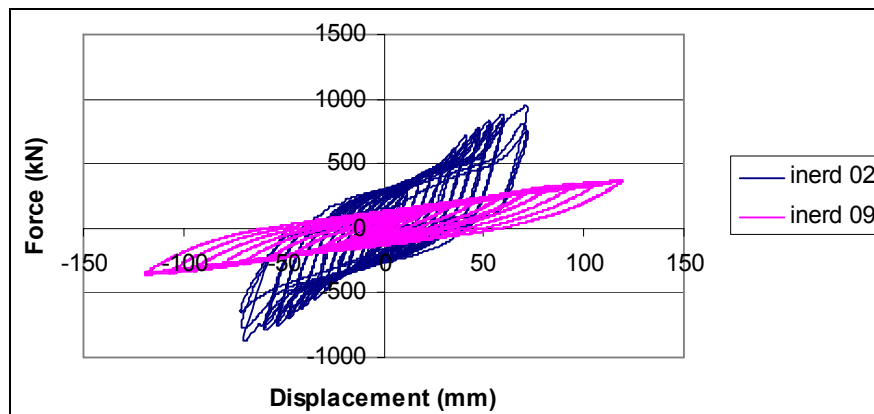


Figure 4.40. Force-displacement behaviour - Pin (02) vs U-device (09)

From a comparison of the results, showed in Tables 4.5 and 4.6, it is possible to notice that pins allow better performance in terms of strength ( $F_{max}/F_y$ ), stiffness (both elastic  $K_y$  and plastic  $K_p$ ), and ductility ( $\Delta v/v_y$ ) than the U-devices.

Table 4.5

	Test	$K_y$ (kN/mm)	$K_p$ (kN/mm)	$\Delta v/v_y$	$F_{max}/F_y$
Pin	1	38,33	9,65	5,91	2,24
	2	36,96	10,55	7,75	2,93
	3	38,44	4,07	3,45	1,26
	4	37,11	8,93	4,11	1,75
	5	42,30	9,34	6,90	2,30
	6	41,18	11,37	5,62	2,28
	7	42,29	4,51	3,77	1,30
	8	41,00	7,92	3,88	1,56
U-Device	9	6,93	1,84	3,91	1,77
	10	9,20	2,26	4,46	1,85
	11	8,83	2,38	3,95	1,80
	12	11,33	2,34	4,51	1,72
	13	15,02	1,69	3,98	1,33
	14	12,76	1,72	4,88	1,52
	15	12,55	1,71	4,35	1,46
	16	10,15	1,93	5,80	1,91

Table 4.6

Test	$v_y$	$F/F_y$	$\Delta v$	$\Delta v/v_y$
1	9	1,8	42	4,67
2	9,2	1,8	48	5,22
5	8,7	1,8	48	5,52
6	8,5	1,8	42	4,94
9	30,3	1,2	60	1,98
10	23,4	1,2	30	1,28
11	29,1	1,2	60	2,06
12	26,3	1,2	60	2,28
13	26,3	1,2	75	2,85
14	21,4	1,2	45	2,10
15	27,1	1,2	75	2,77
16	20,6	1,2	45	2,18

The graphic below, shows the behaviour of both the braced frame and the frame without diagonals. During the test the contribution of the frame is small but when the device recovers from the elastic deformation, there is a point where only the frame dissipates energy; this happens when the force in the frame is bigger than the force in the diagonals, due to ovalization of the holes of the eye-bars. This situation is highlighted in the hysteresis loop of the global (braced) frame response by an evident translation of the curve along the line corresponding to the frame behaviour (without bracings) due to the slippage between the pins and the eye-bar plates.

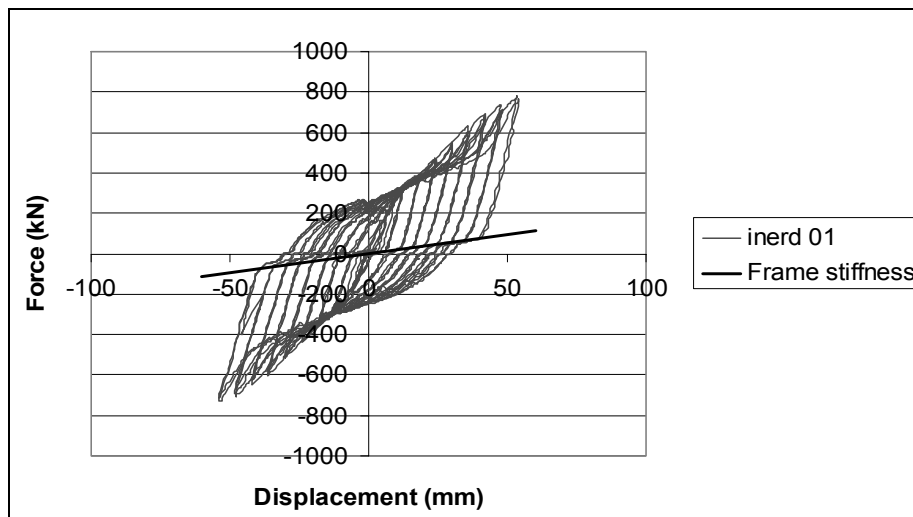


Figure 4.41. F-v, Frame vs Global frame

Analysing all the graphics it can be concluded that the rounded pins with a distance of 70 mm between the eye-bar plates were the best solution for the pins. In relation with the U-Devices, the best performance can be obtained by U2 type with radius 100 mm. and thickness 30 mm.

The Pins dissipate more energy than the U-Devices because the Pins attain the plastic moment earlier than the U-Devices.

It seems that the best dissipative connecting device for concentric bracings is the pin with a rounded section and a large distance between the eye-bar plates.

However, the best performance for the U-Device can be obtained by increasing the thickness and decreasing the radius. From this point of view, it must be considered the practical limit for the production of these devices, in terms of maximum thickness and minimum bending radius allowed by material properties as well as by production technology.

From the safety point of view the pins are better than the U-Devices. In test 2 (Pins) when the dissipative connection broke the diagonal did not fall, as the pin ends were safely restrained by the external eye-bar plates. On the contrary, when a complete failure of a U device occurred (tests 13 and 14), the diagonal fell down.

From a practical point of view the pins are easier to be set in place and to be removed than the U-Devices.

A possible improvement might be represented by modifying the detail of the connection of the eye-bar plates to the diagonal.

Instead of welding the plates to the diagonal (as in present research), they can be welded to an end plate, bolted to the diagonal member by means of high strength pre-tensioned bolts.

This might improve:

- the “easiness” of the operation, when replacing the damaged device;
- eliminate eventual geometrical and technological constraints in coupling diagonal shapes and eye-bar distances

#### **4.5. Theoretical assessment of dissipative connections and of frames with concentric bracings using dissipative connections.**

The investigations performed in the National Technical University of Athens included analytical studies on the monotonic and cyclic behaviour of the INERD connections and studies on the static and dynamic response of X-braced frames with INERD connections. The analyses referred to pin connections.

##### **4.5.1. Analysis of pin INERD connections**

###### **General**

The behaviour of the pin INERD connections has been studied by means of three models with varying degrees of complexity, as following:

- FE model
- Beam model
- Simple beam model

The purpose of the first two models was to give a better insight of the connection response and to allow for the development of the third, simple engineering model. Evidently, only the last simple model is intended for use for design purposes. In the following, a description of the models will be given, as well as their results compared with the experimental ones.

###### **FE model**

Finite Element Models, as applied in the present studies, provide useful information for the monotonic and cyclic response of the connections at large inelastic deformations. The analyses were made using the general purpose programme ABAQUS, version 6.4. In a first phase, the geometric and mechanical properties of the analysed connections were identical to the test specimens experimentally investigated in Lisbon. In the following figures they are referred to as Type A-D.

The contact between the eye-bars and the pin, was modelled either with node-to-node gap elements, or by applying special interaction properties between the appropriate surfaces, as ABAQUS provides a vast variety of contact properties (e.g. stiffness, friction etc.) to select from. Making use of the double symmetry properties allowed for modelling of one quarter of the connection that included one half of an external and one half of an internal eye-bar and a quarter of the pin (Fig. 4.42). Monotonic loads were applied in the analysis through axial displacement control up to 50 mm. The cyclic loading (for specimen D alone) was applied in cycles that were 5mm larger than the previous ones.

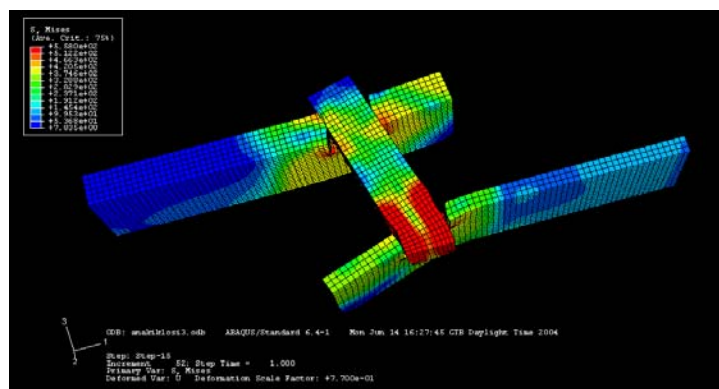


Figure 4.42: FE model for the pin connection in the deformed state (1/4 of connection)

The connection response by means of the relevant force-displacement curves are presented for specimen A to D in Figures 4.43. Positive values represent loading in which the eye-bars are in compression. The comparison between experimental and FEM results indicate the following:

- The monotonic curves represent skeleton curves for higher displacements.
- The initial stiffness at monotonic loading is higher than for cyclic loading in the tests.
- This effect could not be captured in the analysis, where the initial stiffness is similar to that for cyclic loading.
- Strain hardening effects are present at large displacements for monotonic loading but not for cyclic loading.
- The cyclic curves indicate pinching in the response, which is due to the enlargement of the holes in the eye-bars due to large bearing stresses at the contact with the pin.
- Pinching in the analysis occurred at approximately the same “yield” load.
- The strength for negative loading (eye-bars in tension) is larger than for positive loading (eye-bars in compression) due to transverse bending in opposite direction of the eye-bars that follow the curvature of the pin (Fig. 4.42) which magnify the span (distance between external eye-bars).
- Contact through surfaces is better suited than gap elements.
- All connections were subjected to large displacements (more than 50 mm) without failure.
- A generally good agreement between experimental and analytical results is observed.

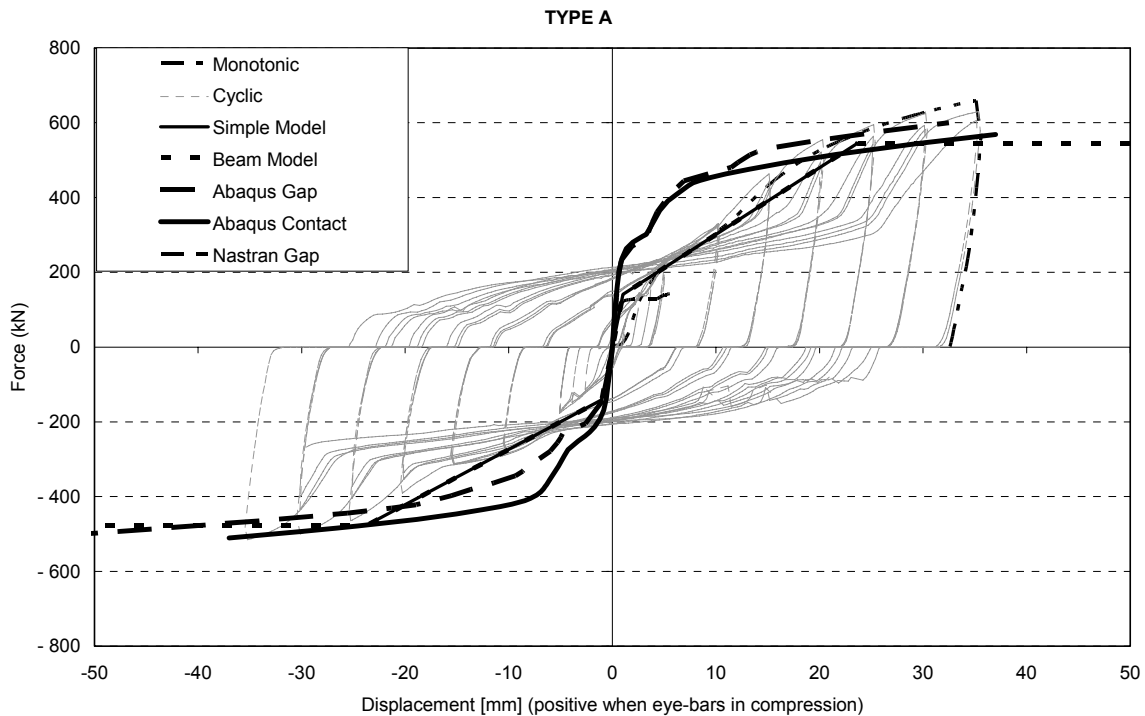


Figure 4.43a: Force-displacement curves for Type A model

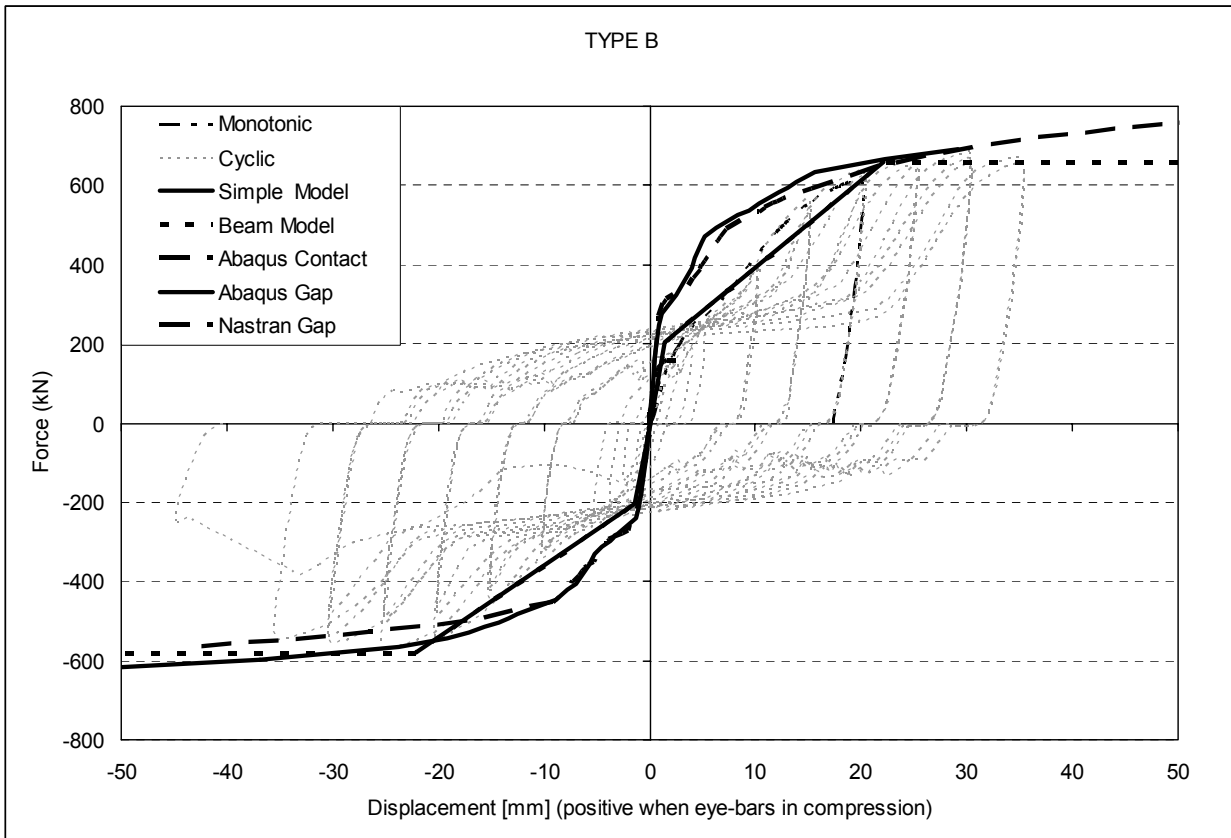


Figure 4.43b: Force-displacement curves for Type B model

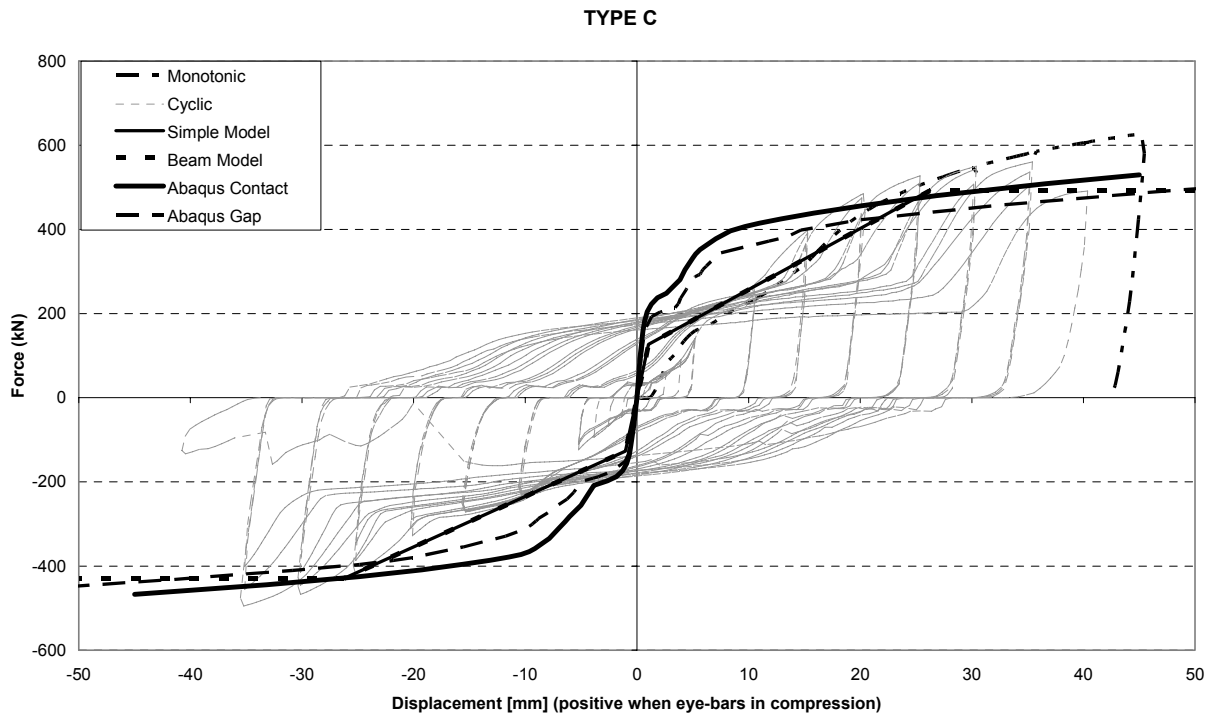


Figure 4.43c: Force-displacement curves for Type C model

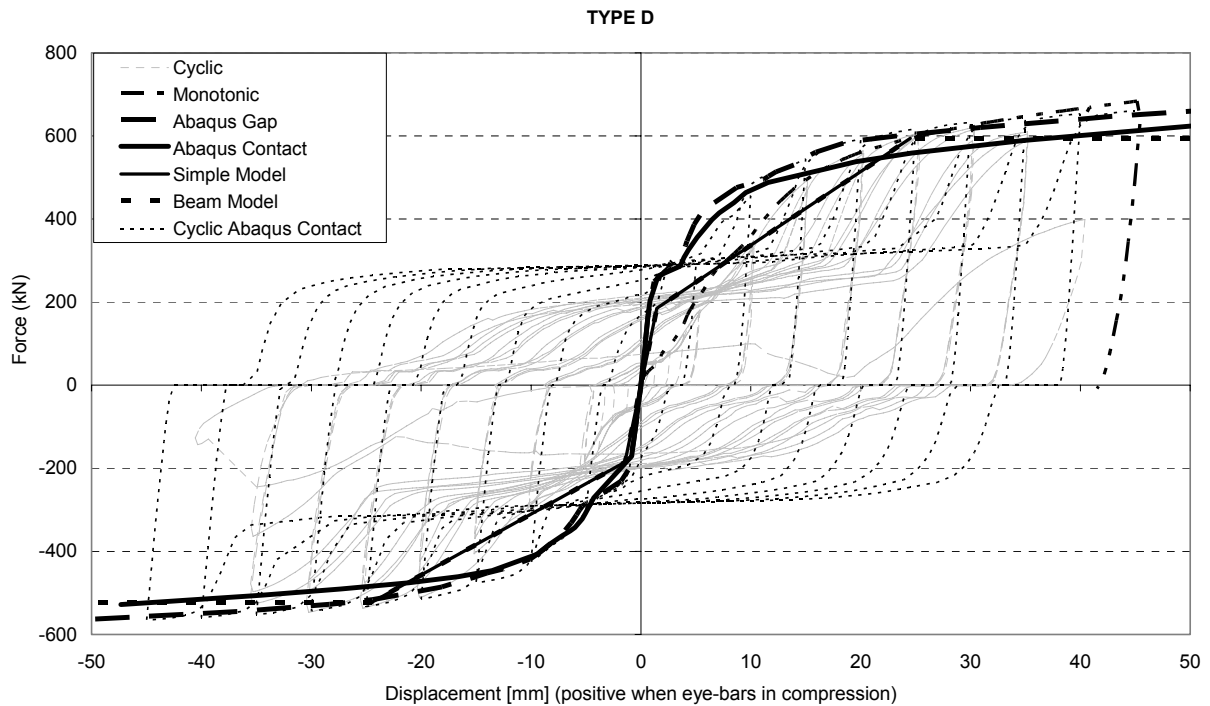


Figure 4.43d: Force-displacement curves for Type D model

After gaining confidence on the results of the FEM analysis, parametric studies on the connection were performed. These studies gave following indications on the performance of the connection:

- The yield point of the connection mainly depends on the dimensions and the material properties of the pin.
- The strength of the connection is additionally dependent on the thickness of the external eye-bars. Thicker eye-bars increase the clamping effect on the pin in the inelastic region and therefore the connection strength.
- The thickness effect is relevant for thicknesses of the eye-bars up to 75% of the pin thickness. Further increase in thickness does not affect the connection strength.
- The connection strength for positive and negative loading is almost the same for thicknesses of the eye-bars higher than the above value (75% of the pin thickness).
- For lower thicknesses the strength of the connection decreases, especially for negative loading (eye-bars in tension). This is due to transverse bending in the opposite direction of the eye-bars that increases the span.
- The difference of strength between positive and negative loading gives an indication on the effect of the transverse bending.
- In order to minimize the negative effect of the transverse bending (up to 90%), the thickness of the external eye-bars should be larger than 0.5 of the pin thickness.

Beam model

In this model, the pin is modelled as a simply supported beam with linear rotation springs at the end supports (Fig 4.44b). The overall span is equal to the clear distance plus one thickness of the outer eye bars. The forces in the outer eye bars are equilibrated by opposite forces in the inner eye bars (Fig 4.44a).

The beam is loaded by the forces in the inner eye bars, which are considered as uniformly distributed across the inner eye-bars.

The system is solved by a second order, plastic zone analysis using the SOFiSTiK general purpose beam program. The beam is divided into 10 elements for which the stiffness is determined continuously at each loading step. The reduction in stiffness is due to the gradual plasticity of the cross sections. The material is modelled by a bilinear  $\sigma - \epsilon$  - Diagram. Strain hardening starts after the attainment of the

yield stress. As an approximation, strain hardening is considered with a constant slope  $E_t = \frac{f_u - f_y}{\epsilon_u - \epsilon_y}$ .

The values of  $f_u$  and  $f_y$  were adopted from the results of the tensile specimen of the material, while the ultimate strain was taken as  $\epsilon_u = 30\%$ .

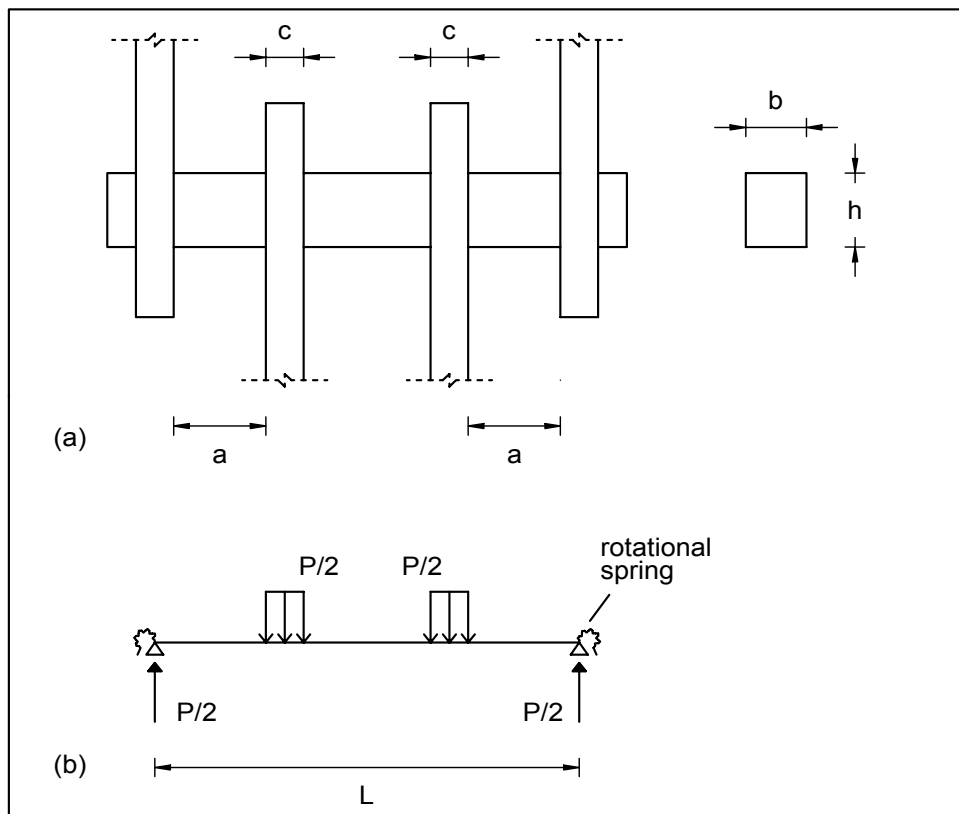


Figure 4.44: Beam model. Geometry and loading

The development of the moments at the axis of the loading and the end supports are qualitatively shown as a function of loading in Figs. 4.45b and 4.45c. The moment diagram along the beam (pin) at various stages of loading is shown in Fig. 4.45d, while the pin stiffness in Fig. 4.45e.



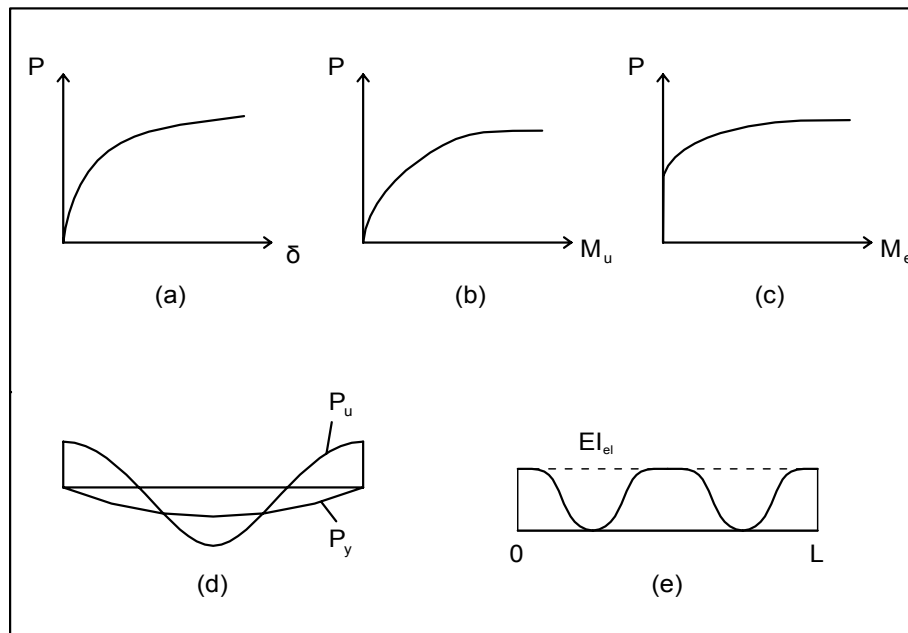


Figure 4.45: Response of Connection

a) Deflection under the loading, b) Moment under the loading,  
 c) Moment at end support, d) Moment diagrams, e) Stiffness along the beam

Following observations can be made:

- At the initial stage of loading, the pin behaves as a simple supported beam. This is due to the fact that the relatively stiffness of the beam is much higher than the stiffness of the end springs, so that they “attract” almost no moments.
- This happens more or less until yielding starts in the sections under the applied loading, after which the beam stiffness in this region is gradually decreasing.
- At subsequent loading, moments at the end supports develop, since the spring stiffness is becoming larger relatively to the beam.
- This occurs until yielding starts at the beam near the end supports.
- For further loading, the stiffness of the beam under the loading points and at the ends reduces significantly, so that the deflections increase very much. The moments increase very slowly.
- The final maximal moments in the middle and at the ends at the ultimate state are between the values of the full plastic moments, using  $f_y$  and  $f_u$  as ultimate stresses.

The analytically determined curves of the beam model for the experimentally tested connections are shown in Figures 4.43. It may be seen that the beam model is well suited for representing the connection response. However, a simpler model is required for use in practical applications. Such a model is introduced in the next paragraph.

### Simple beam model

The simple beam model is proposed for use in practical applications. This model allows for the representation of the connection response by means of a tri-linear curve (Fig. 4.46b). The overall span is in this case equal to the axial distance of the outer eye bars, while the forces are considered as acting concentrated on the relevant axes (Fig 4.46a).

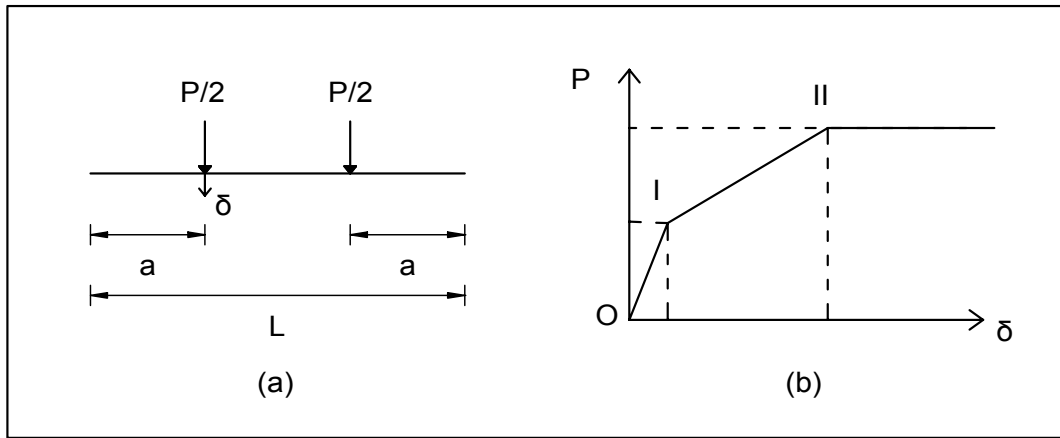


Figure 4.46: Simple beam model  
a) Geometry and loading, b) Response curve

Figure 4.46b indicates that the connection response may be described by two separate systems, one between points O and I and one between points I and II.

The first system corresponds to a four-point loaded beam (Fig. 4.47a). It describes the connection behaviour in the early loading stages, up to the attainment of the plastic moment of the pin. The maximal values of the total force and the beam deflection under the loads (point I in Fig. 4.47b) may be determined from:

$$P_y = P_I = \frac{2M_p}{a} \quad [4-1]$$

$$\delta_y = \delta_I = 1,5 \cdot \frac{M_p}{EI} \cdot l^2 \cdot \frac{\alpha}{6} \cdot (3 - 4\alpha) \quad [4-2]$$

where:

$M_p = W_{pl} \cdot f_y$  = plastic moment of the pin based on the yield stress

$EI$  = elastic stiffness of the pin

$l$  = overall span

$$\alpha = \frac{a}{l}$$

Eq. [4-2], without the factor 1,5, provides the deflection according to the elastic solution. The factor 1,5 is introduced in order to take approximate into account the stiffness reduction of the cross-section beyond the yield moment of the pin  $M_y$ .

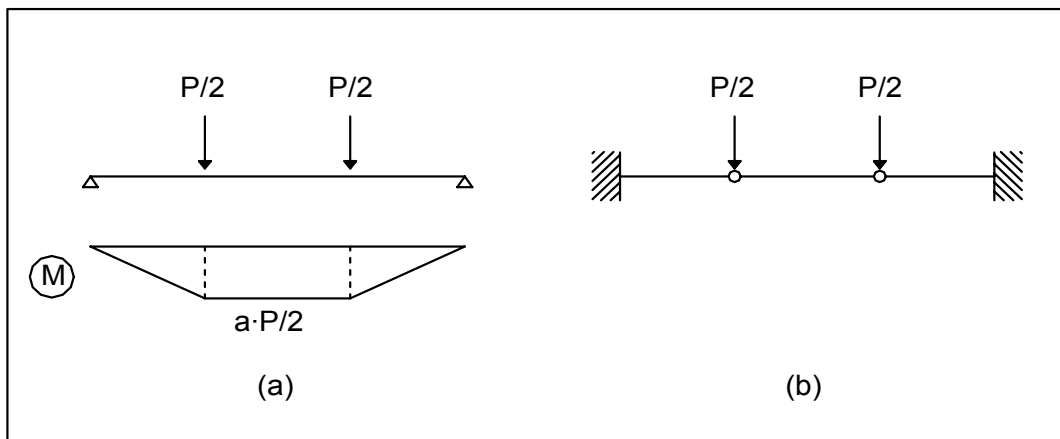


Figure 4.47: Simple beam model  
a) early and b) late loading stages

As observed before, the system changes after the attainment of the plastic moment of the pin under the loading points in that some clamping is provided at the ends and end moments develop (Fig. 4.47b).

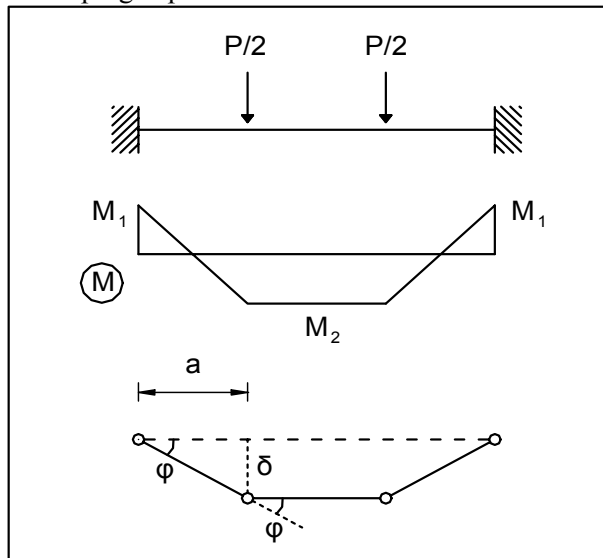


Figure 4.48: Mechanism of the simple beam model

For this system it is possible to derive the ultimate load and the relevant displacements. Figure 4.48 shows the final moment distribution along the beam and the relevant inelastic deformations for the case where the eye-bars are in compression. The works of the internal moments and the external forces may be written as:

$$U_{\text{int}} = (M_1 + M_2) \cdot \varphi \quad [4-3a]$$

$$U_{\text{ext}} = \frac{P \cdot \delta}{2} \quad [4-3b]$$

The kinematics' relation is written as:

$$\delta = \varphi \cdot a \quad [4-3c]$$

The equation of the above works, considering the system kinematics, provides the ultimate load of the beam:

$$P_u = P_{II} = \frac{2 \cdot (M_1 + M_2)}{a} \approx \frac{4 \cdot M_u}{a} \quad [4-4]$$

where

$M_u = W_{pl} \cdot f_u$  = plastic moment of the pin based on the ultimate tensile stress

$a$  = axial distance between external and internal eye-bars

Eq. [4-4] provides conservative results for the ultimate load, in that it neglects the influence of the friction at end supports. However, this influence is counterbalanced by the lateral displacements of the inner eye-bars at large cyclic deflections which enhance the span, so that finally this effect may be conservatively neglected.

The deflection at ultimate loading may be determined from eq. [4-3c]. The plastic rotation may be written as:

$$\varphi = \kappa_u \cdot l_p \quad [4-5]$$

where:

$$\kappa_u = \text{ultimate curvature} = \frac{2 \cdot \varepsilon_u}{h}$$

$l_p$  = length of the “plastic hinge”  $\approx h$  (height of the pin cross section)

Taking into account an ultimate strain  $\varepsilon_u = 10\%$ , the plastic rotation becomes:

$$\varphi_u = 0,2 \text{ radians} \quad [4-6a]$$

The ultimate deflection at point II is then equal to:

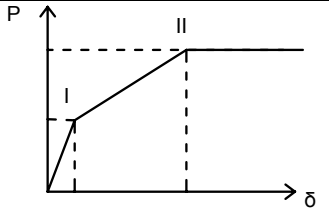
$$\delta_{II} = 0,2 \cdot a \quad [4-6b]$$

The deformation capacity may be derived from similar relationships, taking into account an ultimate strain  $\varepsilon_u = 20\%$ . Under this assumption, it is:

$$\delta_{lim} = 0,4 \cdot a \quad [4-7]$$

The final relations are summarized in Table 4.7. It must be noted, that a minimum thickness for the external eye-bars shall be provided, in order to limit their transverse deflections.

Table 4.7: Forces and deflections of pin connection

	Force P	Deformations $\delta$
Point I “yielding y”	$P_y = \frac{2 \cdot M_p}{a}$	$\delta_y = 1,5 \cdot \frac{M_p}{EI} \cdot l^2 \cdot \frac{\alpha}{6} \cdot (3 - 4\alpha)$
Point II “ultimate u”	$P_u = \frac{4 \cdot M_u}{a}$	$\delta_{II} = 0,2 \cdot a$
Deformation capacity		$\delta_{lim} = 0,4 \cdot a$
$M_p = W_{pl} \cdot f_y$ , $M_u = W_{pl} \cdot f_u$ , $W_{pl} = b \cdot h^2 / 4$ (for rectangular pins) $l$ = pin length, $h$ = pin height, $b$ = pin width $a$ = axial distance between internal and external eye-bars $\alpha = a/l$ $f_y$ = yield stress of pin $f_u$ = tensile strength of pin		

The analytically determined curves of the simple beam model for the experimentally tested connections are shown in Figures 4.43. It may be seen that this simple model is well suited for representing the connection response in both the strength and the deformation. For that reason it is proposed for use in practical applications as will be shown later.

The elastic stiffness of the connection is defined by:

$$k_e = \frac{P_y}{\delta_y} = \frac{8EI}{l \cdot a^2 \cdot (3 - 4\alpha)} \quad [4-8a]$$

The tangential post-elastic stiffness is expressed by:

$$k_t = \frac{P_u - P_y}{\delta_u - \delta_y} = \frac{2 \cdot (2f_u / f_y - 1)}{a^2 \cdot [0,2 / M_p - l \cdot (3 - 4\alpha) / 4EI]} \quad [4-8b]$$

The post-elastic (strain hardening) ratio is equal to:

$$r = \frac{k_t}{k_e} = \frac{(f_u / f_y - 0,5) \cdot l \cdot (3 - 4\alpha)}{0,4EI / M_p - 0,5 \cdot l \cdot (3 - 4\alpha)} \quad [4-9]$$

The pin deflection is given by following expressions:

$$\text{For } P \leq P_y: \quad u_p = P / k_e \quad [4-10a]$$

$$\text{For } P_y < P \quad u_p = \frac{P_y}{k_e} \cdot \left( 1 + \frac{P / P_y - 1}{r} \right) \quad [4-10b]$$

### 4.5.2. Frame and connection kinematics

In frames with dissipative pin INERD connections, inelastic action is expected to concentrate in the pins. It is therefore important to derive the frame and connection kinematics, in order to derive the required connection deformations as a function of the interstorey drifts. Inversely, from the deformation capacity of the connection, it is important to derive the resulting interstorey drifts in a performance level design.

The frame geometry at the displaced position is shown in Fig 4.49a. It may be seen that at a lateral frame displacement  $\Delta\delta$ , the elongation of the diagonal's length is equal to  $\Delta d$ . The same applies to the shortening of the other diagonal which is not shown here. The relations that follow are derived for the brace under tension. For the brace under compression similar expressions apply.

Considering a small change of the diagonal's inclination  $\varphi$ , the relation between horizontal frame displacement and diagonal elongation is given by:

$$\Delta d = \Delta\delta \cdot \cos\varphi = \Delta\delta \cdot \frac{l}{d} \tag{4-11a}$$

The entire elongation of the diagonal may be attributed to the inelastic deformations of the pin. Any elastic deformations of the pin or the brace itself are neglected, as of minor importance. Accordingly, it is (Fig. 4.49b):

$$\Delta d = 2 \cdot u_p \tag{4-11b}$$

where  $u_p$  is the inelastic transverse pin deformations (relative displacements between eye-bars).

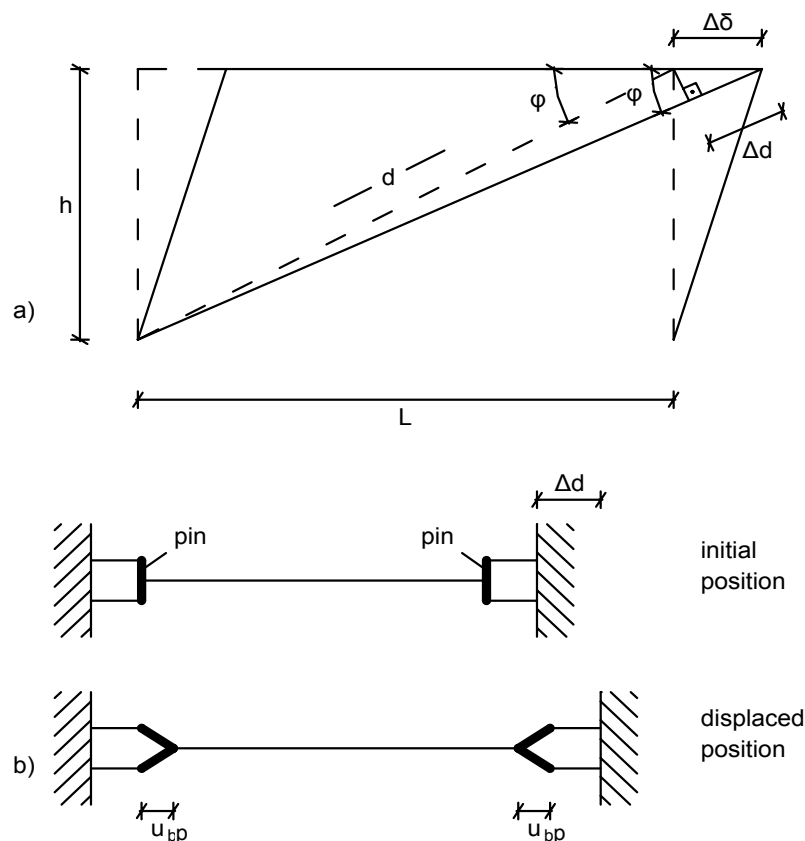


Figure 4.49: Lateral drift vs. pin deformations

The lateral drift ratio of the frame is given by:

$$D = \frac{\Delta\delta}{h} \quad [4-11c]$$

The combination between the above expressions gives:

$$u_p = D \cdot \frac{l \cdot h}{2 \cdot d} \quad [4-11d]$$

After elimination of the length of the diagonal  $d$  and some algebraic manipulation, following expression may be derived:

$$u_p = \frac{\Delta\delta \cdot \cos\varphi}{2} = \frac{D \cdot h \cdot \cos\varphi}{2} \quad [4-12]$$

where:

$\Delta\delta$  = lateral drift

$D$  = lateral drift ratio

$h$  = storey height

$\varphi$  = angle of inclination of the diagonal

The relationship between the force in the diagonal and the lateral force in an X-braced frame with two active diagonals is as following:

$$F = \frac{P}{2 \cdot \cos\varphi} \quad [4-13]$$

where:

$F$  = compression or tension force in the diagonal

$P$  = lateral force in the frame

$\varphi$  = angle of inclination of the diagonal

The validity of eqs. (12) and (13) was verified by the results of the Milan tests on complete frames. Figure 4-11 shows indicative experimental results for Frame 02 of Milan and the corresponding force and displacements in the connection (and the braces) as derived from the above relations (which are indicated in Figure 4-11 as “delta”). The good agreement is obvious, which shows that indeed, both diagonals are active even at large displacements.

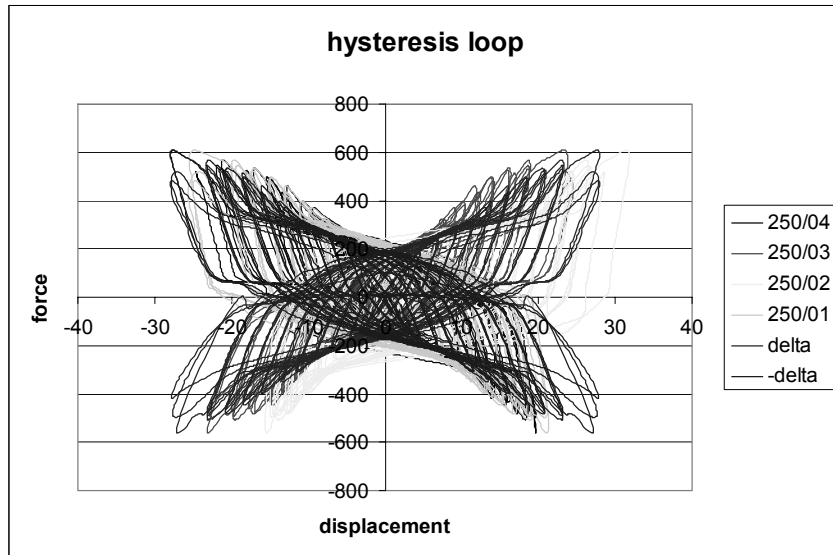


Figure 4.50: Axial force in the braces vs. pin deformations (as recorded in Milan test frame 02 and analytically derived)

Figure 4.51 shows the required pin deformations at 2,5% drift. It may be seen, that for usual inclinations of braces (around 45°) and usual storey heights (around 3,5 m), the required connection deformations (< 35 mm) may be easily accommodated by the pin INERD connections. According to Table 4.7, the distance between eye-bars should be chosen as:

$$a > \frac{35}{0,4} = 87,5 \text{ mm}$$

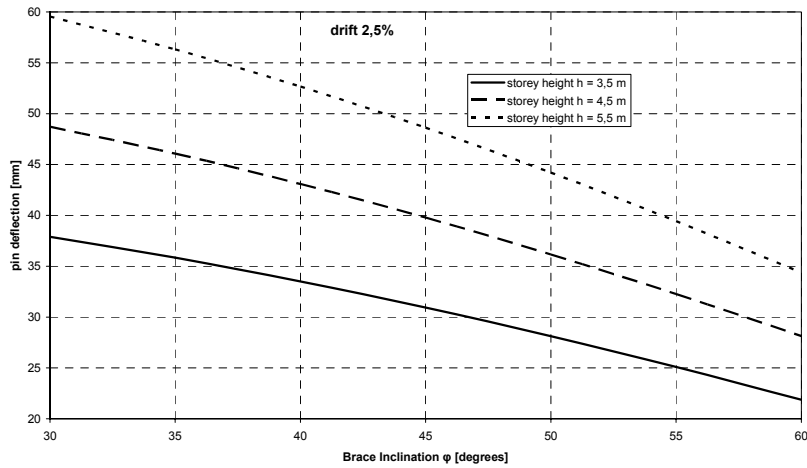
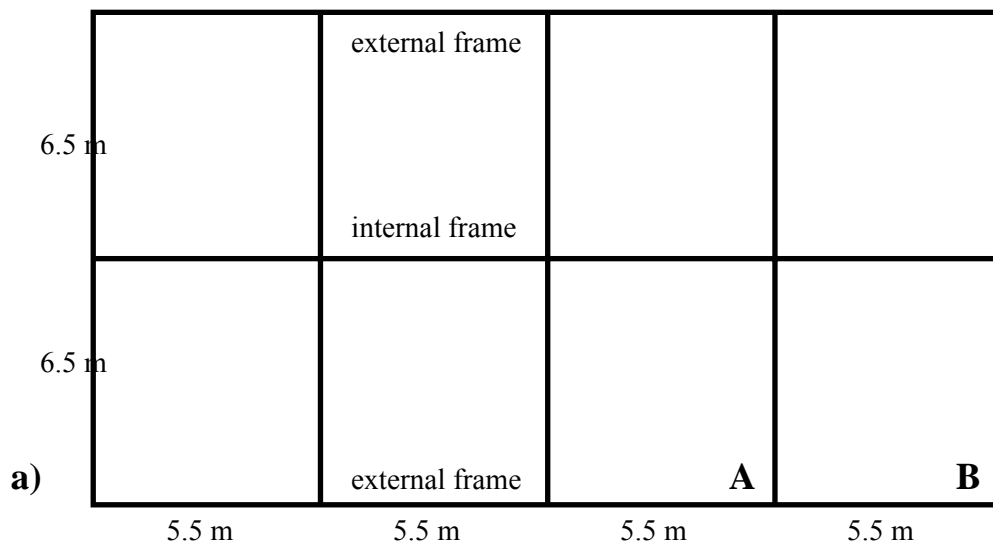


Figure 4.51: Required pin deformations



### 4.5.3. Response of braced frames with INERD connections under static loading

The response of braced frames with INERD connections under static loading has been studied by means of pushover analyses. The building that is examined consists of three frames at 6.5 m intervals (Fig. 4.52a). The beam-to-column connections are simple (hinged) connections. Lateral stability is provided by X-bracing in the external frames (Fig. 4.52b). For conventional braced frames, the connections at brace end are simple hinged connections. The influence of the INERD connections has been studied by introduction at brace ends of axial springs that represent the connection behaviour.



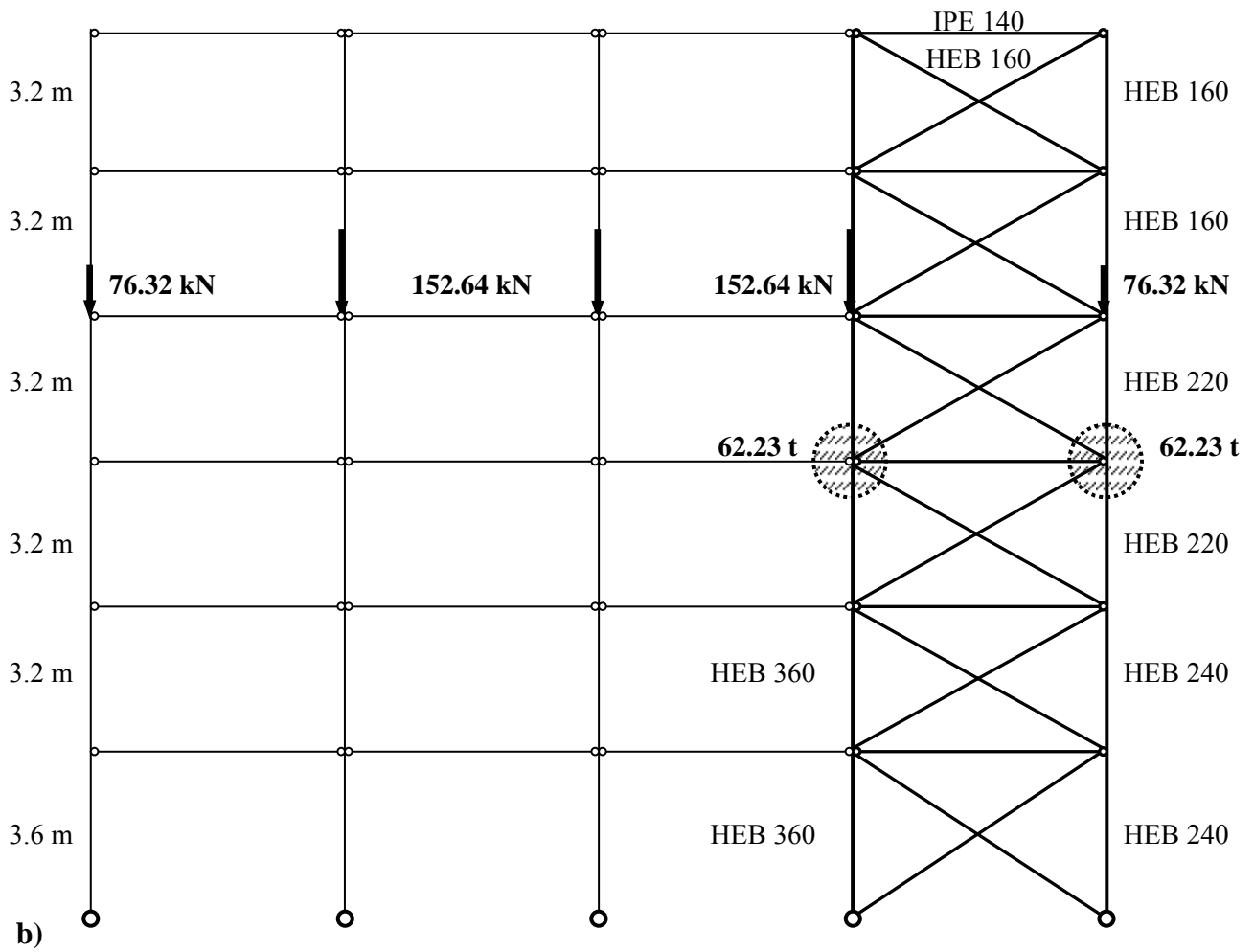


Figure 4.52: Examined building: a) plan, b) external frame

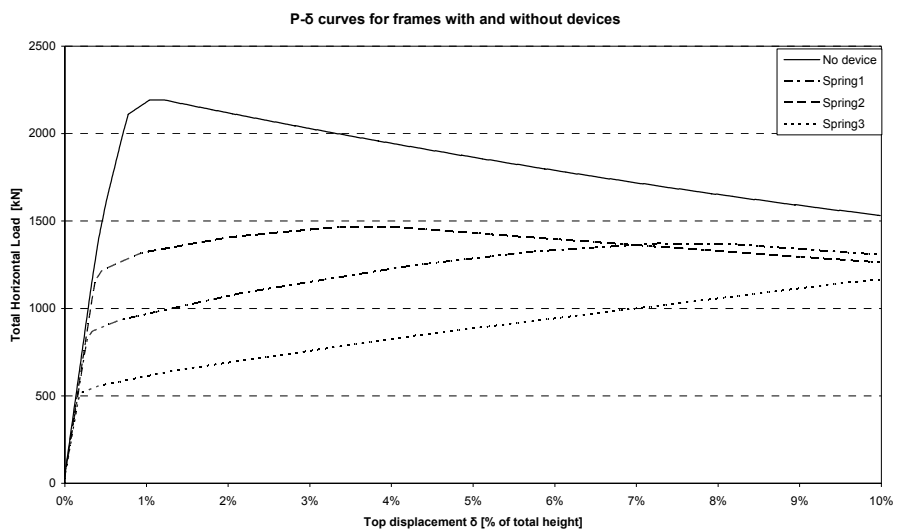


Figure 4.53: Force-displacement curves of conventional frame (“No device”) and frames with INERD connections (“Springs 1-3”)

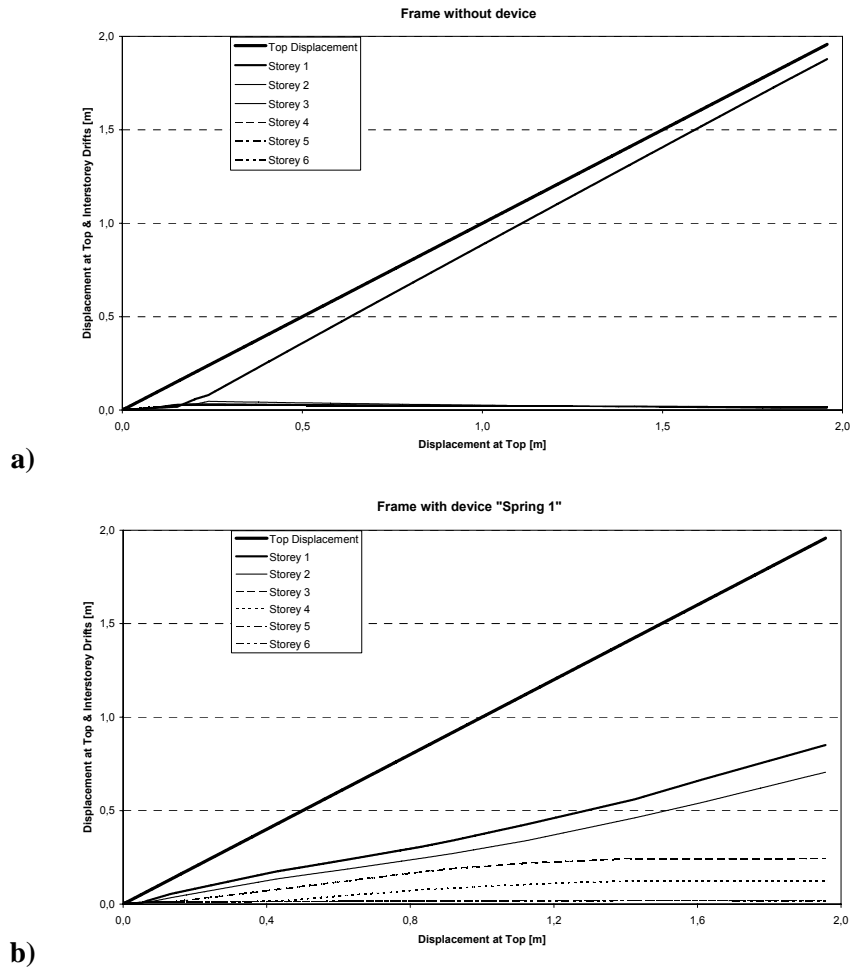


Figure 4.54: Distribution of drifts over the height a) for conventional frame, b) with frame with INERD connection

A pushover analysis with triangular distribution of lateral loads over the height of the building was performed by means of the DRAIN2Dx frame analysis program. Figure 4.53 shows the base shear – top displacement curves for the various frames. The initial stiffness of all frames is similar. However, the conventional braced frame exhibits larger strength, but also a steep unloading branch. For frames with INERD connections, yielding starts at lower forces, but the unloading branch, if existent, starts at larger drifts and is flat. This indicates that conventional frames may face instability problems once the braces buckle. On the contrary, frames with INERD connections may yield earlier (dependent on the connection strength), but are more ductile.

Figure 4.54 shows the distribution of the inter-storey drifts for the conventional frame (“pin”) and the frame with INERD connection 1 (“spring 1”). It may be seen that inelastic action for the conventional frame concentrates entirely on the first floor, where the diagonals buckle. On the contrary, in the frame with INERD connections, all floors (i.e. all connections) exhibit non-linear deformations and plasticity spreads over the entire building.

#### 4.5.4. Response of braced frames with INERD connections under seismic loading

The response of braced frames with INERD connections under seismic loading has been studied by means of inelastic dynamic time history analyses. A large number of X-braced frames with and without INERD connections have been subjected to various real and artificial seismic records. The studies were performed by application of different analysis programmes (ETABS v.8 Nonlinear, SAP v.8 Nonlinear,

DRAIN2DX, OPENSEES). An overview of the studies and relevant results are given in the detailed report of NTU Athens. In the following, one such study will be presented.

The building under consideration is square in plan with 6 bays of 5,5 m and storey height 3,8 m. Braces are placed in the perimeter of the building. Figure 4.55 shows a perimeter frame, which stabilises half of the building in the relevant direction. All connections are simple (hinges). The building has been dimensioned according to Eurocodes 3 and 8 for  $PGA = 2,4 \text{ m/sec}^2$ ,  $q = 4$  and final spectral acceleration  $SA = 1,6 \text{ m/sec}^2$ . The cyclic law for the connections has been formulated according to the tests results of Lisbon and Milan.

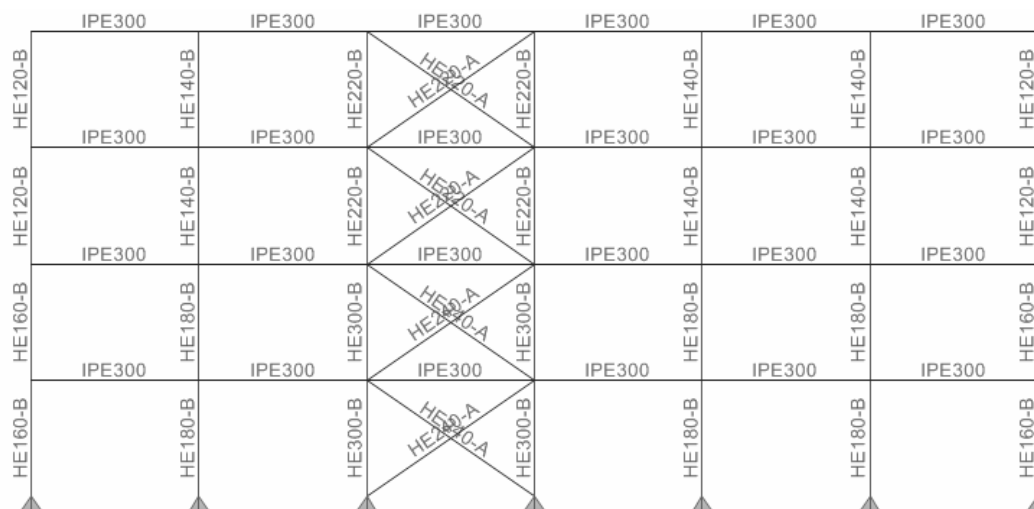


Figure 4.55: Braced frame under consideration

Pin INERD connections with different strength have been introduced at brace ends. “Hyst 1” with yield load 310 kN for all braces and “Hyst 2” with yield load 670 kN at the two lower and 500 kN at the two higher storeys. The frames were subjected to four real records (Aigion 1995 and Thessaloniki 1978, Greece, Kobe 1995, Japan, Vrancea 1977, Romania) and one artificial record corresponding to the EC 8 spectrum used for design. The records were appropriately scaled in order to reach limit drifts of 1%, 2,5% and 5% corresponding to Occupancy, Life Safe and Collapse performance levels according to FEMA 274 for moment resisting frames. Additionally, the scaling factor for first yield was also recorded.

Indicative results for the frame “Hyst 2” and the Kobe record are shown in Figures 4.56 to 4.60. The Kobe record used here has a  $PGA 9,0 \text{ m/sec}^2$  and a Spectral acceleration ( $S_a$ ) at the fundamental period of the building  $18,8 \text{ m/sec}^2$ . Figure 4.56 shows dynamic pushover curves for the individual storeys, Figures 4.57 and 4.58 the base shear and first storey drift vs. time for the record scaled so that the maximum drift is 2,5%, Figure 4.59 the connection force at the first floor and the relevant dissipated energy and Figure 4.60 the hysteretic behaviour of the connection for the record scaled so that the maximum drift is 5% (Collapse performance level).

Following observation can be made:

- All floors participate in the inelastic action, with exception of the 4<sup>th</sup> floor (Fig. 4.56).
- The Life Safe performance level (2,5% maximal drift) is achieved at a scale factor of the Kobe record 0,27 (Fig. 4.56), i.e. a  $PGA$  of  $2,40 \text{ m/sec}^2$  (equal to the design  $PGA$ ) and a  $S_a$  of  $5,0 \text{ m/sec}^2$  (equal to **3 times** ( $=5,0/1,6$ ) the design  $S_a$ ) indicating the good performance of the structure with the INERD connections.
- Good performance was achieved for a very demanding record, with long duration and large number of cycles (Fig. A2-18).

- The ground motion was well filtered, so that the maximum drift of 2,5% was achieved only once, where in general the drifts remained well below that value between 0,5% and 1,5% (Fig. 4.58).
- However, for maximum drift 2,5%, the residual drift is 0.8% (Fig. 4.58).
- The Collapse performance level (maximum drift 5%) was achieved for a scale factor of 0,54 (Fig. 4.56), i.e. for a PGA twice as large as the design PGA.
- For this record, the strong motion period during which energy was dissipated was about 20 sec. During this period only once a very high force developed in the connection (Fig. 4.59). Nevertheless, yielding of the device occurs in 3-4 more cycles.
- Even at the Collapse performance level only the connections yielded. The braces were protected from buckling and were active for both compression and tension
- The required connection deformations at the Collapse performance level were around 80 mm. This value is high, but can be achieved by the INERD connections.
- The above value proves the validity of eq. [4-12], i.e. the concentration of inelastic action in the connections. Indeed, the brace inclination is  $\varphi = \arctan\left(\frac{3,8}{5,5}\right) = 34,6^\circ$  and eq. [4-12] gives

$$u_p = \frac{D \cdot h \cdot \cos \varphi}{2} = \frac{0,05 \cdot 3800 \cdot \cos 34,6}{2} = 78 \text{ mm} \approx 80 \text{ mm}.$$

- For the Life Safe performance level the required deformation is around 40 mm, which can be easily achieved by the INERD connections, as the test results from Lisbon and Milan showed.

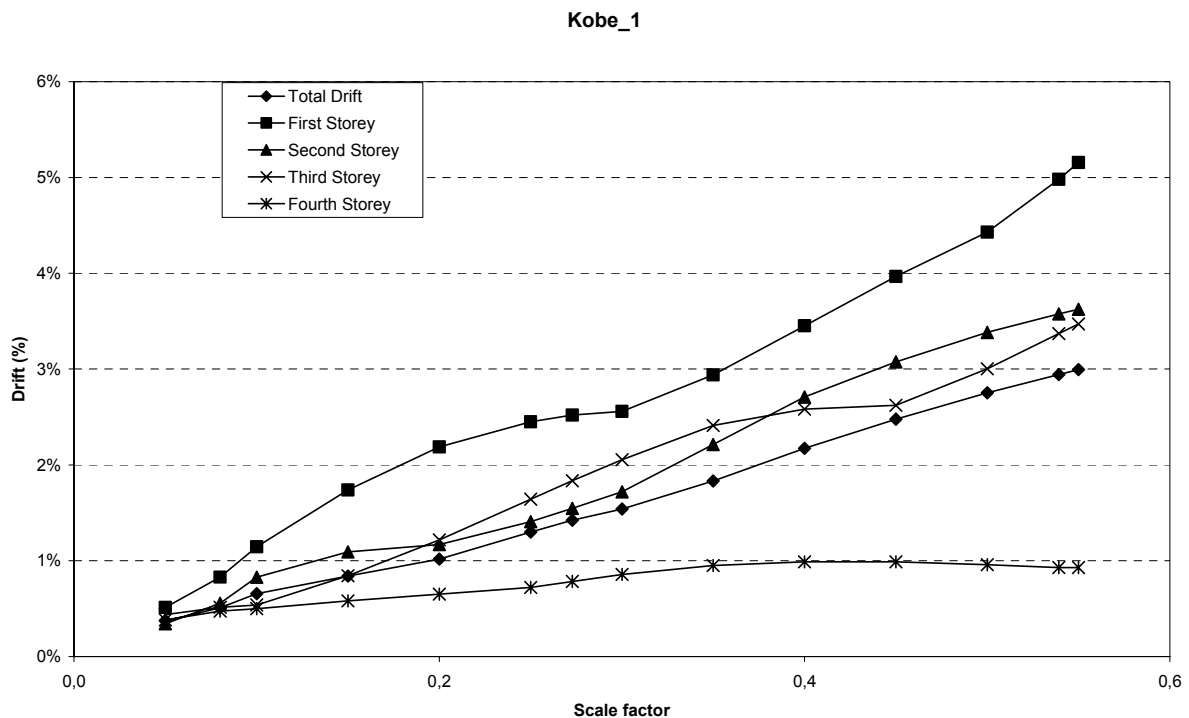


Figure 4.56: Development of storey drifts

Kobe\_1 - Failure at 2.5% drift for first storey

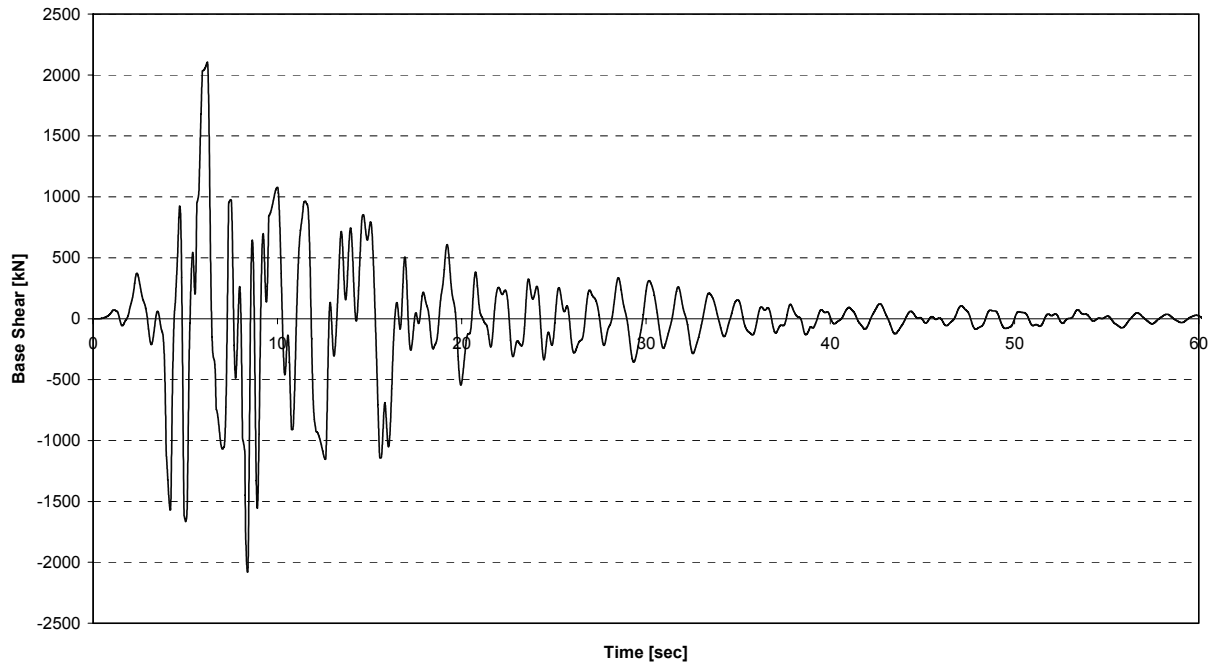


Figure 4.57: Base shear vs. time for 2.5% drift

Kobe\_1 (PGA = 2.41m/sec<sup>2</sup>) - First Storey Drift (2.5% limit)

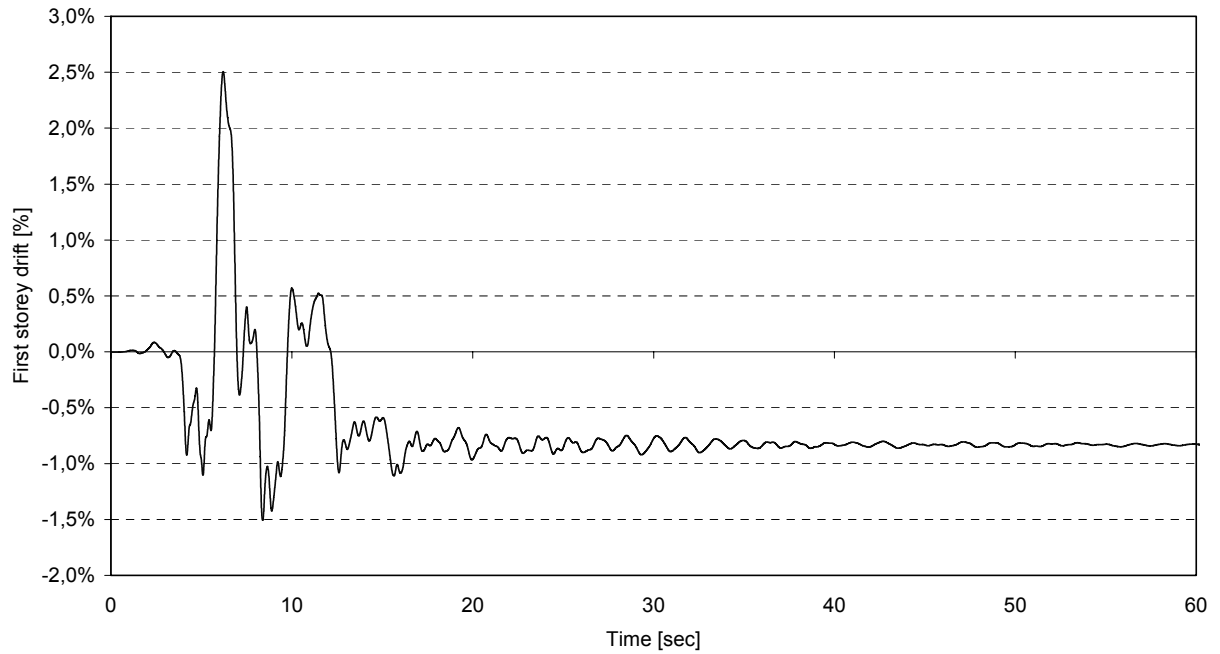


Figure 4.58: First storey drift vs. time

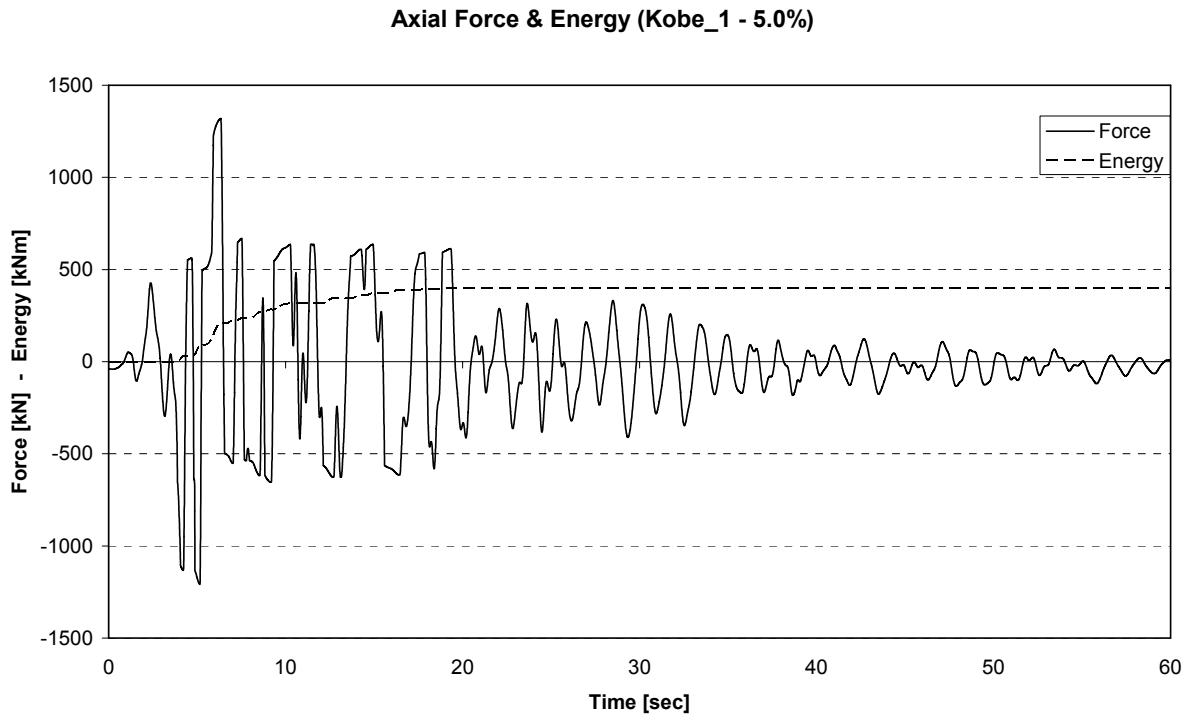


Figure 4.59: First floor connection force and dissipated energy vs. time for 5% drift

4x6d Frame - Kobe\_1 - Hysteretic curve of first storey device for 5% storey drift

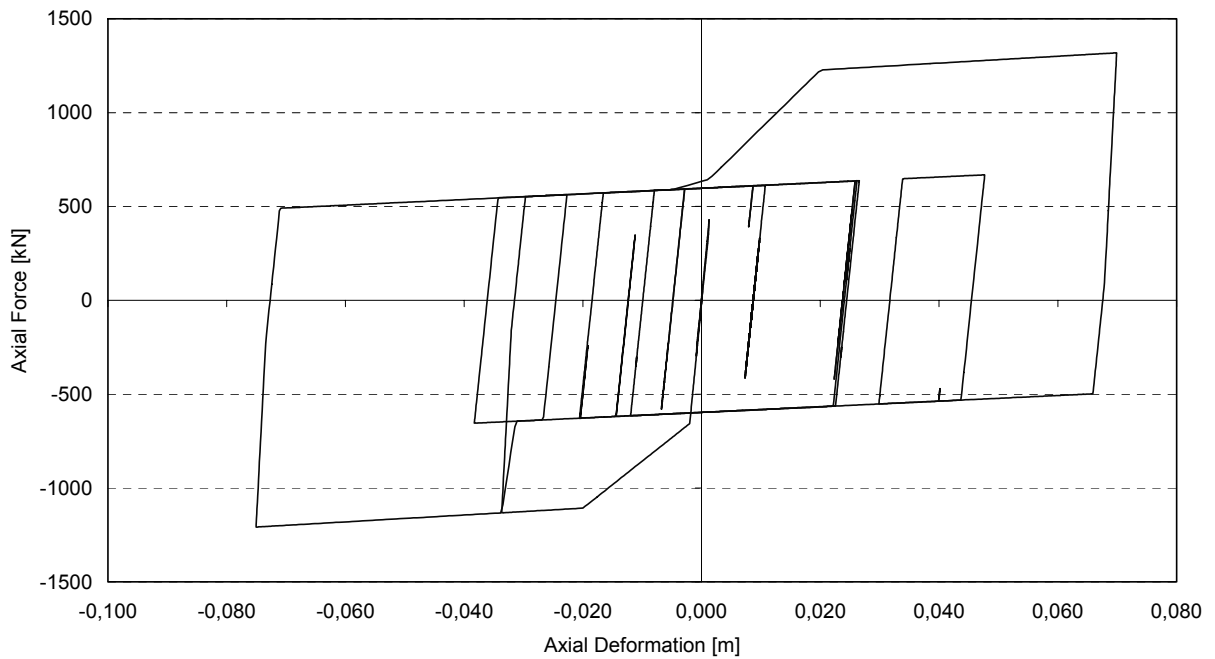


Figure 4.60: Hysteretic curve for the first storey connections at 5% drift

Results for all the records are summarized in Table 4.8. This Table gives also values of the achieved behaviour factors according to two definitions:

$$q_1 = \frac{PGA \text{ at failure}}{PGA \text{ at yield}} \quad [4-14]$$

$$q_2 = \frac{Elastic \text{ Base Shear for } PGA \text{ at failure}}{Elastoplastic \text{ Base Shear for } PGA \text{ at failure}} \quad [4-15]$$

It may be seen that:

- The PGA and Sa values for which the various performance levels are reached depend on the record characteristics.
- The limit PGA for the Life Safe limit state is above the design PGA (except for the artificial and the Vrancea records).
- For all cases, the limit Sa for the Life Safe limit state is well above the design Sa.
- The behaviour factors are, as expected, dependent on the performance level due to the different degree of plasticity.
- The behaviour factors are for both definitions well above the initial value of  $q = 4$  for which the frame was designed.



Table 4.8: Results for “Hyst 2” devices (All records)

Device: «Hyst2b & Hyst2t»

q <sub>1</sub>	Aigion_L				q <sub>2</sub>
	Scale Factor	P.G.A.	Spectral Acceleration	q <sub>1</sub>	
<i>yield (drift3)</i>	0,1806	0,89	0,37		
1,0%	0,6183	3,03	1,25	3,4	2,3
<i>yield</i>	0,1912	0,94	0,39		
2,5%	1,9951	9,78	4,05	10,4	5,0
5,0%	3,3898	16,62	6,88	17,7	7,6

**value for unscaled record: 4,9031 2,0288**

	Thessaloniki_L				
	Scale Factor	P.G.A.	Spectral Acceleration	q <sub>1</sub>	
<i>yield (drift3)</i>	0,5286	0,75	0,42		
1,0%	3,1720	4,47	2,53	6,0	3,4
<i>yield</i>	0,6948	0,98	0,55		
2,5%	6,5762	9,28	5,25	9,5	4,7
5,0%	13,3366	18,81	10,64	19,2	7,3

**value for unscaled record: 1,4108 0,7978**

	Kobe_1				
	Scale Factor	P.G.A.	Spectral Acceleration	q <sub>1</sub>	
<i>yield</i>	0,0254	0,23	0,48		
1,0%	0,0909	0,82	1,71	3,6	2,4
2,5%	0,2661	2,41	5,00	10,5	5,4
5,0%	0,5403	4,89	10,15	21,3	9,4

**value for unscaled record: 9,0448 18,7879**

	Record1_X				
	Scale Factor	P.G.A.	Spectral Acceleration	q <sub>1</sub>	
<i>yield (drift3)</i>	0,6313	1,55	0,25		
1,0%	2,4421	5,99	0,95	3,9	2,6
<i>yield</i>	0,6488	1,59	0,25		
2,5%	5,7726	14,16	2,25	8,9	4,3
5,0%	9,4373	23,15	3,68	14,5	6,2

**value for unscaled record: 2,4530 0,3902**

	Vrancea				
	Scale Factor	P.G.A.	Spectral Acceleration	q <sub>1</sub>	
<i>yield</i>	0,0876	0,17	0,49		
1,0%	0,2975	0,58	1,65	3,4	2,3
2,5%	0,7123	1,39	3,95	8,1	4,4
5,0%	1,1194	2,18	6,21	12,8	6,0

**value for unscaled record: 1,9493 5,5448**

#### **4.6. Conclusions on dissipative connections in concentric bracings.**

The research work on connections was developed by means of 3 logical and complementary steps:

1. The behaviour of the connections considered alone and outside of any frame effect was studied in a horizontal test machine at IST Lisbon. In that way, a wide parametrical study on the two types of connections initially designed by the INERD research group could be made, with as much as 100 tests. It allowed to assess the best possible design for the “devices”. (see 4.3)
2. The experimental response of frames with concentric bracing was studied in a dedicated set up at Politecnico di Milano. (see 4.4). 16 of these full scale tests have been performed.
3. At the National Technical University of Athens, theoretical or numerical approaches of the behaviour of the connections and of the behaviour of representative frame structures using the INERD connections were made to assess the practicability of this new technology. (see 4.5)

The research on dissipative INERD connections leads to the following conclusions, which are common to IST and Milano tests programs.

For pin connections, rounded pins have a better performance than the rectangular ones, as they can sustain a larger force. For small cycles the rectangular section (with slightly larger inertia) is stronger. For large deformations (large amplitude cycles) the rounded section have a better performance, because the torsional effects are smaller. The best performance is obtained with the maximum distance between the eye-bar plates, since it maximizes the energy absorption in the device.

In the case of U connections, the best behaviour is obtained with a large thickness and a small radius. This correspond to practical limit for the production of U devices, in terms of maximum thickness and minimum bending radius allowed by material properties as well as by production technology.

When comparing the behaviour of pin and U connections, it appears that pins allow better performance than the U-devices in terms of strength, stiffness (both elastic  $K_y$  and plastic  $K_p$ ), and ductility ( $\Delta v/v_y$ ). The pins dissipate more energy because they attain the plastic moment earlier than the U-Devices.

The tests on frames in Milano allow some additional conclusions related to the application of dissipative connections in real frames:

- From the safety point of view the pins are better than the U-Devices: when the pin is broken, the diagonal does not fall, as the pin ends are safely restrained by the external eye-bar plates. On the contrary, when a failure of a U device occurs, the diagonal fall down.
- From a practical point of view the pins are easier to be set in place and to be removed than the U-Devices.
- An improvement of pin connections could be obtained by welding the eye bars to an end plate rather than to the diagonal. The end plate could then be bolted to the diagonal member by means of high strength pre-tensioned bolts. This would improve the “easiness” of the operation, when replacing the damaged device and eliminate eventual geometrical and technological constraints in coupling diagonal shapes and eye-bar distances.

The theoretical or numerical approaches of the behaviour of the connections and of the behaviour of representative frame structures using the INERD connections developed at the National Technical University of Athens lead to the following conclusions:

- Dissipative connections improve the seismic performance of frames with concentric bracings.
- The connections protect the braces from buckling and concentrate the inelastic deformation into the connection.
- The introduction of the dissipative connections does not unduly reduce the structural stiffness and create no serviceability problems with horizontal deformations, like it is the case in

classical design in which the inevitable cyclic buckling of diagonals is difficult to consider in design.

- When the energy dissipation is located in the INERD connections and not in the members, more dissipative zones are activated over the structure, which improves its ductility and can be translated into higher values of the behaviour factor  $q$ .
- The mechanical characteristics of the pin connections may be described by simple formulae developed in the project and which are supported by experimental and numerical evidence.
- Frames with concentric bracings using INERD connections achieve limit drifts similar to those of moment resistance frames for all performance levels.
- Code relevant design rules for frames with dissipative INERD connections have been formulated. They are presented in the “Designers report” on the CD-ROM.
- Practical recommendations for the selections of the connection characteristics and the member verifications have been formulated. They are presented in the “Designers report”

Globally, the INERD project has demonstrated that the proposed innovations brought unquestionable positive results and new concepts of the interest for construction practice and for safety.



## **5. GENERAL CONCLUSION AND FUTURE WORK.**

The INERD project proposed two innovative seismic design concepts:

- A first innovation aiming at the improvement of the seismic resistance of reinforced concrete structures; it consists in the local use of composite structural elements in structures which for the rest essentially remain reinforced concrete structures.
- A second innovation aiming at the improvement of the seismic resistance and a better control of design of frames with concentric bracings; it consists in localising dissipative zones in the connections of the diagonals, rather than in the diagonals themselves.

The most frequent failure mode of reinforced concrete (R.C.) moment frame buildings is the so called “soft storey” mechanism. It consists in a localisation of buildings seismic deformations and rupture in the bottom storey, either by shear and bending failure of the column itself or by shear failure of the column panel zone. The proposed innovation is the use of a composite column at those very sensitive places: an encased H steel profile could provide reliable resistance in bending, shear and compression and enough ductility to transform a brittle element into a reliable dissipative element. The innovation is also in one proposal for the design of such components in the context of reinforced concrete structures: the steel section is meant and designed as a safety belt or a ductile fuse, not like an explicit composite column.

In order to refer to a realistic situation, the first step of the research on the cyclic plastic behaviour of composite columns consisted in designing reference reinforced concrete buildings of which the RC sections were designed for 3 different ductility levels. This work was made by the University of Trento and then the design conditions for the encased steel profiles were evaluated the INERD research group and a decision was taken which balances safety, economy and feasibility. Other parameters considered in the definition of the tests specimens were the type of stiffening of the steel column web and the bending axis of the steel profile. Three different anchorages of the steel profiles were selected. Half of the specimens were designed to address the behaviour of the column panel zone and the other half the shear and bending behaviour of column outside of the panel zone. The experimental activity was shared between the University of Liege and Trento, each Institution addressing one of those two problems. A total of 38 specimens were tested, out of which 10 were reference reinforced concrete elements necessary for comparison purposes. The testing activity has demonstrated that composite columns possess the capacity to form stable and dissipative mechanisms in plastic bending coupled to compression. In addition, the composite component generates a serious increase in resistance and ductility of the beam column panel zone. The proposed innovation is thus operative: composite columns can be applied as foreseen to the lower storeys of reinforced concrete to avoid “soft storey” mechanism. In parallel to the experimental work, analytical and numerical work has been made in order to develop design relationships related to all aspects of the proposed innovation: strength of plastic mechanisms in bending and shear, in the panel zone and outside of the panel zone, strength of anchorage zone, reliability of composite aspects at ultimate strength. Again Trento and Liege contributed for the aspect of the problem on which they had focused their experimental activity.

The research work provided data to make a first calibration of design formula of column strength under coupled axial force and bending. The improvement in strength and ductility has been assessed. In addition, the formulas developed to design the composite shear panel zone as well as those for the design of the anchorage of the steel profile can also be applied to the design of pure composite frames, which means that the information from the research is wider in application than strictly for the mitigation of soft storey failures in RC structures.

However, there remain gaps in knowledge. One is due to the quality of the concrete which was too high to represent correctly the reality of many countries. Another gap corresponds to the narrow range of values of the axial force achieved in tests. Furthermore, the composite panel zones which have been tested were also confined by transverse reinforcements; these ones can be unnecessary and are certainly costly, due to the geometrical complexity of that zone in which all types of reinforcements are present: horizontal longitudinal, vertical longitudinal, vertical transverse, encased steel profile. This detail can certainly be

improved. It requires tests on design in which the shear strength of the panel zone rely only on the composite aspect of the column section. Then there is the problem of expanding the obtained results to the complete range of available H steel sections. This can be done by numerical modelling, using the INERD test results for calibration. This research activity, considering the ductility in cyclic plastic bending combined to compression, would be concluded by the definition of easy to use tables for designers.

The demonstrated effectiveness of localised encased steel profiles in reinforced concrete structures can open a market to applications of rolled steel sections in the market of reinforced concrete structures, especially for the application to “pilotis” type of structures which for architectural reasons are preferred with slender columns at ground level. Also, in countries where the quality of the concrete material is not well controlled, the proposed innovation, which prevents the soft storey failures, is a good tool to prevent disasters.

For the second innovation, which consists in localising dissipative zones in the connections of the diagonals, rather than in the diagonals themselves, the complete story had to be written within the INERD project: original design of dissipative connections, their characterisation, studies of the response of complete structures using the connections, development of design relationships for the connections.

So the process started by a brain storming involving the six partners of the INERD project. Potential design, their strength and weakness were discussed and two potentially best designs of dissipative connections were decided. Tests specimens were designed by a group involving NTUA, Politecnico di Milano and IST, considering practical aspects, including the capacity of test rigs. The first activity of the research was a characterisation of the behaviour of the connections alone, outside of any frame effects. This work, bearing on a total 100 tests was achieved by IST Lisbon. It was followed by 16 tests on frames using such connections, which were made at Politecnico di Milano. All the tests data were processed into various types of graphs, from the classical load displacements curves up to low cycle fatigue Wöhler type curves.

For the so called “U” type of connections, tentative developments of numerical models were made both in Lisbon and Milano; they came across serious difficulties due to the high geometrical non linearity of the deformation of the “U”. For the other type of connection, so called “pin”, the complete way in modelling was made at NTUA, involving numerical modelling by means of two softwares, followed by the development of complete analytical formulas and completed by simplified analytical formula ready for designers use.

In parallel, a study was made at NTUA in order to study by numerical modelling the peculiarities of the response of complete frames with concentric bracings which incorporated dissipative connections at the ends of diagonals. In those models, the experimental load displacements characteristics were used for the characterization of the load displacement laws of connections.

From this comprehensive experimental – numerical – analytical research activity, a set of conclusions can be drawn.

Dissipative connections are applicable to concentric braced frames. Knowledge for pin connections is now sufficient to provide all data necessary for design. The whole research way concluded positively, up to the point that the necessary steps for patenting and looking after licences have been made. Dissipative “pin” connections can be made of a very well controlled steel, so that their resistance is very well calibrated, allowing a more precise and less expensive design of the complete frame than in the standard situation in which the designer has to deal with the variability of steel characteristics by means of overstrength factors. When the energy dissipation is located in the INERD connections and not in the members, more dissipative zones are activated over a structure, which improves its ductility and can be translated into higher values of the behaviour factor  $q$ . The dissipative device can easily be replaced after the earthquake, which avoids the total replacement of the yielded diagonal which is needed in classical design. Trade Marks are under way for both the U and the pin connections.

Future research steps on the subject of dissipative connections would be useful to better assess the practical application field of dissipative connections, meaning the definition of the building height to which they best apply and the assessment of their use in other typologies of frames with bracings, like V or  $\Lambda$  bracings for instance.

As a general conclusion, it can be said that the challenge in the INERD project was to go from the “concepts” mentioned at the beginning to results applicable in constructional practice and it can be considered that the INERD research work has been up to the challenge: the research efforts developed by all partners have concluded in a number of “ready for use” design approaches. This success is due to a clear definition of the objectives and of the research steps and to the complementarity and the commitment of all contributors along the project duration.





## 5. LIST OF REFERENCES

- ACI American Concrete Institute (1995): Building code requirements for structural concrete (ACI 318-95). Farmington Hills, MI.
- AISC (1997), Seismic provision for structural steel buildings, Task Committee 113.
- Aschheim M, Gulkan P., Sezen H. (2000): Chapter 11: Performance of Buildings, in Kocaeli, Turkey earthquake of August 17, 1999 Reconnaissance Report. Earthquake Spectra. Supplement A to Volume 16, 237–279.
- Benats Valérie, "Développement du concept d'assemblages dissipatifs dans des structures parasismiques en treillis", Université de Liège, thesis, a.a. 2000-2001.
- Chou C.C., Uang C.M. (2002): Cyclic Performance Of A Type Of Steel Beam To Steel-Encased Reinforced Concrete Column Moment Connection. Journal of Constructional Steel Research 58, 637-663.
- ECCS (1986): Recommended Testing Procedure for Assessing the Behaviour of Structural Steel Elements under Cyclic Loads. ECCS Publication n° 45.
- ECSC Project 7210-PR-316 (2001): Earthquake Resistant Design: the INERD Project.
- Hibbitt, Karlsson & Sorensen Inc (2003): ABAQUS - User's Manual, Version 6.3. Vol.1-3, 2003.
- Kanno R., Deierlein G.G. (2000): Design Model Of Joints For Rcs Frames. Composite Construction in Steel and Concrete IV – Proc. of Engrg. Found. Conference, Banff, May 28 – June 2, Banff, Alberta, 947-958.
- Krawinkler H. (1978): Shear in Beam-Column Joints in Seismic Design of Steel Frames. Engineering Journal AISC Vol. 3.
- Mander J.B., Priestley M.J. N., Park R. (1988): Theoretical Stress-Strain Model For Confined Concrete. Journal of Struct. Engrg., ASCE, vol. 114, No 8, 1804-1826.
- Ministry of Public Works and Settlement (1975): Specification for structures to be built in disaster areas. Government of Republic of Turkey.
- Penelis G.G., Kappos A.J. (1997): Earthquake-Resistant Concrete Structures. E & FN Spon, London.
- prEN 1991-1-1:2001: Actions on structures, Part 1-1: general actions, densities, self-weight, imposed loads for buildings. Final Draft, July 2001.
- prEN 1992-1:2001: Design of concrete. Part 1: general rules and rules for buildings. Draft n° 2, January 2001.
- prEN 1993-1-1:2000: Design of steel structures. Part 1.1: general rules. Draft n° 2, August 2000.
- prEN 1994-1-1:2001: Design of composite steel and concrete structures. Part 1-1: general rules and rules for buildings. Draft n° 3, March 2001.
- prEN 1998-1:2001: Design of structures for earthquake resistance. Part 1: general rules, seismic actions and rules for buildings. Draft n°3, May 2001.
- Scawthorn C.R. (2000): Turkey earthquake of August 17, 1999: Reconnaissance Report. Technical Report MCEER-00-0001. Buffalo, N.Y.: Multidisciplinary Center for Earthquake Engineering Research, State University of New York, NY. Editor. the Marmara.
- Sezen H., Elwood K.J., Whittaker A.S., Mosalam K.M., Wallace J.W., Stanton J.F. (2000): Structural Engineering Reconnaissance of the August 17, 1999 Kocaeli (Izmit), Turkey Earthquake. PEER 2000/09. Technical Report. Berkeley, CA.: Pacific Earthquake Engineering Research Center, University of California, CA. <http://nisee.berkeley.edu/turkey>.

- Turkish Standards Institute (1985). TS-500 Building Code Requirements for Reinforced Concrete. Ankara, Turkey.
- Plumier A., Stoychev L., Doneux C., “Composite columns to mitigate soft storey in reinforced concrete structures submitted to earthquake”, in the Proceedings of the Colloquium on Recent Advances and New Trends in Structural Design; Timisoara 7-8 May 2004. ISBN 973-638-119-6.
- Ferrario F., Bursi O.S. and Colombo A., “Analysis and design of RC beam-to-column joints with encased steel profiles subjected to seismic actions”, in the Proceedings of the 4th European Conference on Steel and Composite Structures - Eurosteel 2005, Maastricht, The Netherlands, June 8-10, 2005.
- Doneux C., Plumier A., “Mitigation of seismic soft storey failures in reinforced concrete structures by composite steel-concrete columns”, in the Proceedings of the 4th European Conference on Steel and Composite Structures - Eurosteel 2005, Maastricht, The Netherlands, June 8-10, 2005.
- Vayas I., Thanopoulos P., “Behaviour of seismic resistant braced frames with innovative dissipative (INERD) connections”, in the Proceedings of the 4th European Conference on Steel and Composite Structures - Eurosteel 2005, Maastricht, The Netherlands, June 8-10, 2005.
- Plumier A., Doneux C., Stoychev T., Demarco T., “Mitigation of storey failures of RC Structures under Earthquake by Encased Steel Profiles “, in the Proceedings of the 4<sup>th</sup> International Conference on Advances in Steel Structures(ICASS’05).Shanghai 13-15 June, 2005.
- Vayas I., Calado L., Castiglioni C., Plumier A., Thanopoulos P., “Innovative dissipative (INERD) connections for seismic resistant steel frames”, in the Proceedings of the International Symposium on Steel Structures ISSS’05, Seoul, Korea, 2005.
- Calado Luis and Castiglioni Carlo A., “Design Of Steel Dissipative Connections Under Cyclic Loadings”, in the Proceedings of the 4<sup>th</sup> International Conference on Advances in Steel Structures(ICASS’05).Shanghai 13-15 June, 2005.
- Castiglioni Carlo A. and Calado Luis, “Seismic Behaviour Of Steel Braced Frames With Dissipative Connections”, in the Proceedings of the 4<sup>th</sup> International Conference on Advances in Steel Structures(ICASS’05).Shanghai 13-15 June, 2005.
- Calado Luis and Castiglioni Carlo A., “Design Of Steel Dissipative Connections Under Cyclic Loadings”, in the Proceedings of the 1<sup>st</sup> International Conference on Advances In Experimental Structural Engineering (AESE 2005). Nagoya July 19-21, Japan, 2005.
- Castiglioni Carlo A. and Calado Luis, “Seismic Behaviour Of Steel Braced Frames With Dissipative Connections”, in the Proceedings of the 1<sup>st</sup> International Conference on Advances In Experimental Structural Engineering (AESE 2005). Nagoya July 19-21, Japan, 2005.
- Dell'anna Sergio, "Behaviour of dissipative connections for concentric bracings of steel frames in seismic areas", Politecnico di Milano, thesis, a.a. 2003-2004.
- Feligioni Sandro, "Characterization of dissipative connections for concentric bracing systems of steel frames in seismic areas", Politecnico di Milano, thesis, a.a. 2003-2004.
- Lazzarotto Luca, "Dissipative connections for concentric bracing systems in steel frames in seismic areas", Politecnico di Milano, thesis, a.a. 2003-2004.